Endogenous and Chemical Modifications of Model Proteins

by

Valerie T. Ressler

B.A. Chemistry
Macalester College, 2011

M.S. Chemistry
College of William & Mary, 2013

Submitted to the Department of Chemistry
in Partial Fulfillment of the Requirements for the Degree of

DOCTOR OF PHILOSOPHY
IN CHEMISTRY

at the

Massachusetts Institute of Technology

February 2019

Signature of Author: Signature redacted

Department of Chemistry
January 14, 2019

Certified by: Signature redacted

Ronald T. Raines
Firmenich Professor of Chemistry
Thesis Supervisor

Accepted by: Signature redacted

Robert W. Field
Haslam and Dewey Professor of Chemistry
Chairman, Departmental Committee on Graduate Students

This doctoral thesis has been examined by a committee of professors
from the Department of Chemistry as follows:

Signature redacted

Matthew D. Shoulders
Whitehead CD Associate Professor
Thesis Committee Chair

Signature redacted

Ronald T. Raines
Firmenich Professor of Chemistry
Thesis Supervisor

Signature redacted

Laura L. Kiessling
Novartis Professor of Chemistry
Thesis Committee Member

Endogenous and Chemical Modifications of Model Proteins

by

Valerie T. Ressler

Submitted to the Department of Chemistry on
January 15, 2019 in Partial Fulfillment of the Requirements
for the Degree of Doctor of Philosophy in
Chemistry

Abstract

Protein modifications are ubiquitous in nature, introducing biological complexity and functional diversity. Of the known post-translational modifications, glycosylation is one of the most common and most complex, yet some of the biological implications of this modification remain poorly understood. The development of chemical tools to mimic these modifications is helping to elucidate their biological roles and improve the range of biopharmaceuticals. To probe the biochemistry of endogenous glycosylation and to test the efficacy of novel synthetic modifications, tractable protein scaffolds are needed.

Previously, members of the pancreatic-type ribonuclease (ptRNases) superfamily have been utilized as model protein scaffolds. They are a class of highly conserved, secretory endoribonucleases that mediate diverse biological functions through the cleavage of RNA. The prototypical family homolog, human ribonuclease 1 (RNase 1), has been observed as a differentially glycosylated protein in vivo and been shown to tolerate a wide range of chemical manipulations. It has also emerged as an ideal candidate for protein-based drug therapy. The goal of this thesis is to showcase the biological potential of RNase 1 as a model endogenously glycosylated protein and as a protein payload for evaluating intracellular delivery systems.

In CHAPTER 1, I summarize the current knowledge about ptRNases including their biochemical characterization, conservation of *N*-glycosylation, and therapeutic potential.

RNase 1 possesses three *N*-glycosylation sites giving rise to enormous heterogeneity in biological samples, with unknown implications. In CHAPTER 2, I demonstrate that glycosylation of RNase 1 enhances protein stability and attenuates enzymatic activity.

In CHAPTER 3, I utilize a previously developed diazo compound to enhance delivery of a therapeutically relevant RNase 1 variant. The modification is shown to be reversed upon entry into the cell, presenting a novel approach for delivering native, functional proteins to the cytosol.

Intracellular delivery of another model protein, Cytochrome C (CytoC), has shown therapeutic promise as well. In CHAPTER 4, I demonstrate that synthetic glycosylation with a large, monofunctionalized dextran conveys CytoC into the intracellular space, triggering apoptosis.

Finally, CHAPTER 5 outlines future directions for the study of RNase 1 glycosylation and expanding the utility of the established diazo and dextran-based delivery systems. Taken together, this thesis explores a wide variety of protein modifications, demonstrating biochemical effects of endogenous glycosylation and enhanced delivery of protein payloads with chemical tools.

Thesis Supervisor: Ronald T. Raines

Title: Firmenich Professor of Chemistry

Acknowledgments

I would like to express my sincere thanks to the many people who have encouraged me and supported me on my journey through graduate school. First and foremost, I would like to thank Professor Ronald Raines for allowing me to be a part of his amazing research group and giving me the opportunity to pursue research in his laboratory. My time in the Raines lab has allowed me to work on a wide range of projects with many brilliant people. As a result, I have evolved into a confident, independent scientist and thinker.

I have been fortunate to be a part of several successful projects that would not have been possible without my fantastic collaborators. Thanks to Henry Kilgore, Kalie Mix, and Wen Chyan for their insightful contributions and hard work that helped drive these projects forward. I also want to thank my predecessor Rob Presler for establishing the foundation for the glycosylation project. I have to thank my undergraduate assistant, Jamie Wood, for her dedicated work with enzyme activity assays and her organization skills that helped keep our biochemistry experiments moving seamlessly.

I have to thank the Raines lab as a whole, both past and present, who have routinely given me their time and attention. I especially have to thank Ian Windsor, Trish Hoang, Jim Vasta, Robert Newberry, and Caglar Tanrikulu for their thoughtful discussions and eagerness to lend a helping hand. I am grateful to have been a part of such a wonderful lab that has encouraged me to grow personally and professionally. It has been a pleasure to be a part of such a fun, close-knit group.

I would like to thank the Department of Chemistry at the University of Wisconsin for their assistance and guidance in starting my graduate career. Brian Esselman and Nick Hill were instrumental in cultivating my passion for mentoring and teaching. I would also like to thank the

Department of Biochemistry at the University of Wisconsin for their support of my work and funding me through a William H. Peterson Fellowship.

The move to Massachusetts Institute of Technology was monumental and helped along by many people. The Kiessling lab members have been a great source of advice, encouragement, and laughter as we reassembled our labs and found our way in this new space. Brian Pretti and Jennifer Weisman welcomed us to MIT and have since been wonderful resources as we re-established the lab and joined the Chemistry Department. I am particularly grateful to Professor Laura Kiessling and Professor Matt Shoulders for their flexibility in acting as my new thesis committee at MIT. I appreciate their time and helpful suggestions throughout my time here.

I have to thank Alex Justen, Greg Jones, Will Czaplyski, Kaila Margrey, and Emily Garnett for being incredible friends and sources of comfort during the last years of graduate school – you have provided endless amounts of encouragement and for that I am forever grateful.

My sincere thanks to my family, Tripps, Resslers, and Frybergers, your support has always allowed me to follow my dreams, wherever they may lead. I would especially like to thank my mom and brother, Miles, for their herculean efforts at Southwest Airlines and American Airlines that allowed my husband to log more than 25,000 air miles on trips to visit me in Boston (the circumference of the Earth is 24,901 air miles). Finally, thank you to Daniel Ressler for his unwavering support and patience.

Table of Contents:

List of figures and schemes

List of tables

Abbreviations

Ang	Angiogenin
AOX	Alcohol oxidase
APAF1	Apoptotic peptidase activating factor 1
Asn	Asparagine
ATCC	American Type Culture Collection
bp	Base pair
cDNA	Complementary deoxyribonucleic acid
CHO	Chinese hamster ovary
CLIC	Clathrin- and caveolin-independent carriers
CMV	Cytomegalovirus
CytoC	Cytochrome C
Dex	Dextran
DLS	Dynamic light scattering
DNA	Deoxyribonucleic acid
DNase	Deoxyribonuclease
DSF	Differential scanning fluorimetry
dsRNA	Double-stranded ribonucleic acid
E. coli	*Escherichia coli*
ER	Endoplasmic reticulum
ESI	Electron spray ionization
FAM	Fluorescein
FPLC	Fast protein liquid chromatography
GlcNac	*N*-Acetylglucosamine
Glu	Glucose
HEPES	4-(2-hydroxyethyl)-1-piperazineethanesulfonic acid
His	Histidine
HPLC	High performance liquid chromatography
K_D	Dissociation constant
kDa	Kilodaltons
LC-MS	Liquid chromatography-mass spectrometry
Lys	Lysine
MALDI	Matrix-assisted laser desorption-ionization
Man	Mannose
Met	Methionine
MIM	Mitochondrial inner membrane
mRNA	Messenger ribonucleic acid
MTS	3-(4,5-Dimethylthiazol-2-yl)-5-(3-carboxymethoxyphenyl)-2-(4-sulfophenyl)-2H-tetrazolium
nt	Nucleotides
NLS	Nuclear localization sequence
OST	Oligosaccharyltransferase
P. pastoris	*Pichia pastoris*
PBS	Phosphate-buffered saline
PCR	Polymerase chain reaction

PNGase F	Peptide-*N*-glycosidase F
Poly(A)	Poly(adenylic acid)
Poly(C)	Poly(cytidylic acid)
PTM	Post-translational modification
ptRNase	Pancreatic-type ribonuclease
RI	Ribonuclease inhibitor
RNA	Ribonucleic acid
RNase	Ribonuclease
rRNA	Ribosomal ribonucleic acid
S. cerevisiae	*Saccharomyces cerevisiae*
SA	Sinapinic acid (3,5-dimethoxy-4-hydroxy cinnamic acid)
SAXS	Small-angle X-ray scattering
SDS-PAGE	Sodium dodecylsulfate polyacrylamide gel electrophoresis
SEM	Standard error of the mean
Ser	Serine
SLS	Static light scattering
ssRNA	Single-stranded ribonucleic acid
TAMRA	5-Carboxytetramethylrhodamine
Thr	Threonine
tiRNA	Transfer RNA halves
TOF	Time of flight
tRNA	Transfer ribonucleic acid

Chapter 1

Understanding Endogenous and Chemical Protein Modifications

1.1 Introduction

The amino acid residues of proteins are amenable to a vast array of modifications due to a sea of reactive moieties including carboxylic acids, amides, amines, alcohols, and thiols. Alterations of protein side chains drastically enhances the diversity of protein structures and functions by up to two orders of magnitude.[1] This diversity drives new chemistry, new recognition events, modulates enzyme activity, and targets proteins to specific locations.

Glycosylation is the most prevalent post-translational modification (PTMs), with at least 50 % of human proteins glycosylated in vivo.[2] Glycans can be attached to the amino acid side chains in various ways, including through amide linkages to Asn side chains (*N*-glycosylation), through glycosidic linkages to side chains of Ser/Thr (*O*-glycosylation), or through C–C linkages to the C2 position of Trp (*C*-mannosylation).[3] The glycans themselves can be structurally complex and seem to impart additional information, as protein glycosylation is crucial for protein secretion, immune surveillance, auto-immunity, and tumor metastasis.[4-5] Given the abundance and significance of protein modifications such as glycosylation, extensive work has attempted to mimic these features synthetically. In fact, chemical modification of proteins has emerged as an important tool to probe biological systems and create therapeutic conjugates.[6-7] Multiple synthetic approaches have been specifically designed to exploit proteins for therapeutic gain.

Model protein systems are needed to probe both naturally occurring and synthetically installed alterations. One such group of enzymes is termed the pancreatic-type ribonucleases (ptRNases) and constitutes an extensive superfamily that has been the subject of intense biochemical, structural, and evolutionary studies. Many members of this family are known to be glycosylated in vivo though the biological implications of this functionalization remain poorly

understood. Moreover, previous work with these model proteins has demonstrated their compatibility with a variety of chemically installed modifications.

Herein, I review the current knowledge of this enzyme superfamily, exploring the impact of natural and synthetic alterations on the biochemistry and utility of the prototypical member, ribonuclease 1 (RNase 1). Of all of the human ptRNases, RNase 1 has the most widespread and robust tissue expression, yet its biological functions remain poorly understood largely due to its heterogeneity as a glycoprotein. Understanding the biochemical implications of RNase 1 glycosylation could inform studies about RNase 1 in biological contexts, either as an exogenous or endogenous protein. Previously designed recombinant ptRNases have shown immense promise as anticancer agents and serve as ideal candidates for developing more effective intracellular delivery strategies.

1.2 The pancreatic-type ribonuclease superfamily

1.2.1: Biochemical characteristics of ptRNases

The pancreatic-type ribonucleases are a class of highly conserved secretory proteins that accomplish diverse biological functions by catalyzing the cleavage of RNA. These secreted endoribonucleases are perhaps the best characterized enzyme family of the past century and have been found in all vertebrate species.[8] Insights into the structure and biological functions of ptRNases have emerged from extensive work with RNase A, the bovine homolog that was originally isolated from pancreatic tissue of cows in the early 20th century.[9] As a readily available molecular byproduct of the meatpacking industry, RNase A became a model protein that ushered in the "golden age of biochemistry".[10] During this period, studies with RNase A provided seminal information to many areas of biochemical research as the first enzyme for which an amino acid sequence was determined, the first well-characterized enzyme mechanism,

and the third enzyme for which a crystal structure was determined.[11] Work with RNase A contributed to Nobel-prize winning studies on protein folding,[12] protein chemical structure,[13] and protein solid-phase synthesis;[14] laying the foundation for identification and characterization of other ptRNase family members.

As with RNase A, other ptRNases have been well characterized as being small in size, generally cationic, and highly stable. They also share specific structural features, including a disulfide-bonded tertiary structure and the ability to cleave various RNA substrates. A conserved catalytic triad (His12, Lys41, and His119) enables ptRNases to hydrolyze the P-$O^{5'}$ bond on the 3' end of RNA with some preference for pyrimidine nucleobases, with a preference for cytidine over uridine (Figure 1.1). Human RNase 1 is the most catalytically active of all the human ptRNases. It displays activity against single-stranded RNA (ssRNA)[15] as well as a distinct activity against double-stranded RNA (dsRNA). [16] Presumably, positively charged, non-catalytic residues contribute to the binding and destabilization of the dsRNA to access a single strand for hydrolysis. In humans, thirteen different ptRNases have been identified and characterized, with all of the encoding genes clustered on chromosome 14. Eight of the human ptRNases have been classified as "canonical" ptRNases, while the remaining five differ in one or more of the catalytic residues or lack cationic character. Many of the human ptRNases exhibit tissue-specific expression and distinct biological functions.

1.2.2: Known biological functions of the human ptRNase superfamily

Based on phylogenetic reconstructions, the ptRNase family is rapidly evolving and expanding, and some members are under positive selection for increased diversification. Their diverse biological functions range from angiogenesis to host defense. The human homolog of RNase A,

RNase 1, was associated early-on with the pancreas and was largely miscast as solely a digestive enzyme. More recent work has identified RNase 1 as the primary ribonuclease in human serum, where it has implications in the blood coagulation cascade. Human RNase 2 and 3 (eosinophil-derived neurotoxin : EDN; and eosinophil cationic protein: ECP) are secreted by granules in eosinophils, a specialized type of white blood cells involved in immune responses. Both RNase 2 and 3 display antimicrobial and antiviral activities that rely on their catalytic activity.[17-19] RNase 4 and 5 (ANG) promote angiogenesis and neuroprotection by targeting a unique substrate located in the nucleolus.[20-21] Human RNases 6–8, which are expressed in highest levels in tissues such as in the lung, the skin, and the placenta, have displayed antimicrobial activity and broad-spectrum cytotoxicity. As previously mentioned, RNases 9–13 differ from the "canonical" enzymes in their structural features and catalytic activity, and their biological functions are still emerging. Despite their incredible diversity, all human ptRNases are bound and inhibited by a conserved cytosolic protein, ribonuclease inhibitor (RI).[22]

Intriguingly, *N*-linked glycosylation has been identified as a common feature of many of the human ptRNases in vivo, yet the significance of this modification has remained a mystery. The position of glycosylation sequons varies across the human ptRNases with some conservation of sites between closely related RNase 2 and 3. The structures of the appended glycans also differs between the human ptRNases and might endow different biological functions. Here, we focus on the endogenous glycosylation of human RNase 1 and pursue different tools for delivery of it and other model proteins.

1.3 Human ribonuclease 1

1.3.1: Secretion and glycosylation of RNase 1 in vivo

As secreted proteins, the translation and processing of all ptRNases, including RNase 1, begins in the endoplasmic reticulum (ER). The newly synthesized ptRNase undergoes a series of modifications in the ER to ensure proper protein folding, including signal-peptide cleavage, disulfide-bond formation, and *N*-glycosylation.[23] A host of folding factors such as molecular chaperones, lectin chaperones, and substrate-specific chaperones assist in the entire process and serve as quality control checkpoints.[24] *N*-Glycosylation is a highly conserved and major biosynthetic function of the ER, with approximately 80% of secreted proteins having a glycan attached at specific Asn residues.[25] *N*-Linked glycans are appended in response to the sequon Asn-Xaa-Ser/Thr (where Xaa can be any amino acid residue besides Pro) by an oligosaccharyltransferase (OST). Nonetheless, the presence of a sequon within a protein is not sufficient to guarantee glycosylation of a site, giving rise to macroheterogeneous forms known as glycoforms. Molecular analyses have revealed that the acceptor sequence must be located in a flexible region of polypeptide[26] and interact sufficiently with the OST active site.[27] In fact, the majority of *N*-glycosylation sites exist in potential loop and turn domains of proteins as is the case with most ptRNase glycosylation sites.[28] For glycosylation to occur, the multimeric OST complex transfers a preassembled carbohydrate consisting of three glucoses, nine mannoses, and two *N*-acetyl glucosamines ($Glc_3Man_9GlcNAc_2$) to the Asn side chain of RNase 1.[29]

The *N*-linked oligosaccharide undergoes processing and remodeling by glucosidases and mannosidases within the ER to remove all three glucose residues and one mannose residue before the ptRNase is shuttled to the Golgi. The transport between organelles appears to be tightly regulated through various protein–protein interactions that are still being elucidated.

Glycan maturation occurs in the Golgi to yield a $Man_5GlcNAc_2$ core heptasaccharide in mammalian systems prior to secretion into the extracellular matrix.[30] The final oligosaccharide structure attached to the ptRNase depends on the cell type, its enzymatic equipment, and its disease state,[31] giving rise to a microheterogeneous mixture. The inherent heterogeneity of glycosylated proteins, both on the macro and micro level, has complicated their production in recombinant systems and limited thorough biochemical characterization.[32-33]

1.3.2: RNase 1 homologs across vertebrate species

Interestingly, the notation RNase A arose not from a substrate specificity for the adenine (A) nucleobase, but rather due to it being the primary ribonuclease expressed in the cow pancreas.[34-35] The sequence for RNase A contains a potential site of glycosylation such that RNase A is unmodified, whereas "RNase B", "RNase C", and "RNase D" are *N*-glycosylated forms of RNase A.[36-37] The glycosylation occurs at a single residue, Asn34, which serves as a substrate for endogenous cellular oligosaccharyltransferase. In the case of RNase A, the different glycoforms correspond to the attachment of a $Man_{5-9}GlcNAc_2$ glycan at Asn34 with RNases B,C, and D differing in the number of mannoses.

Pioneering work with RNase A and its glycoforms revealed the widespread conservation of RNase 1 across both mammalian and non-mammalian species.[38] Evolutionary analysis of vertebrate RNase 1 proteins identified multiple *N*-glycosylation sequons that occur in rapidly evolving sections of the enzyme.[8, 39-40] Among the sites, Asn34 emerges as the most widely conserved across RNase 1 homologs and is consistently glycosylated in biological samples from various species, including in humans.[41-43] It has been postulated that RNase A plays a major role in digesting RNA from microflora in ruminants and species with ruminant-like digestion, given

its high expression in the pancreas and salivary glands. Previous work has suggested that selection pressures encouraged the glycosylation of Asn34 in monogastric animals (*e.g.*, humans and mouse) and decreased the level of glycosylation in ruminants (*e.g.*. cow and goat).[44] This trend reinforces the distinction between the digestion-related RNase A and other RNase 1 homologs, such as human RNase 1. The widespread conservation of RNase 1 homologs and maintenance of multiple glycosylation sites implies a significant biological role that remains poorly understood.

1.3.3: Evolutionary trends in glycosylation of RNase 1 homologs

Human RNase 1 is one of the most heavily glycosylated of all the RNase 1 homologs with three sites that can undergo *N*-linked glycosylation (Asn34, Asn76, and Asn88). This specific tri-glycosylation pattern seems to have evolved more recently in ape and great ape species, with the exception of orangutans lacking Asn88. The three sites are distinct from one another in that they occur in unique environments within the protein. The local environment has been shown to have a significant impact on the level of occupancy for a given glycosylation site. Endogenous glycosylation machinery recognizes sequences that end in either Ser or Thr, yet higher levels of glycan attachment were observed with sequences ending with Thr.[28] The highly conserved Asn34 in human RNase 1 matches the non-ruminant ancestral carbohydrate attachment site, Asn-Met-Thr, that favors glycosylation.[44] Residue Asn76, which occurs as Asn-Ser-Ser, is located distal to the enzymic active site and appears to have evolved more recently, as it is mainly limited to apes. Lastly, Asn88 exists in the sequence Asn-Gly-Ser and is situated closer to the RNA binding cleft. Characterization of RNase 1 from different tissue samples, including tumors, revealed drastically different glycosylation patterns. As predicted by the differences in the

sequences, RNase 1 isolated from human pancreas had Asn34 glycosylated in almost all cases, whereas Asn76 and Asn88 had glycans attached in about half and a minor amount of the proteins, respectively.[42]

1.3.4: Biological distribution and glycosylation of human RNase 1

Although human RNase 1 was originally grouped with bovine RNase A as a purely digestive enzyme, growing evidence has led to the hypothesis that RNase 1 has a broader role in humans. In fact, RNase 1 expression has been detected in a wide variety of tissues[40] and bodily fluids beyond the digestive tract, with highest levels of secretion from endothelial cells.[41] Since these cells line the interior surface of blood vessels, RNase 1 circulates freely through the body at a concentration of 400 ng/mL (or ~20 nM).[45-46] Human RNase 1 has been observed in other bodily fluids including, milk,[47] urine,[48] seminal plasma, and cerebrospinal fluid.[49] Interestingly, the glycosylation pattern for RNase 1 varies by fluid, with urinary forms being the most heavily glycosylated with all three sites occupied.[50]

The variable glycosylation of RNase 1 has undetermined biological implications, but has been explored as a potential biomarker for pancreatic cancer. Pancreatic cancer remains one of the most difficult cancers to diagnose, mainly due to a lack of early definitive symptoms. Originally, elevated serum levels of RNase 1 were considered to be a marker for pancreatic cancer, but other studies observed significant increases in serum RNase 1 expression for a multitude of conditions.[51-54] Recently renewed efforts have noted aberrations in the glycosylation of RNase 1 in cancer, specifically increased glycan occupation of Asn88 in serum samples from pancreatic cancer patients.[55] As mentioned above, Asn88 is rarely glycosylated in samples from

healthy patients. Thus, detecting changes in glycosylation at this position shows promise as a novel diagnostic marker for pancreatic cancer.[42]

1.3.5: Production of recombinant RNase proteins

The recombinant expression of various ptRNases in *Escherichia coli*, the most widely used heterologous protein expression system,[56] has enabled thorough characterization and significantly expanded the application of these proteins. ptRNases can be expressed in relatively high concentrations with this prokaryote-based system, though the proteins aggregate as inclusion bodies and must be refolded as part of the purification process. Production in *E. coli* yields large quantities of pure ptRNases that lack PTMs including *N*-glycosylation.

Previous attempts to produced authentically glycosylated RNases employed eukaryotic expression hosts, including *Saccharomyces cerevisiae*[56] and Chinese hamster ovary (CHO) cells.[57] While these hosts possess the cellular machinery necessary to glycosylate recombinant proteins, the observed glycosylation pattern is strongly dependent on the cell type and might not be biologically representative. Many yeast systems including *S. cerevisiae* have been found to append immunogenic high mannose glycans and high levels of undesired *O*-glycosylation, a major limitation for production of recombinant glycoproteins.[58] Mammalian-based systems, such as CHO or HEK cells, suffer from low yields of recombinant glycoproteins. In addition, the secretion of endogenous ptRNases by mammalian cells complicates the production of recombinant ptRNases, necessitating a tag-based approach.

In recent years, *Pichia pastoris* (*P. pastoris*) has emerged as a successful expression host due to its high efficiency,[59] reduced *O*-linked glycosylation,[60] and ability to secrete fully folded proteins.[61-62] Though *P. pastoris* has been observed to append shorter chain glycans than does *S.*

cerevisiae, the resulting *N*-glycans are often highly antigenic and detrimental for therapeutic protein production.[63] To overcome this limitation, extensive work focused on generating strains capable of mimicking mammalian-like glycosylation patterns.[64] Glycoengineering efforts have eliminated hyper-mannosylation of yeast glycans and introduced elements required to produce human-like glycans.[65-66] One such highly engineered strain known as the *Pichia* Glycoswitch® System has a key disruption of the gene encoding for a mannosyltransferase in the yeast Golgi as well as the addition of heterologous genes encoding enzymes that append human-like glycans (Figure 1.2).[67-68] The Superman 5 (M5) strain produces large quantities of glycosylated proteins with a human-like $Man_5GlcNAc_2$ heptasaccharide and could be promising as an expression system for producing glycosylated forms of ptRNases.

1.4 RNase 1 therapeutics

1.4.1: Therapeutic potential of RNase 1

Understanding the endogenous modifications of RNase 1 is a crucial step towards harnessing their unique biochemistry therapeutically. Previously engineered forms of RNase 1 are currently in phase I clinical trials as cancer therapeutics.[69-70] Several features of RNases—stability to harsh conditions, robust activity, and tolerance of modifications—make them ideal candidates for targeted protein therapies.[71] Moreover, RNases are naturally endocytosed into cells, a process largely driven by Coulombic interactions between the positively charged protein and the negatively charged glycocalyx that coats cells.[72] The putative model of ptRNase-mediated cytotoxicity requires an initial cell-surface binding, followed by internalization through energy-dependent endocytosis.[73] Interestingly, RNase 1 retains activity and conformational stability even under acidifying conditions like those found in endosomes. Upon translocation into the cytosol, RNases capable of evading the inhibitor protein can degrade intracellular RNAs such as

tRNA, mRNa, rRNA, triggering apoptosis (Figure 1.3).[74] Thus, RNase 1 and other ptRNases provide exciting potential as cytotoxins.

1.4.2: Internalization of ptRNases and specificity for cancer cells

Circulating ptRNases, as either an endogenous protein or an exogenous therapeutic agent, readily interact with a variety of cell surfaces. Studies of ptRNases-uptake revealed that the process does not appear to be driven by receptor-mediated endocytosis, but rather through multiple internalization pathways (Figure 1.4).[75] A predominant theory was that the cationic ptRNases associate with anionic cell-surface features to facilitate binding and subsequent internalization. In fact, previous work has demonstrated that reducing the negative charge on a cell surface by diminishing the biosynthesis of heparan sulfate and chondroitin sulfate decreases the internalization of ptRNases.[72] A similar decrease in internalization was observed by decreasing the positive charge of an ptRNase, further emphasizing the importance of Coulombic forces in mediating this interaction.[76] Extensive mechanistic work has equated ptRNase internalization to that of cell-penetrating peptides and has inferred that uptake occurs through both clathrin-coated vesicles and macropinosomes.[77]

Surprisingly, ptRNases seem to naturally target cancer cells. The surface of cancer cells is more negatively charged than that of homologous normal cells, in large part due to increases in glycosaminoglycans, phospholipid composition, or glycosphingolipid exposure,[78] and might explain the susceptibility of cancer cells to ptRNase-based therapeutics. More recent work focused on characterizing ptRNase interactions with specific components of the glycocalyx and identified Globo H, a known cancer antigen, as a strong binding partner of RNase 1.[79] Globo H is a neutral glycosphingolipid found on the outer membrane of epithelial cells like those in

mammary, uterine, pancreatic, and kidney tissues.[80-81] The overabundance of Globo H on the surface of MCF-7 breast cancer cells originally led to its classification as a tumor-associated antigen; however, it has since been associated with a range of other cancer types and served as the basis for an anti-cancer vaccine.[82-83] RNase 1 binds immobilized Globo H with a relatively high affinity in the low micromolar–high nanomolar range and is pH dependent. Moreover, the expression of Globo H correlates with cell susceptibility to ptRNases. The broad expression of Globo H on multiple cancer cell lines provides a promising target to direct ptRNase-based therapeutics to cancer cells.

1.4.3: Previous approaches to engineer RI Evasion

Another key aspect of ptRNase-mediated toxicity is evasion of the cellular "sentry", RI, which is expressed ubiquitously in human cells.[40, 84] Various strategies have been deployed to endow ptRNases with the ability to evade RI without perturbing other factors, such as cellular internalization. The chemotherapeutic potential of ptRNases was first observed with onconase® (ONC), a RNase 1 homolog isolated from the oocytes of the northern leopard frog, *Rana pipiens*. ONC was found to be both cytotoxic and cytostatic toward tumor cell lines and inhibited the growth of xenograft tumors in mice.[85-86] The observed cytotoxicity of ONC was attributed to an extremely low affinity for mammalian RI due to evolutionary differences. High levels of renal toxicity however, have limited the clinical efficacy of this protein therapy.[87-88]

Mammalian-derived ptRNase protein therapies display markedly less immunogenicity than does ONC and have higher catalytic activity towards RNA substrates. Though mammalian ptRNases are typically bound and sequestered by cytosolic RI in an evolutionarily conserved manner, the rational design of mammalian ptRNases has reduced the affinity for RI.[89] Site-

directed mutagenesis and chemical modifications of ptRNase have been used to disrupt binding interactions at the interface with RI.

The attachment of a single pendant poly(ethylene glycol) (PEG) moiety to a specific residue of RNase A reduced interactions with RI sufficiently to decrease the proliferation of cancer cells and inhibit tumor growth.[90-91] The crucial site on RNase A for PEG functionalization was buried in the interface with RI such that the additional steric bulk reduced the binding affinity from the femtomolar range to nanomolar (a 10^6-fold change). Further, the addition of the PEG chain lowered renal clearance, which typically affects small proteins. The same region of RNase 1, namely residues 85–94, has been altered through site-directed mutagenesis to minimize contact with RI. This surface loop appears to be highly flexible and tolerated multiple manipulations to generate a more cytotoxic variant of RNase 1, ERDD (L86E/N88R/G89D/R91D).[92] To date, the most RI-evasive variant of RNase 1, DDADD (R39D/N67D/N88A/G89D/R91D), contains mutations in the previously mentioned surface loop and two other residues known to interact with RI (Figure 1.5).[76] The installation of carboxylates at strategic positions within RNase 1 reduced the interaction with RI to a micromolar affinity in vitro, but they also significantly reduced the overall net charge of the protein. The loss of cationicity was detrimental to the cellular internalization and thus cytotoxicity of DDADD RNase 1.

The development of ptRNase-based therapeutics has revealed a dueling system of equilibria related to protein charge. Specifically, the internalization of ptRNases relies largely on Coulombic interactions with anionic moieties on the cell surface, yet more cationic proteins bind more tightly to RI. Given the current understanding of ptRNase-based therapeutics and their

innate specificity for cancer cells, we have employed them as model proteins to assess intracellular delivery strategies.

1.5 Delivery of therapeutic proteins

1.5.1: Challenges to intracellular delivery

Many of today's top selling drugs are proteins that offer many benefits over traditional small molecule-based therapeutics. Still, a major roadblock in the advancement of biopharmaceuticals is the delivery of these macromolecules into the cell to act on specific targets. Whereas ptRNases have some endogenous strategies to enter the cell, most proteins do not readily penetrate the cellular membrane and must instead act on extracellular targets. The mammalian cellular membrane presents a formidable obstacle as cells have evolved to tightly regulate their contents and the influx of extracellular material.[93-94] In addition, the eukaryotic cell surface is coated in a dense forest of polysaccharides that make up the glycocalyx and can be up to 500 nm thick.[95-96] The dynamic, hydrophilic glycocalyx is anionic in nature and can repel anionic proteins and nucleic acid-based therapeutic agents.[96-97] Beneath the glycocalyx, the amphipathic plasma membrane itself spans 5 nm.[98] Though small, lipophilic molecules might diffuse across this layer, most proteins are too large and must rely upon other means of internalization, such as endocytosis or phagocytosis.[99] Unfortunately, once inside the cell, protein therapeutics face the additional problem of escaping vesicular structures (*e.g.*, endosomes) and accessing the cytosol.[100] Therapeutics that become entrapped in endosomes are later degraded by specific enzymes in the lysosome.[101] Though protein-based therapeutics have high-specificity and potency, they face many challenges in reaching intracellular action sites and require enhanced delivery methods.

1.5.2: Current approaches to cellular delivery

Extensive efforts have focused on developing new techniques to enhance the cytosolic delivery of biologicals, without causing detrimental off-target effects.[102] Two delivery strategies that have been broadly used are carrier-based delivery and covalent modification. The carrier-based approach uses modular systems to encapsulate protein cargo through reversible associations. Liposomes, lipoplexes, and nanoplexes have all shown promise as supramolecular carriers for delivering different biological cargoes to intracellular targets.[103-107] Covalent modification of cargo proteins includes the irreversible attachment of cell-penetrating peptides,[108-109] supercharged proteins,[110-111] or conjugation to nanocarriers to improve cellular uptake.[112] Although these strategies improve protein delivery, they possess several drawbacks, including low efficiency, reduced biological activity,[113-114] immunogenicity,[115] and decreased protein stability.[116-117] Most of these delivery strategies increase the endocytosis of biological cargoes, but do not facilitate endosomal escape and entry into the cytosol. Thus, therapeutic payloads might still be entrapped in endosomes and degraded by cellular processes.

The ever-growing catalog of therapeutically relevant proteins requires the expansion of delivery strategies to include more biocompatible modifications. In order to evaluate the efficacy of such novel modifications for enhanced cellular internalization, amenable protein scaffolds (*i.e.*, cargoes) will be needed.

1.6 Chemical biology tools for enhanced delivery

1.6.1: Diazo compounds as tools for chemical biology

Though diazo groups ($R_2C{=}N_2$) have been a common reagent in synthetic organic chemistry for more than a century, [118-120] their applications in biological settings have only recently gained attention.[121-122] For decades, concerns about toxicity[123-125] and potentially explosive reactivity

limited the usefulness of diazo compounds in chemical biology. The extreme reactivity arises from the high basicity of these compounds, as protonation of the α carbon leads to the formation of a diazonium species ($R_2HC–N_2^+$) that rapidly releases nitrogen gas.[126] Recent advances have allowed access to "stabilized" diazo compounds that are mild, yet powerful, tools for chemical biologists. The tuned diazo compounds are designed with functional groups that allow the electron density to be delocalized beyond the α carbon. In addition to their broad applications and tunable reactivity, diazo compounds are easily accessed by conversion of the parent azido group in a one-step "deimidogenation" reaction with an appropriate phosphine.[127-128]

1.6.2: Diazo-mediated esterification of protein side chains

Diazo compounds are well known to esterify carboxylic acids through *O*-alkylation of the carboxyl group. This modification provides a unique opportunity in chemical biology as a means to esterify proteins and other biomolecules. The resulting linkage would be susceptible to cleavage by non-specific esterases in mammalian cells, thereby providing a temporary masking strategy.[129-131] Previous attempts to label proteins with diazo reagents were limited in that they required a large molar excess (>10^3-fold) of diazo compound[132-134] and were not chemoselective.[135] Amino, sulfhydryl, and phenolic side chains were indiscriminately alkylated under these conditions, resulting in irreversible modifications to proteins.

To overcome limitations with diazo-mediated labeling, various stabilized diazo scaffolds were evaluated for their ability to selectively esterify protein carboxyl groups in an aqueous environment.[122, 136] The anointed diazo compound possessed the desired features and was used to esterify the carboxyl groups of green fluorescent protein (GFP), thus remodeling the surface to be less anionic and more hydrophobic.[137] The esterification strategy efficiently labeled multiple

carboxyl groups of GFP and drastically enhanced cellular uptake, even at 4 °C with its suppressed endocytosis. Remarkably, esterified GFP does not appear to rely on endocytosis and can enter cells directly by translocating through the plasma membrane, similar to a prodrug.[130] A model protein of the ptRNase family, ANG, was also labeled with the chosen diazo compound and treated with cellular extract to confirm the bioreversibility of this modification. Hence, diazo-mediated esterification is well poised as a tool to deliver native cargo to the cytosol of cells given its selectivity for carboxylic acids and bioreversibility.

1.6.3: Large monofunctionalized dextrans for enhanced cellular uptake

Polysaccharides represent a major class of biomolecules, but have historically garnered less attention than their protein, nucleic acid, and lipid counterparts. Dextrans are a well-characterized, versatile class of polysaccharides with applications in biology, medicine,[138] food science,[139] and commercial goods.[140] Isolated from *Lactobacillales*, a family of gram-positive bacteria, dextran biopolymers consist of glucose monomers linked through α–1,6 glycosidic linkages, with occasional branches connected to the main chain by α(1-4) and α(1-3) linkages.[141] The widespread use and availability of dextrans in biochemistry has spurred their commercialization, with fluorophore-conjugated dextrans serving as a tracking agent for macro- and micropinocytosis or as an imaging reagent in co-localization studies focused on endocytosis.[142-143]

Recently, a novel type of large monofunctionalized dextran was observed to exhibit unusually high cytosolic transport of a fluorogenic probe.[144] This specific dextran displayed an ability to permeate throughout the cell without the aid of transfection reagents, electroporation methods, or membrane perturbation. The enhanced uptake phenomenon was preserved across

multiple cell lines, with dispersion throughout the cytosol and the nucleus. The cellular entry of the dextran conjugate was attributed to a combination of receptor-mediated endocytosis and pinocytosis, as has been observed in other work with dextrans.[145] This dextran carrier presents an ideal platform for delivering protein-based therapeutic payloads. Synthetic glycosylation of protein therapeutics has been routinely exploited to enhance in vivo efficacy by improving stability and pharmacokinetic profiles.[146]

1.6.4: Therapeutically relevant model proteins

To assess novel intracellular protein delivery strategies, ideal protein cargoes are needed. As discussed above, ptRNases have shown promise as model proteins for multi-faceted drug design. ptRNase variants are readily produced in microbial hosts, easily purified, and are stable to even the harshest conditions. In addition, they are incredibly tolerant of modifications and possess biological readouts for cellular internalization. Though ptRNases seem to preferentially target cancer cells over non-cancerous cells,[73, 147] only a small fraction of the endocytosed protein is able to translocate into the cytosol and degrade cellular RNA.[77] Thus, ptRNases are especially well-suited for enhanced delivery strategies as therapeutic agents.

Cytochrome C (CytoC) is another useful model protein [148] to assist in the development of delivery technologies. In biological systems, CytoC plays a dual role in regulating both cellular energetic metabolism and apoptosis.[149] It functions in the mitochondrial intermembrane (MIM) space to transfer electrons in the oxidative phosphorylation pathway, facilitating the production of adenosine triphosphate (ATP).[150] Interestingly, the release of CytoC from mitochondria into the cytosol initiates a cascade of events triggering apoptosis through the intrinsic pathway. Once in the cytosol, CytoC binds to apoptosome activating factor 1 (APAF 1), which heptamerizes to

form an apoptosome. The apoptosome mediates activation of caspase-9, thereby triggering a caspase cascade, whereby the executioner caspases 3 and 7 are activated.

The intracellular delivery of exogenous CytoC presents a promising, but challenging therapeutic target. CytoC is a cationic, 12.3–kDa protein with an exceptionally large dipole moment and an affinity for anionic lipids.[150-152] These characteristics prevent unmodified CytoC from entering mammalian cells. Thus, CytoC is an ideal protein scaffold that is commercially available and provides a direct biological readout for cellular internalization—cell death.

1.7 Prospectus

Pancreatic-type ribonucleases, specifically RNase 1, have been extensively studied over the past century. Still, many mysteries remain regarding the biochemistry of these enzymes in their endogenous glycosylated state. Though differential glycosylation patterns have been observed in vivo and even been considered as biomarkers for pancreatic cancer, the biochemical implications of this modification are still unknown. Recently, RNase 1 has emerged as a promising chemotherapeutic agent and is an ideal candidate for engineering modifications to enhance cytosolic delivery. Newly developed chemical tools have been shown to enable cellular internalization and show promise in expanding the use of protein therapeutics. Further study of protein modifications, whether installed by endogenous or synthetic mechanisms, would advance our knowledge and guide their use as therapeutic agents.

The central aim of this thesis is to demonstrate the broad potential of protein modifications and explore their implications in vitro and in cellulo. I produced individual RNase 1 glycoforms and evaluate their biochemical properties, then used these data to speculate on the conservation of glycosylation sequons. Additionally, I have worked to functionalize RNase 1 and another model protein, CytoC, as a means to test novel intracellular delivery strategies.

Importantly, I demonstrate that bioreversible and irreversible methods can be harnessed to deliver challenging protein payloads. Together, the studies in this thesis provide an intriguing view into modifications of RNase 1 and CytoC, either endogenously with glycosylation or as a strategy to enhance intracellular delivery.

A

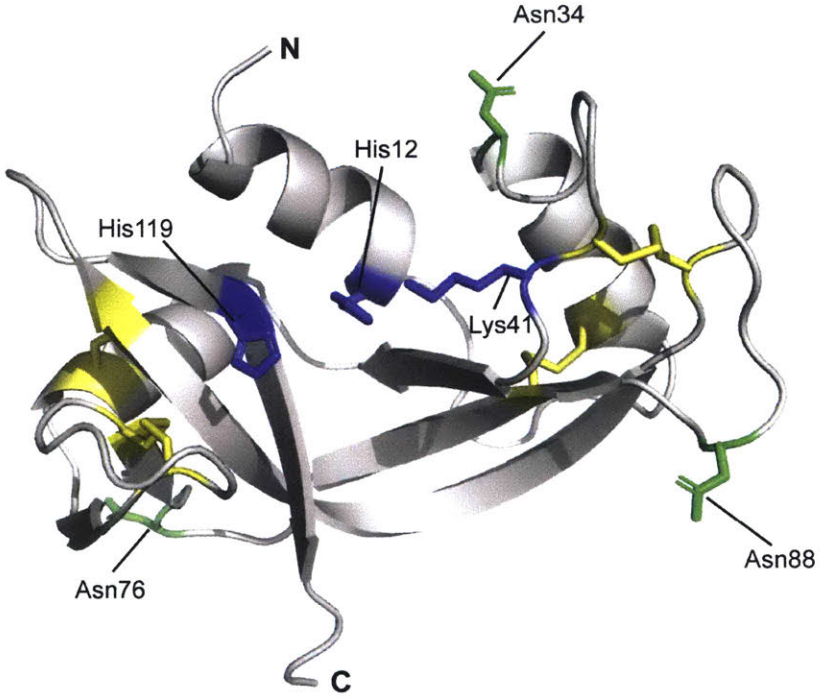
N
Asn34
His12
His119
Lys41
Asn88
Asn76
C

B

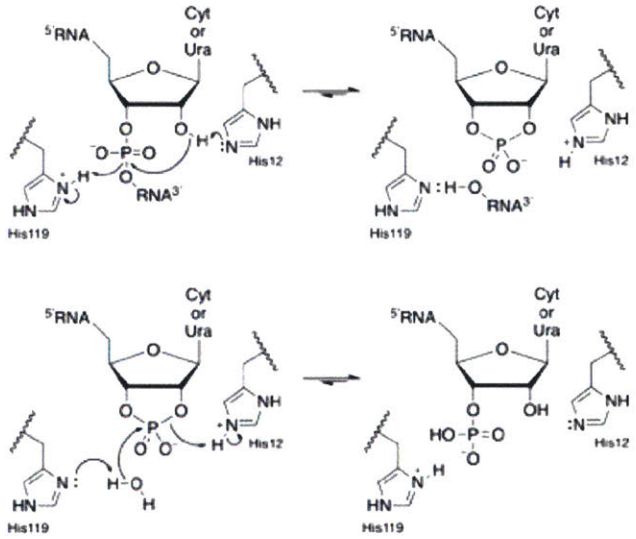
5'RNA
Cyt or Ura
His12
His119
RNA3'
OH

Figure 1.1. Structural features and catalytic mechanism of ptRNases. *A.* PyMOL rendering is based on PDB entry 1z7x. Relevant side chains are shown as sticks. Active–site residues His12, Lys41, and His119 are shown in blue. The three *N*-glycosylation sites at Asn34, Asn76, and Asn88 are shown in green. The four intramolecular disulfide bonds are highlighted in yellow. *B.* Mechanism of transphosphorylation and hydrolysis of RNA catalyzed by ptRNases. Figure is adapted from reference 8.

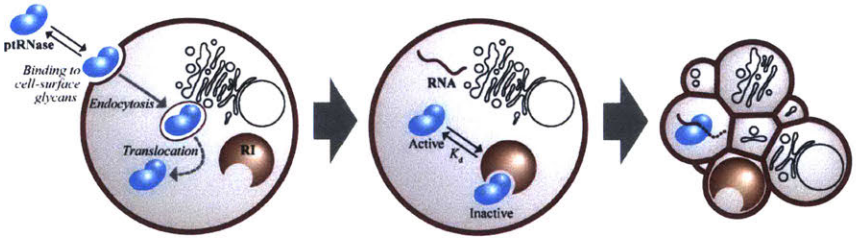

ptRNase Internalization RI-Evasion *in cellulo* Cell-Growth Inhibition and Apoptosis

Figure 1.2. Putative mechanism of ribonuclease cytotoxicity. The cellular uptake of ptRNases is largely charge-driven and requires association with glycans on the cell membrane, absorptive endocytosis, and interaction with cytosolic RI. Upon evasion of RI, cytotoxic ptRNases will readily degrade cellular RNA and induce apoptosis.

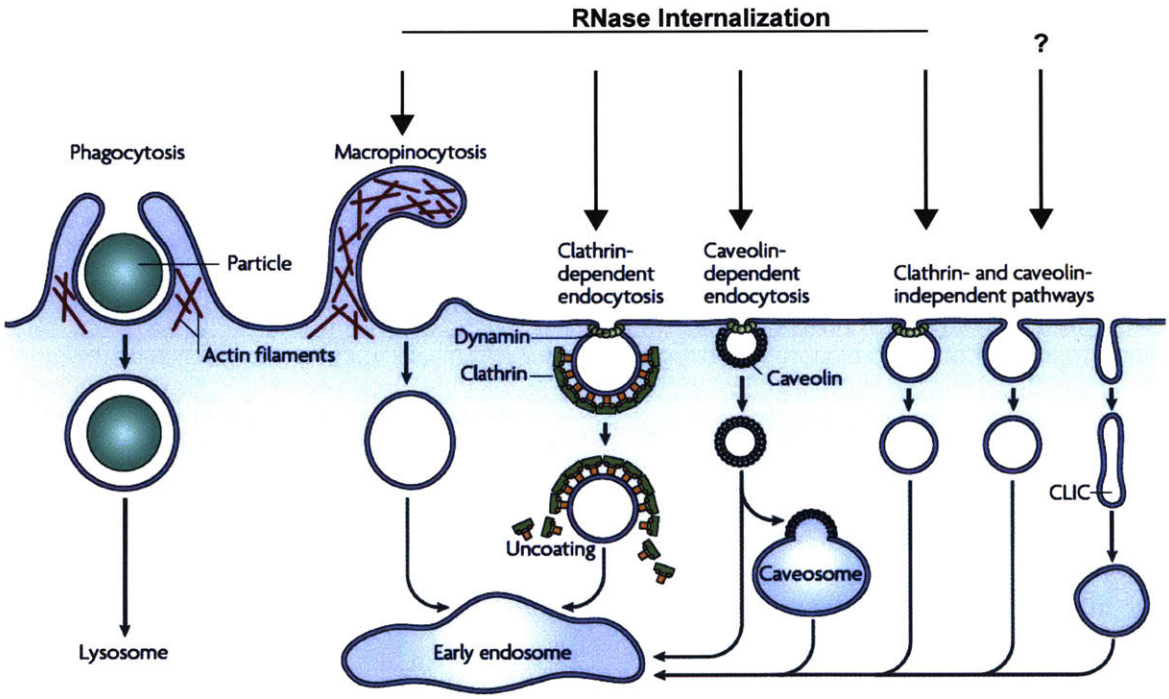
RNase Internalization
?
Phagocytosis
Macropinocytosis
Particle
Actin filaments
Clathrin-dependent endocytosis
Caveolin-dependent endocytosis
Clathrin- and caveolin-independent pathways
Dynamin
Clathrin
Caveolin
CLIC
Uncoating
Caveosome
Lysosome
Early endosome

Figure 1.3. Pathways for cellular internalization utilized by ptRNases. A representation of the main pathways and routes used by ptRNases for cellular entry. Phagocytosis and micropinocytosis correspond to the uptake of large particles and fluid, respectively. Both these processes require the rearrangement of actin filaments. Endosomal uptake can require dynamin (GTPase), clathrin (coat protein), and caveolin (structural protein). However, some internalization occurs in the absence of all these elements to become encapsulated in clathrin- and caveolin-independent carriers (CLIC). Internalization of RNase A was found to be partially dependent on micropinocytosis and dynamin- and clathrin-dependent endocytosis, as indicated by the arrows above the image. Figure adapted from reference 75 and 77.

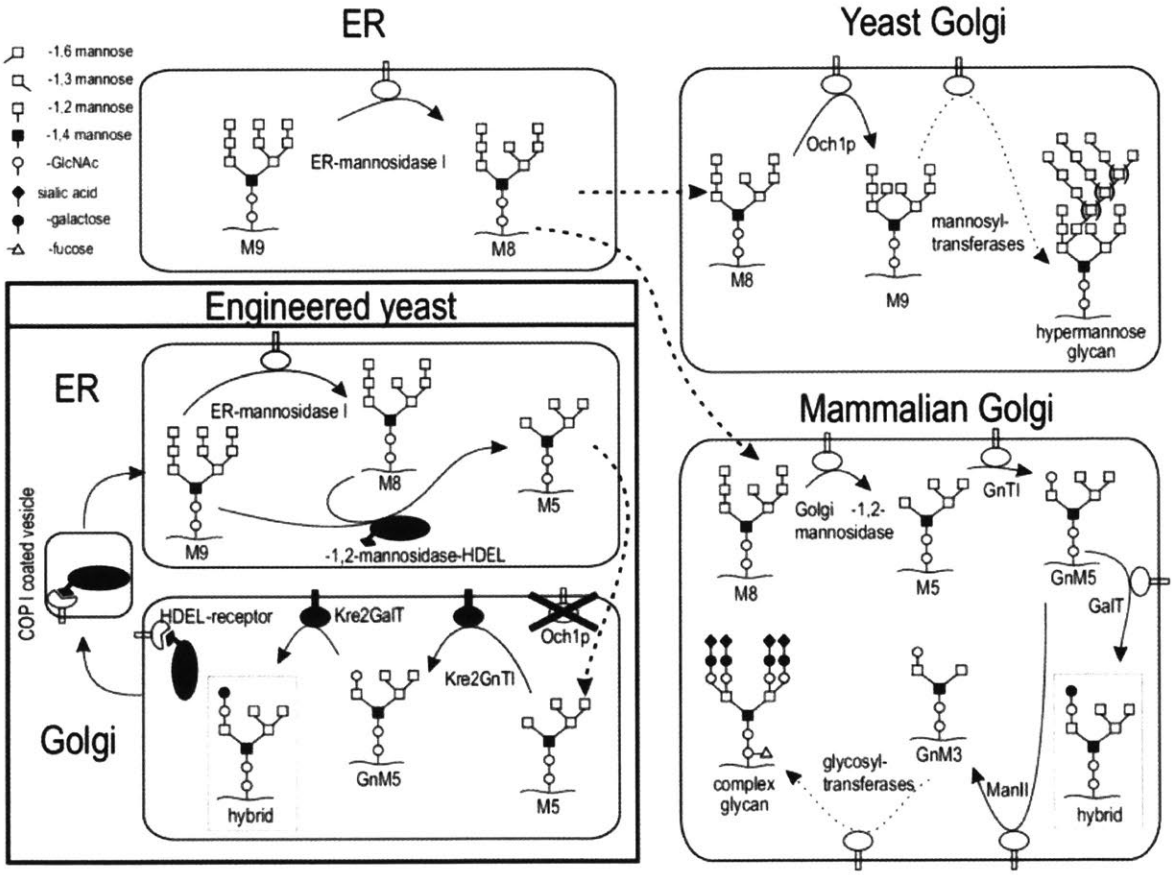
ER
Yeast Golgi
-1,6 mannose
-1,3 mannose
-1,2 mannose
-1,4 mannose
-GlcNAc
sialic acid
-galactose
-fucose
ER-mannosidase I
M9
M8
Och1p
mannosyl-
transferases
M8
M9
hypermannose
glycan
Engineered yeast
ER
ER-mannosidase I
M8
M5
M9
-1,2-mannosidase-HDEL
COP I coated vesicle
HDEL-receptor
Kre2GalT
Och1p
Kre2GnTI
Golgi
GnM5
M5
hybrid
Mammalian Golgi
Golgi -1,2-
mannosidase
GnTI
M8
M5
GnM5
GalT
glycosyl-
transferases
GnM3
ManII
complex
glycan
hybrid

Figure 1.4. Schematic of *N*-glycosylation in different organisms. In eukaryotes, the glycosylation of secreted proteins proceeds through the ER and the Golgi with multiple glycosidases and glycosyltransferases involved in generating a mature glycoprotein. Typical yeast hosts append undesirable hypermannose glycans to recombinant proteins. Recent advances in yeast engineering have resulted in the "humanization" of the glycosylation pathways, producing "human-like" glycans. We utilize the M5 cell line specifically to generate different glycoforms of human RNase 1. Figure was adapted from reference 67.

A

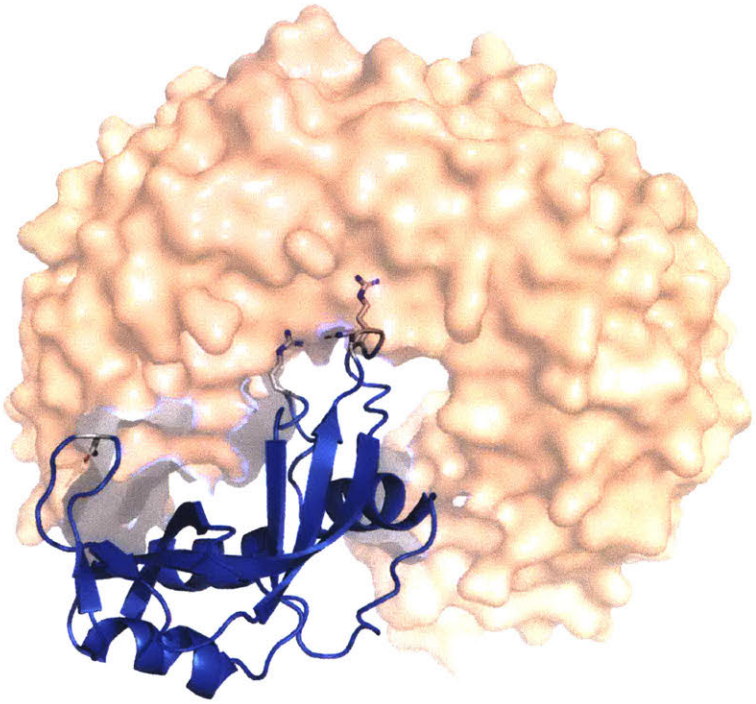

B

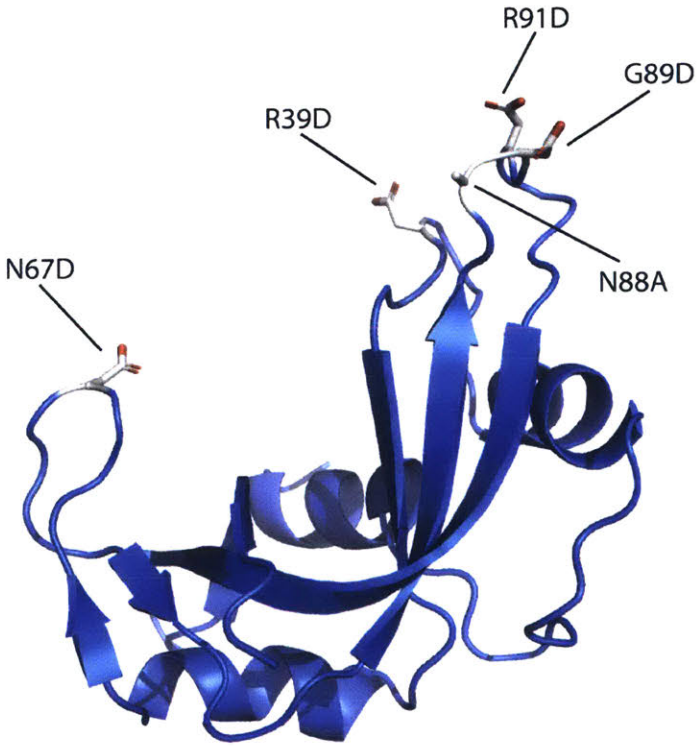

Figure 1.5. Structures of human RNase 1 variants and RI. *A.* PyMOL renderings are based on PDB entry 1z7x. *A.* Ribbon diagram of wild-type RNase 1 in complex with inhibitor protein (RI) shown in red. Important side chains for binding of RNase 1 are depicted as sticks. *B.* Ribbon diagram of RI-evasive variant DDADD RNase 1 with side chains that have been engineered to evade RI.

Chapter 2

Consequences of the Endogenous *N*-Glycosylation of Human Ribonuclease 1.

Contributions: I designed and carried out all experiments, and wrote the manuscript.

This chapter has been submitted as *Consequences of the endogenous N-glycosylation of human ribonuclease 1* to *Biochemistry*.

2.1 Abstract

Ribonuclease 1 (RNase 1) is the most prevalent human homolog of the paradigmatic enzyme, RNase A. RNase 1 contains sequons for *N*-linked glycosylation at Asn34, Asn76, and Asn88 and is *N*-glycosylated at all three sites *in vivo*. The effect of *N*-glycosylation on the structure and function of RNase 1 is unknown. By using an engineered strain of the yeast *Pichia pastoris*, we installed a heptasaccharide ($Man_5GlcNAc_2$) on the side chain of Asn34, Asn76, and Asn88 to produce the authentic triglycosylated form of human RNase 1. Unlike an asparagine residue, a glutamine residue is not a substrate for cellular oligosaccharyltransferase. We also used the *P. pastoris* strain and strategic asparagine-to-glutamine substitutions to produce the three diglycosylated and three monoglycosylated forms of RNase 1. We found that the *N*-glycosylation of RNase 1 at any position attenuates its catalytic activity but enhances both its thermostability and its resistance to proteolysis. *N*-Glycosylation at Asn34 generates the most active and stable glycoforms, in accord with its sequon being highly conserved among vertebrate species. These data provide new insight on the biological role of the *N*-glycosylation of a human secretory enzyme.

2.2 Introduction

Pancreatic-type ribonucleases (ptRNases) are a family of secretory endoribonucleases that enable various biological functions in vertebrates by catalyzing the cleavage of RNA. Members of this family are characterized by their small size and high conformational stability.[153-154] Insights into the structure and function of ptRNases have emerged from a bovine prototype—RNase A. The mass production of RNase A as a byproduct of the meatpacking industry provided seminal information on the biological chemistry of proteins,[9, 38, 155-158] including the first enzymatic reaction mechanism.[159]

The "A" in RNase A refers not to an *a*denine nucleobase, but to RNase A being the predominant ribonuclease in the cow pancreas.[34-35] RNase A is unglycosylated, whereas "RNase B", "RNase C", and "RNase D" are *N*-glycosylated forms of RNase A.[36, 160] The glycan is added to the side chain of the Asn34 residue by oligosaccharyltransferase, which acts on Asn-Xaa-Ser/Thr sequons,[161-164] where Xaa represents any residue other than proline.[165] RNase A has only one sequon.

The most prevalent human homolog of RNase A is RNase 1, which is present in many bodily fluids[47-48] and circulates at ~0.5 μg/mL.[45] In RNase 1, Asn34, Asn76, and Asn88 are in Asn-Xaa-Ser/Thr sequons (Figure 2.1A). An analysis of RNase 1 in human serum has shown that each of these sites is *N*-glycosylated *in vivo*.[42] (There are no apparent *C*-, *O*-, or *S*-linked glycans.) The three sites of human RNase 1 are, however, *N*-glycosylated differentially depending on tissue- and cell-type.[41, 50, 166] Moreover, Asn34 is glycosylated in nearly all isolates, whereas Asn76 and Asn88 are occupied in half or a small fraction of isolates, respectively.[42, 167] These occupancies are consistent with the observed preference for the glycosylation of Asn-Xaa-Thr rather than Asn-Xaa-Ser sequences.[28]

The consequences of the glycosylation of human RNase 1 are unknown.[168] A phylogenetic analysis reveals multiple *N*-glycosylation sequons, many of which occur in rapidly evolving segments of the enzyme (Figure 2.2).[39] Of the potential *N*-glycosylation sites, Asn34 is conserved most widely, and the analysis of isolates confirms that this site is *N*-glycosylated in a range of diverse species.[43, 169] The specific triglycosylation pattern observed in human RNase 1 appears to have evolved more recently with hominids, with only orangutans lacking Asn88. Accordingly, all three *N*-glycosylation sites are worthy of consideration.

In this work, we present the first biochemical analysis of glycosylated human RNase 1. First, we establish a heterologous production system that generates high yields of individual RNase 1 glycoforms. Then, we measure the biochemical characteristics of each glycoform, including catalytic activity and overall protein stability. The ensuing data provide biochemical insight into the impact of glycosylation on RNase 1 and, specifically, the potential evolutionary significance of glycosylation at Asn34.

2.3 Methods

2.3.1: Strategy for producing human RNase 1 glycoforms

Previous studies of human RNase 1 have relied on the aglycosylated enzyme produced by heterologous expression in *Escherichia coli*. Detailed investigations of *N*-glycosylated RNase 1 have been hindered by the intrinsic heterogeneity of isolated RNase 1. This heterogeneity arises from both the differential utilization of particular *N*-glycosylation sites (macroheterogeneity) and the variable glycan composition at each site (microheterogeneity). RNase 1 glycoforms have been produced by recombinant DNA technology in Chinese hamster ovary cells[170] and *Saccharomyces cerevisiae*,[56] but such systems suffer from the microheterogeneity and macroheterogeneity of human isolates, as well as the presence of non-human glycans.

Recently, a highly engineered strain of methylotrophic *Pichia pastoris* yeast has emerged as an ideal platform for glycoprotein biosynthesis.[171] The *Pichia* Glycoswitch® System has been altered by a disruption in the gene encoding for a mannosyltransferase as well as the addition of heterologous genes encoding enzymes that append human-like glycans.[67-68] The Superman 5 (M5) strain produces large quantities of protein with a $Man_5GlcNAc_2$ heptasaccharide that is identical to the core *N*-linked glycosylation structure in human proteins, attached to Asn-Xaa-Ser/Thr sequences.

With its three sequons, RNase 1 has seven possible macroscopic glycoforms (Figure 2.1D). Even though replacing an asparagine residue with glutamine is a conservative substitution, Gln-Xaa-Ser/Thr sequences are not substrates for oligosaccharyltransferase.[162-164] Accordingly, the production of a particular glycoform of RNase 1 can be designated by replacing an asparagine codon with a glutamine codon.

Hence, we chose to use the M5 strain of *P. pastoris* and strategic aspargine→glutamine substitutions to generate the glycoforms of RNase 1.

2.3.2: Materials

The M5 strain of *P. pastoris* was from Research Corporation Technologies (Tucson, Arizona). The BL21(DE3) strain of *Escherichia coli* cells was from Novagen (Madison, WI).

A fluorogenic substrate, 6-FAM–dArU$(dA)_2$–6-TAMRA and DNA oligonucleotides were from Integrated DNA Technologies (Coralville, IA). Poly(cytidylic acid) was from Sigma–Aldrich (St. Louis, MO). A 50,000× solution of SYPRO Orange Protein Gel Stain was from Life Technologies (Grand Island, NY). All other chemicals and reagents were of commercial reagent grade or better, and were used without further purification.

Aqueous solutions were made with water that was generated with an arium Pro water purification system from Sartorius (Bohemia, NY) and had resistivity ≥18 $M\Omega \cdot cm^{-1}$. Phosphate-buffered saline (PBS) was 10 mM Na_2HPO_4 and 1.8 mM KH_2PO_4 buffer, pH 7.4, containing NaCl (137 mM) and KCl (2.7 mM). Buffered glycerol-complex medium (BMGY) was 100 potassium phosphate buffer, pH 5.0, containing peptone (2% w/v), yeast extract (1% w/v), yeast nitrogen base without amino acids (1.34% w/v), glycerol (1% w/v), and biotin (0.4 μg/mL). Buffered methanol-complex medium (BMMY) was 100 mM potassium phosphate buffer, pH 5.0, containing peptone (2% w/v), yeast extract (1% w/v), dextrose (2% w/v), yeast nitrogen base without amino acids (1.34% w/v), methanol (1% v/v), and biotin (0.4 μg/mL). BMGY and BMMY were sterilized by autoclaving prior to use. Yeast extract peptone–dextrose solution (YPD) was 100 mM potassium phosphate buffer, pH 5.0, containing peptone (2% w/v), yeast extract (1% w/v), dextrose (2% w/v), and agar (2% w/v). The solution was sterilized by autoclaving, poured into 60 mm × 15 mm plates, and allowed to cool to room temperature. Dialysis was performed with 3.5-kDa MWCO tubing from Spectrum Labs (Rancho Dominguez, CA). A Spectra Multicolor Broad Range Protein Ladder from Thermo Fisher Scientific (Waltham, MA) was used a molecular weight standard for SDS–PAGE.

2.3.3: Instrumentation

Chromatography was conducted using an ÄKTA Pure system from GE Healthcare Life Sciences (Piscataway, NJ) and the results were analyzed with the UNICORN Control System. HiTrap SP HP, HiTrap SP Sepharose FF, HiTrap ConA 4B, and HiLoad® 26/600 Superdex® 75 pg columns for protein purification were from GE Healthcare Life Sciences.

Protein concentrations were determined with a NanoVue Plus spectrophotometer from GE Healthcare Life Sciences by absorbance at 280 nm using Beer's law, $\varepsilon = 0.53$ mL·mg^{-1}·cm^{-1}, and the molecular weight of the unglycosylated protein.

Differential scanning fluorimetry (DSF), which requires thermal denaturation and the simultaneous monitoring of fluorescence, was performed with a ViiA 7 Real-Time PCR system from Applied Biosystems (Foster City, CA). Denaturation data were obtained with ViiA 7 version 2.0 software and analyzed further by Protein Thermal Shift version 1.4 software, both from Applied Biosystems.

The intact molecular mass of RNase 1 glycoforms was determined by MALDI–TOF mass spectrometry using a microflex LRF instrument from Bruker (Billerica, MA) and by ESI mass spectrometry using a 6530 Accurate-Mass Q-TOF LC/MS from Agilent (Santa Clara, CA).

2.3.4: Conditions

All procedures were performed in air at ambient temperature (~22 °C) and pressure (1.0 atm) unless indicated otherwise.

2.3.5: Plasmid preparation for expression in P. pastoris

A cDNA that encodes N34Q/N76Q/N88Q RNase 1 (QQQ) was synthesized from synthetic DNA oligonucleotides by Gibson assembly[172] using the kit from New England Biolabs (Ipswich, MA) (Figure 2.S1). The synthetic gene was inserted into the pPICZ expression vector, which has a neomycin phosphotransferase (NeoR)/G418 resistance gene and was from Thermo Fisher Scientific. The vector encodes DNA for an RNase 1 glycoform fused to the α-mating factor signal sequence with expression under the control of a strong methanol-inducible promoter.

cDNAs coding RNase 1 glycoforms were made by site-directed mutagenesis of the QQQ pPICZα plasmid using synthetic oligonucleotides (Figure 2.S2) and the Phusion site-Directed Mutagenesis Kit from Thermo Fisher Scientific. After target-plasmid amplification, the parent template plasmid was degraded by digestion with 1 unit of *Dpn*I restriction endonuclease from New England Biolabs, which was added to the PCR reaction mixture. The resulting nuclease-resistant target plasmid was transfected into *E. coli*. Plasmids were isolated from the resulting colonies, and the sequence of the cDNA that encodes RNase 1 was assessed for the desired modification.

2.3.5: Transformation and selection of RNase 1 glycoform expression plasmids

In preparation for transformation into *P. pastoris*, plasmids were linearized by digestion with 1 unit of *Pme*I restriction endonuclease from New England Biolabs at 37 °C overnight. The aqueous DNA solution was washed with 1 volume of 25:24:1 phenol/chloroform/isoamyl alcohol that was saturated with 10 mM Tris–HCl buffer, pH 8.0. The aqueous (*i.e.*, upper) layer containing the linearized DNA was transferred to a new tube, and $1/10^{th}$ volume of 3 M sodium acetate, pH 5.0, was added. A twofold excess of isopropanol was added, and the resulting solution was then subjected to centrifugation at 14,000*g* at 4 °C for 1 h to pellet the DNA. After spinning, the supernatant was removed by careful decantation, and the DNA pellet was resuspended in ethanol (70% v/v) to remove excess salts. The solution was subjected to centrifugation at 14,000*g* at 4 °C for 1 h, and the supernatant was removed by careful decantation. Excess ethanol was evaporated by allowing the DNA pellet to sit at room temperature for 10 min. The pure linearized DNA was resuspended in water.

P. pastoris strain M5 was transformed by the addition of linearized DNA (1 μg) to an aliquot of electrocompetent *P. pastoris* cells, followed by incubation on ice for 5 min. After transfer to an ice-cold 2-mm electroporation cuvette, cells were pulsed at 1.5 kV with an electroporator from Bio-Rad Laboratories (Hercules, CA). Cells were resuspended immediately in an ice-cold 1-mL solution of sorbitol (1.0 M) and allowed to recover for 2 h at 30 °C without shaking. After recovery, 200 μL of resuspended cells were spread on YPD-agar plates containing G418 (0.50 mg/mL) from Thermo Fisher Scientific and incubated at 30 °C for 2 days. To test for the ability of transformed cells to secrete RNase 1 into the culture medium, colonies were used to inoculate 10 mL of BMGY. The resulting culture was allowed to grow for 48 h, and then subjected to centrifugation. The resulting pellet was suspended in 5 mL of BMMY. Aliquots of methanol (each 1% v/v) were added to the culture at intervals of 12 h during an incubation period of 60 h. The supernatants were collected and the level of ribonucleolytic activity was assessed by a zymogram assay as described below.

2.3.3: Production and purification of RNase 1 glycoforms in P. pastoris

Colonies producing a high level of ribonucleolytic activity were used to inoculate 10 mL of BMGY. After shaking at 250 rpm for 48 h at 30 °C, the starter culture was used to inoculate 200 mL of BMGY in a 2-L baffled shaker flask. After growth for another 48 h at 30 °C, the large-scale cultures were subjected to centrifugation at 5,000 rpm for 10 min. The cell pellet was resuspended in 100 mL of BMMY containing EDTA (0.5 mM) and allowed to grow for 60 h at 30 °C, with aliquots of methanol (each 1% v/v) added every 12 h to induce gene expression. The culture was subjected to centrifugation at 5,000 rpm for 10 min. The supernatant was concentrated and exchanged into 50 mM sodium acetate buffer, pH 5.0, using a Vivaflow 200

tangential flow concentrator from Sartorius (Bohemia, NY). After a further five-fold dilution in 50 mM sodium acetate buffer, pH 5.0, the sample was applied to a HiTrap SP Sepharose FF cation-exchange column and eluted with a linear gradient of NaCl (0–1.0 M). The eluted fractions were pooled and dialyzed overnight against 5 L of 20 mM Tris–HCl buffer, pH 7.4. containing NaCl (0.50 M), $MnCl_2$ (1 mM), and $CaCl_2$ (1 mM). RNase 1 glycoforms were purified from the retentate by lectin-affinity chromatography using a HiTrap ConA 4B column, which was eluted with a solution of methyl α-D-mannopyranoside (0.50 M). RNase 1 glycoforms were purified further by cation-exchange chromatography using a HiTrap SP HP column before being dialyzed against PBS.

2.3.4: Plasmid preparation for expression in E. coli

A cDNA that encodes Met(–1) RNase 1 in a pET22b(+) expression vector[173] was used to generate wild-type RNase 1 (NNN) in *E. coli* (Figure 2.S1). A synthetic cDNA that encodes the N34Q/N76Q/N88Q RNase 1 (QQQ) variant flanked by regions of homology near the T7 promoter and terminator found in the pET22b vector was obtained from Integrated DNA Technologies (Figure 2.S1). Linear pET22b was prepared by PCR using primers that complement the DNA that encodes RNase 1 (5′-AAGCCCGAAAGGAAGCTGAGTTGGCTGCTG-3′ and 3′-AAACAAATTGAAATTCTTCCTCTATATGTA-5′). Gene and plasmid fragments were combined with Gibson assembly[172] for expression in *E. coli.*

2.3.5: Production and Purification of RNase 1 from E. coli

The N34Q/N76Q/N88Q variant and wild-type RNase 1 were purified from inclusion bodies as described previously.[174] Briefly, induced cells were lysed at 19.0 kpsi with a benchtop cell disruptor from Constant Systems (Kennesaw, GA). After centrifugation at 10,500 rpm for 45 min, the resulting pellet was suspended in 20 mM Tris–HCl buffer, pH 8.0, containing guanidine–HCl (7 M), EDTA (10 mM), and DTT (0.10 M). This solution was diluted 10-fold by the slow addition of degassed 20 mM acetic acid, then subjected to centrifugation at 10,500 rpm for 45 min. The supernatant was then dialyzed overnight against 16 L of 20 mM acetic acid. After centrifugation at 10,500 rpm for 40 min, the supernatant was added dropwise to folding solution (which was 100 mM Tris–HCl buffer, pH 7.8, containing 100 mM NaCl, 1.0 mM reduced glutathione, and 0.2 mM oxidized glutathione) and allowed to fold for 5 days at 4 °C. The pH of the solution was adjusted to 5.0, and the solution was then concentrated to 10 mL by using an Amicon® Stirred Cell concentrator from EMD Millipore (Billerica, Massachusetts) with Hydrostart® 10-kDa filters from Sartorius. Protein in the resulting solution was purified by gel-filtration chromatography using a HiLoad® 26/600 Superdex® 75 pg column and elution with 50 mM sodium acetate buffer, pH 5.0, containing NaCl (0.10 M) and sodium azide (0.05% w/v). The protein was purified further by cation-exchange chromatography using a HiTrap SP HP column before being dialyzed against PBS.

2.3.6: Zymogram analysis of RNase 1 glycoforms

To verify the production of secreted, properly folded ribonucleases, zymogram assays were performed on conditioned medium using an assay similar to one reported previously.[167] Briefly, a polyacrylamide gel containing SDS (0.1 % w/v), Tris (375 mM), and poly(cytidylic acid) (5.5

mg, incubated at 50 °C prior to addition) was cast. Aliquots of *P. pastoris* cultures were prepared with 2× Laemmli sample buffer, which was 68.5 mM Tris–HCl buffer, pH 6.7, containing glycerol (26.3% w/v), SDS (2.1% w/v), and bromophenol blue (0.01% w/v). After electrophoresis, the gel was washed twice in 10 mM Tris–HCl buffer, pH 7.5, containing isopropanol (20% v/v), and once with 10 mM Tris–HCl buffer, pH 7.5. Then, the gel was incubated overnight in 100 mM Tris–HCl buffer, pH 7.5, to allow the RNase 1 glycoform to refold within the gel. The following day, the gel was washed with 10 mM Tris–HCl buffer, pH 7.5, before staining with an aqueous solution of toluidine blue (0.2% w/v) for 10 min. The gel was rinsed with deionized water and destained in 10 mM Tris–HCl buffer, pH 7.5.

2.3.7: Treatment with peptide-N-glycosidase F

To assess *N*-linked glycosylation, RNase 1 glycoforms were denatured by boiling for 10 min in an aqueous solution of SDS (0.5% w/v) and dithiothreitol (40 mM). The denatured proteins were incubated with peptide-*N*-glycosidase F (PNGase F) (5 U/mL) for 24 h at 37 °C in 0.05 M sodium phosphate buffer, pH 7.4, containing NP-40 (1% v/v), SDS (0.25% w/v), and dithiothreitol (20 mM). Products were analyzed by SDS–PAGE.

2.3.8: Assays of protein phosphorylation

To confirm phosphorylation of proteins expressed from *P. pastoris*, RNase 1 glycoforms were denatured and subjected to SDS–PAGE. The gel was fixed, washed, and stained following the protocol for Pro–Q™ Diamond Phosphoprotein Gel Stain from Thermo Fisher Scientific. Protein bands were observed by excitation at 520 nm and emission at 605 nm on an Amersham Imager

600 from GE Healthcare. The gel was then incubated in Coomassie stain for total protein content.

2.3.9: Assays of single-stranded ribonucleolytic activity

The catalytic activity of each RNase 1 glycoform was determined by measuring the initial velocity of cleavage of a single-stranded RNA substrate in a 96-well plate (Corning) at 25 °C. A solution of 6-FAM–dArU$(dA)_2$–6-TAMRA (0.2 μM) in 0.10 M Tris–HCl buffer, pH 7.5, containing NaCl (0.10 M) was added to each well. After baseline fluorescent readings were recorded, an RNase 1 glycoform was added (final concentration: 50 pM), and the initial velocity of substrate turnover was measured by the increase in fluorescence over time. After 8 min, substrate cleavage was saturated by the addition of RNase A to 5 μM. Values of k_{cat}/K_M were determined as described previously,[175] and represent the mean of at least three independent experiments.

2.3.10: Analysis of double-stranded RNA degradation

Double-stranded RNA degradation was evaluated with a previously designed, stable fluorescent hairpin substrate with the sequence: 5,6-FAM–CGATC(rU)ACTGCAACGGCAGTAGATCG (IDT).[173] This substrate contained a single RNA nucleotide near the fluorescently labeled 5' end. An aqueous solution of the substrate was annealed by heating to 95 °C for 3 min, then slowly cooled to room temperature. A solution of substrate (50 nM) was added to an aqueous solution of RNase 1 (1 μM), and the resulting mixture was incubated at room temperature for 1 min. The reaction was quenched by the addition of 40 units of rRNasin from Promega (Madison, WI), then the products were subjected to electrophoresis on a 20% w/v native acrylamide gel at 10 mAmp.

Formation of the cleavage product was monitored by excitation of FAM at 460 nm and emission at 525 nm on an Amersham Imager 600 from GE Healthcare. The gel was then incubated in SYBR Gold from Invitrogen and imaged for total nucleic acid content.

2.3.11: Assays of conformational stability

The conformational stability of each RNase 1 glycoform was assessed by DSF as described previously.[39] Briefly, an RNase 1 glycoform was dissolved in PBS to a final concentration of 2 μg/μL. SYPRO Orange (which was supplied at a concentration of 10000×) was added to a concentration of 50×. The assay solution was heated from 10 to 95 °C at a rate of 0.2 °C/min. As the solutions were heated, the resulting fluorescence emission was monitored at (623 ± 14) nm after excitation at (580 ± 10) nm. Data were summarized by the value of T_m, which is the temperature at the midpoint of the thermal transition between native and denatured states.

2.3.12: Assays of proteolytic stability

An RNase 1 glycoform (1 mg/mL) was incubated with sequencing-grade modified trypsin (10, 1, or 0.1 μg/mL) in 50 mM Tris–HCl buffer, pH 8.0, containing $CaCl_2$ (1 mM) at 37 °C for 1 h. To terminate the reaction, phenylmethylsulfonyl fluoride (PMSF) was added at a final concentration of 1 mM. The reaction products were analyzed by SDS–PAGE.

2.4 Results

2.4.1 Production, purification, and analysis of RNase 1 glycoforms

The three glycosylation sites within RNase 1 give rise to eight potential macroscopic glycoforms, specifically, one triglycosylated, three diglycosylated, three monoglycosylated, and one aglycosylated variant. We produced each macroscopic glycoform of RNase 1 by strategically

installing Gln-Xaa-Ser/Thr sequences, which do not serve as substrates for oligosaccharyltransferase (Figure 2.S3). Soluble RNase 1 glycoforms were produced by the *P. pastoris* cells and secreted into the medium at ~3 mg per liter of culture.

We employed tangential-flow concentration, ion-exchange chromatography, and lectin-affinity chromatography to isolate each RNase 1 glycoform from the protein-rich culture medium. Purified RNase 1 glycoforms displayed a higher molecular mass than did aglycosylated controls, with shifts in electrophoretic mobility corresponding to the additional number of $Man_5GlcNAc_2$ glycans (Figure 2.3). Treatment of purified RNase 1 glycoforms with PNGase F, an amidase that hydrolyzes the bond between a GlcNAc residue and asparagine side chain, resulted in a single species that migrated similar to aglycosylated RNase 1, consistent with *N*-linked glycan attachment to the RNase 1 core (Figure 2.3).

The molecular mass of each purified RNase 1 glycoform was assessed by both MALDI–TOF and ESI mass spectrometry. The MALDI–TOF spectra indicated the presence of additional mass in the mono-, di-, and triglycosylated RNase 1, but was unable to resolve individual species (Figure 2.S5). The ESI spectra indicated the appendage of the expected number of $Man_5GlcNAc_2$ units in each glycoform (Table 2.1, Figure 2.S6). Some additional mannose units (*i.e.*, microheterogeneity) were apparent in the RNase 1 glycoforms produced by the *P. pastoris* system, as is observed in bovine RNase B.[176]

High resolution analysis of the proteins from the *P. pastoris* system also revealed additional peaks at ~80 Da and ~160 Da above the expected base peak for each sample. The presence of these additional peaks, including with the aglycosylated control (QQQ), indicated further modification of the protein core as a result of expression and secretion by *P. pastoris*. We subsequently analyzed proteins from each expression system with a phosphoprotein-specific

stain and confirmed the phosphorylation of proteins expressed with the yeast system (Figure 2.S7). This additional modification did not have an observable impact on other RNase 1 biochemical attributes. Protein phosphorylation, carried out by various kinases, represents another common modification in eukaryotic systems with a variety of roles in signaling pathways and protein–protein interactions.[177] Secretory pathway-associated kinases have recently garnered attention for their role in phosphorylating extracellular proteins in higher eukaryotes and might be at work in yeast-based systems.[178]

2.4.2 Ribonucleolytic activity of RNase 1 glycoforms

Human RNase 1 catalyzes the cleavage of the P–O5′ bond on the 3′ side of pyrimidine ribonucleotides. The principal catalytic residues, His12, Lys41, and His119 (Figure 2.1A), are conserved in RNase 1 homologs, suggestive of a similar enzymatic reaction mechanism.[159] We assessed whether N-glycosylation impacts the ribonucleolytic activity of human RNase 1. We determined the ribonucleolytic activity of each RNase 1 glycoform with a fluorogenic substrate.[175] A similar level of catalytic activity was observed for all aglycosylated variants, regardless of the expression system used in their production (Table 2.1, Figure 2.4A). Apparently, neither three extra methylene groups (QQQ versus NNN) nor an N-terminal methionine residue (NNN from E. coli) have a measurable effect on enzymatic catalysis by RNase 1. In contrast, all RNase 1 glycoforms exhibited lower ribonucleolytic activity. The monoglycosylated NQQ variant maintained the highest activity of all of the glycoforms.

Previous work has demonstrated that human RNase 1 can readily degrade both ssRNA substrates and dsRNA substrates. We examined the ability of RNase 1 glycoforms to degrade dsRNA using a previously designed hairpin-based substrate containing a single ribonucleotide

embedded within a series of DNA bases and labeled with a fluorophore on the 5' end.[173] We observed the formation of the fluorescent cleavage product in the presence of each human RNase 1 glycoform (Figure 2.S8).

2.4.3 Thermostabilty of RNase 1 glycoforms

N-Glycosylation has been reported to enhance the thermostability of proteins, including other ptRNases.[179-180] We assessed the thermostability of each RNase 1 glycoform using DSF. We found that the Tm values of all aglycosylated variants, regardless of the expression system used in their production, were ~56 °C and indistinguishable (Table 2.1, Figure 2.4B). As with enzymatic catalysis, neither three extra methylene groups (QQQ versus NNN) nor an N-terminal methionine residue (NNN from E. coli) have a measurable effect on the thermostability of RNase 1. In contrast, the addition of a single glycan at any position in RNase 1 increased its thermostability. The most thermostable of the monoglycosylated proteins had N-glycosylation at Asn34 (NQQ) and increased the Tm value by >2 °C to (58.6 ± 0.3) °C. N-Glycosylation at any two sequons resulted in minimal change in thermostability from the corresponding monoglycosylated species. Preventing N-glycosylation at Asn34 (QNN) generated the least stable diglycosylated protein—one having a Tm value (57.3 ± 0.1) °C , which is between the values for the related QNQ and QQN glycoforms. The triglycosylated RNase 1 had the highest thermostability with a Tm value of (59.4 ± 0.3) °C.

2.4.4 Proteolytic stability of RNase 1 glycoforms to trypsin

The proteolytic susceptibility of each RNase 1 glycoform was assessed by analysis with SDS–PAGE (Figure 2.S1) following treatment with trypsin. The aglycosylated forms of RNase 1 were

especially susceptible to trypsin and were largely degraded even at low concentrations of trypsin. Digestion products were observed as lower molecular weight bands even in the presence of trypsin at only 1 μg/mL. Nonetheless, any glycosylation produced an increase in resistance to digestion by trypsin, even at high concentrations of protease. Digestion products were not observed when glycosylated proteins were treated with 1 μg/mL trypsin.

2.5 Discussion

2.5.1 Glycosylation attenuates catalysis by RNase 1

Glycosylation can either enhance or diminish the catalytic activity of an enzyme.[181] Catalysis by RNase 1 relies on the favorable Coulombic interaction between cationic enzymic residues and the anionic phosphoryl groups of an RNA substrate.[182-184] During their purification by cation-exchange chromatography, the glycosylated forms of RNase 1 eluted more readily than did aglycosylated RNase 1, indicating that the pendant heptasaccharide diminishes affinity for an anionic resin. Similarly, *N*-glycosylation appears to reduce affinity for the rate-limiting transition state during catalysis of RNA cleavage, leading to a lower k_{cat}/K_M value (Table 2.1, Figure 2.4A).[180]

Although monoglycosylation diminished the ability of RNase 1 to catalyze the cleavage of RNA (Table 2.1, Figure 2.4A), the impact was not equivalent across the three *N*-glycosylation sites. The least active monoglycoform, with glycosylation only at Asn88 (QQN), retained only ~20% of the activity of the aglycosylated controls. Residue 88 is proximal to the cationic RNA-binding site of RNase 1 (Figure 2.1B). A glycan at appended to Asn88 could hinder access of an RNA substrate to the active site. Glycosylation of Asn76 (QNQ) yielded an enzyme with ~40% of the activity of the aglycosylated protein. Residue 76 is distal from the enzymic active site and the basis for its effect on catalysis is not clear.

In contrast to positions 76 and 88, *N*-glycosylation at position 34 (NQQ) enabled RNase 1 to maintain ~80% of its ribonucleolytic activity. Residue 34 is distal from the active site (Figures 2.1A and 2.1B). Moreover, the orientation of the side chain of Asn34 might allow for appendage of a larger glycan without hindering access of an RNA substrate to the active site. This orientation is consistent with the results of analyses of bovine RNase B, which also has a glycan attached to Asn34.[185]

N-Glycosylation of RNase 1 at multiple sites likewise attenuated catalytic activity. The di- and triglycosylated proteins maintained ~30% and ~10% of control activity, respectively. The addition of multiple glycans could distort the enzymic active site as the large glycans conform to minimize steric interactions with one another. Again, though, Asn34 is the most tolerable position for the installation of a glycan.

2.5.2 Glycosylation increases thermostability

Human RNase 1 has a compact structure with thermostability (T_m ~56 °C) deriving largely from four disulfide bonds that crosslink the protein.[186] Previous studies have demonstrated that *N*-glycosylation improves conformational stability of an amphibian homolog of RNase 1.[180] We find that every permutation of RNase 1 *N*-glycosylation enhances its thermostability (Table 2.1, Figure 2.4B).

The three monoglycoforms of RNase 1 exhibited T_m values between 57 °C and 59 °C. *N*-Glycosylation at Asn34 yields the most significant increase in conformational stability. Its ΔT_m value of slightly more than 2 °C is in accord with previous analyses of RNase B. In that homologous context, *N*-glycosylation of Asn34 site resulted in a ΔT_m value of 1.5 °C.[187] In RNase B, residues near Asn34 are known to be less dynamic than in RNase A.[185]

In terms of thermostability, diglycosylated and triglycosylated RNase 1 followed suit. We found that maintaining glycosylation at Asn34 generated the most stable diglycoforms, NNQ with T_m = (59.1 ± 0.2) °C and NQN with T_m = (58.7 ± 0.2) °C. When *N*-glycosylation at Asn34 was deterred, as in the QNN variant, the value of T_m was only (57.3 ± 0.1) °C. *N*-Glycosylation of all three sites increased the thermostability by ~3 °C, giving a T_m value of (59.4 ± 0.3) °C. These data reveal a gain in stability with multiple *N*-glycosylation that was previously unappreciated within ptRNases.

2.5.3 Glycosylation of RNase 1 enhances proteolytic stability

Previous work has demonstrated that the glycosylation of RNase A[187-189] and other proteins[190-192] diminishes their susceptibility to degradation by proteases. We likewise found that all glycoforms of RNase 1 are resistant to proteolysis compared to the aglycosylated protein (Figure 2.5). Each pendant $Man_5GlcNAc_2$ heptasaccharide has a mass (1.2 kDa) that is nearly 10% that of RNase 1 (14.6 kDa), and is likely to be diffuse and mobile in its conformation. These glycans could shield the main chain from proteases.

2.5.4 Glycosylation in human homologs of RNase 1

N-Glycosylation sequons exist in a majority of human ptRNases (Figure 2.S6). Interestingly, the potential for extensive glycosylation is greatest in two homologs, RNase 2 (EDN) and RNase 3 (ECP), that play crucial roles in host defense through antiviral and antimicrobial actions, respectively.[153-154] Amongst human ptRNases, however, the glycosylation sequons at Asn34, Asn76, and Asn88 are unique features of RNase 1.

2.6 Conclusions

The *N*-glycosylation sequons of RNase 1 have been widely conserved across vertebrates, indicative of biochemical significance. We have reported on the first production and characterization of human RNase 1 glycoforms with all possible permutations of endogenous *N*-glycosylation. We find that the *N*-glycosylation of human RNase 1 improves its resistance to both thermal denaturation and proteolytic degradation but reduces its catalytic activity. Among the observed *N*-glycosylation sites, Asn34 has been conserved most widely across diverse groups of mammals and has displayed the highest level of glycan occupancy in a majority of biological samples. In accord, we find that only the *N*-glycosylation of Asn34 in human RNase 1 significantly improves overall protein stability while maintaining robust catalytic activity.

Table 2.1. Attributes of RNase 1 Glycoforms

Source	RNase 1[a]	Glycans	*m/z* (Da) expected	*m/z* (Da) observed	T_m (°C)[b]	k_{cat}/K_M[c] $10^6\ M^{-1}s^{-1}$	k_{cat}/K_M[c] %
E. coli	NNN	0	14705.52[d]	14698.35	55.9 ± 0.2	1.9 ± 0.2	100
E. coli	QQQ	0	14747.60[d]	14740.03	56.6 ± 0.3	1.9 ± 0.1	100
P. pastoris	QQQ	0	14616.41	14608.88	56.4 ± 0.1	1.9 ± 0.1	100
P. pastoris	NQQ	1	15818.38	15811.70	58.6 ± 0.3	1.5 ± 0.1	79
P. pastoris	QNQ	1	15818.38	15811.91	56.8 ± 0.1	0.74 ± 0.07	39
P. pastoris	QQN	1	15818.38	15811.85	57.2 ± 0.2	0.30 ± 0.04	16
P. pastoris	NNQ	2	17020.36	17015.05	59.1 ± 0.2	0.72 ± 0.04	38
P. pastoris	NQN	2	17020.36	17015.15	58.7 ± 0.2	0.63 ± 0.03	33
P. pastoris	QNN	2	17020.36	17015.23	57.3 ± 0.1	0.21 ± 0.03	11
P. pastoris	NNN	3	18222.33	18218.39	59.4 ± 0.3	0.19 ± 0.09	10

[a]Residues at positions 34, 76, and 88 (Figure 2.1D).
[b]Values were determined by DSF at pH 7.4.
[c]Values were determined by fluorescence spectroscopy for the cleavage of 6-FAM–dArUdAdA–6-TAMRA at pH 7.5.
[d]The proteins produced in *E. coli* have an N-terminal methionine residue.

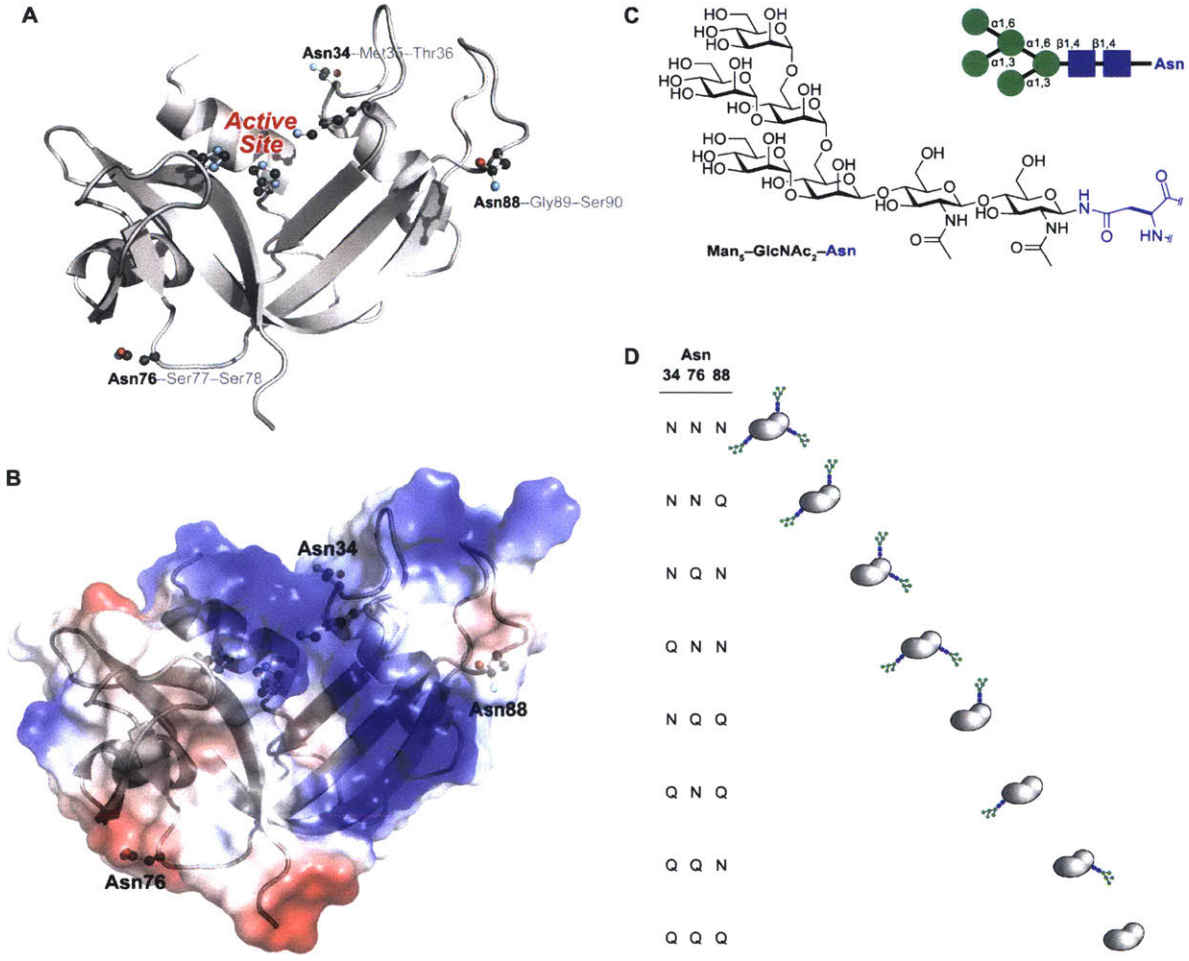
A
Asn34–Met35–Thr36
Active Site
Asn88–Gly89–Ser90
Asn76–Ser77–Ser78
B
Asn34
Asn88
Asn76
C
α1,6
α1,6 β1,4 β1,4
α1,3
α1,3
Asn
Man5–GlcNAc2–Asn
D
Asn
34 76 88
N N N
N N Q
N Q N
Q N N
N Q Q
Q N Q
Q Q N
Q Q Q

Figure 2.1. Three-dimensional structure of human RNase 1. (A) The side chains of the asparagine residues within *N*-glycosylation sequons (Asn34, Asn76, and Asn88) and the active-site residues (His12, Lys41, and His119) are shown explicitly. The image was created with Protein Data Bank entry 1z7x, chain Z[193] and the program PyMOL from Schrödinger (New York, NY). (B) Electrostatic potential map of the surface of human RNase 1. The image was created as in Figure 2.1A. (C) Structure of the core heptasaccharide, $Man_5GlcNAc_2$, that is appended to asparagine residues. (D) Macroscopic glycoforms of human RNase 1 generated by strategic asparagine→glutamine substitution. The three-letter shorthand is used to name each variant.

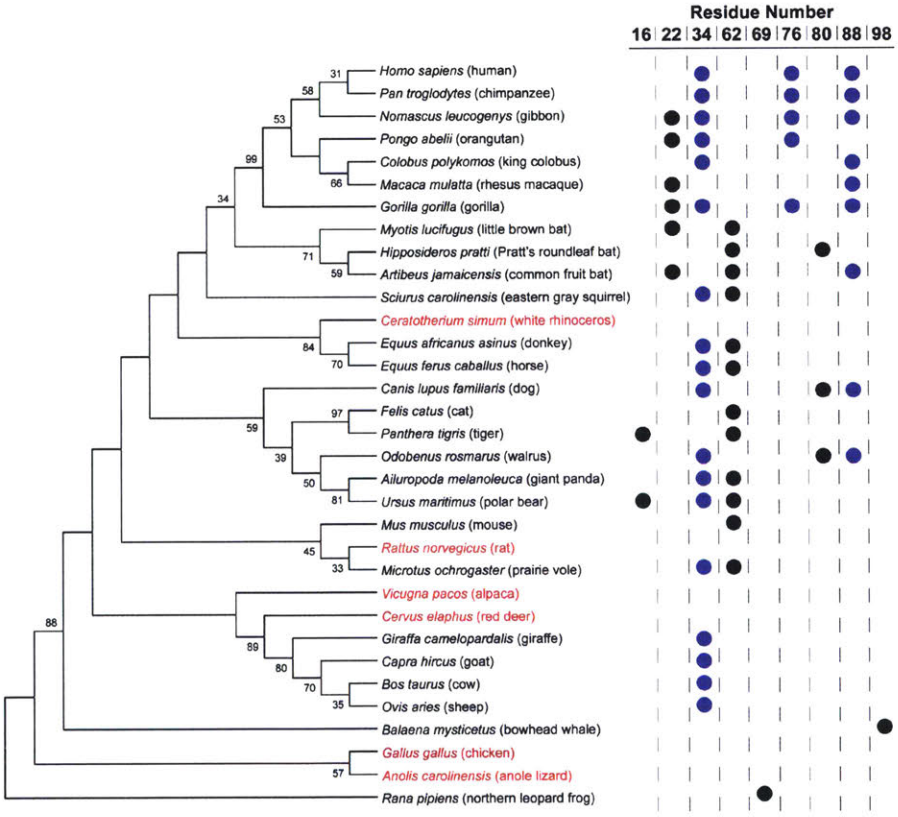
Residue Number
16 22 34 62 69 76 80 88 98
Homo sapiens (human)
Pan troglodytes (chimpanzee)
Nomascus leucogenys (gibbon)
Pongo abelii (orangutan)
Colobus polykomos (king colobus)
Macaca mulatta (rhesus macaque)
Gorilla gorilla (gorilla)
Myotis lucifugus (little brown bat)
Hipposideros pratti (Pratt's roundleaf bat)
Artibeus jamaicensis (common fruit bat)
Sciurus carolinensis (eastern gray squirrel)
Ceratotherium simum (white rhinoceros)
Equus africanus asinus (donkey)
Equus ferus caballus (horse)
Canis lupus familiaris (dog)
Felis catus (cat)
Panthera tigris (tiger)
Odobenus rosmarus (walrus)
Ailuropoda melanoleuca (giant panda)
Ursus maritimus (polar bear)
Mus musculus (mouse)
Rattus norvegicus (rat)
Microtus ochrogaster (prairie vole)
Vicugna pacos (alpaca)
Cervus elaphus (red deer)
Giraffa camelopardalis (giraffe)
Capra hircus (goat)
Bos taurus (cow)
Ovis aries (sheep)
Balaena mysticetus (bowhead whale)
Gallus gallus (chicken)
Anolis carolinensis (anole lizard)
Rana pipiens (northern leopard frog)

Figure 2.2. Putative *N*-glycosylation sites in RNase 1 homologs across an evolutionary spectrum. Circles indicate an asparagine residue within an *N*-glycosylation sequon. The neighbor-joining phylogenetic tree is adapted from ref. [39] and shows bootstrap values >30. Species highlighted in red lack glycosylation sites. The *Bos taurus* (cow) entry is for RNase A; bovine brain ribonuclease has a sequon at residue 62 but not residue 34.[173]

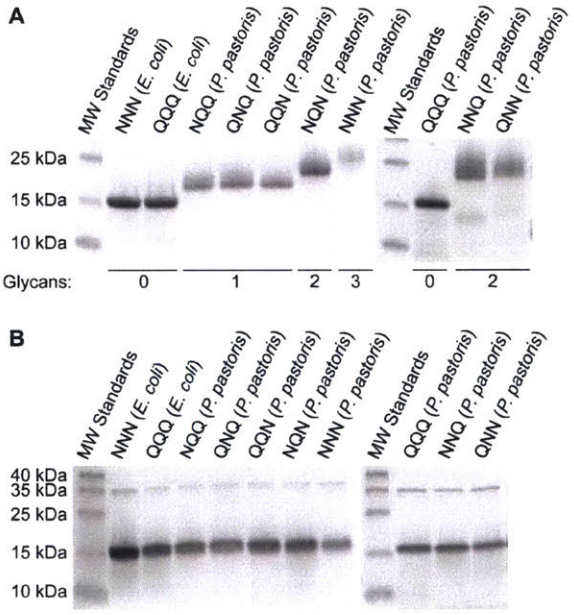
A
MW Standards
NNN (E. coli)
QQQ (E. coli)
NQQ (P. pastoris)
QNQ (P. pastoris)
QQN (P. pastoris)
NQN (P. pastoris)
NNN (P. pastoris)
MW Standards
QQQ (P. pastoris)
NNQ (P. pastoris)
QNN (P. pastoris)
25 kDa
15 kDa
10 kDa
Glycans:
0
1
2
3
0
2
B
MW Standards
NNN (E. coli)
QQQ (E. coli)
NQQ (P. pastoris)
QNQ (P. pastoris)
QQN (P. pastoris)
NQN (P. pastoris)
NNN (P. pastoris)
MW Standards
QQQ (P. pastoris)
NNQ (P. pastoris)
QNN (P. pastoris)
40 kDa
35 kDa
25 kDa
15 kDa
10 kDa

Figure 2.3. SDS–PAGE gels showing purified RNase 1 glycoforms. The enzymes were subjected to electrophoresis in a 15% w/v gel and visualized by staining with Coomassie blue. (A) Purified proteins. (B) Purified proteins after treatment with PNGase F (35.5 kDa).

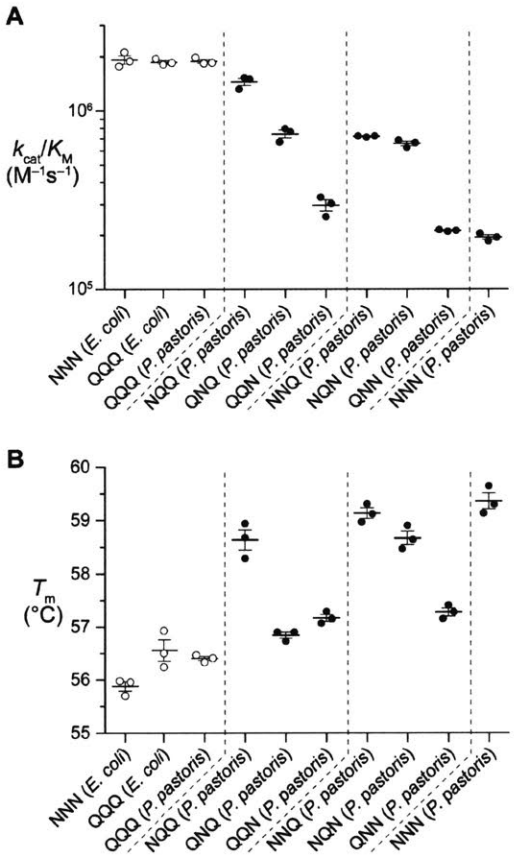
A
k_{cat}/K_M ($M^{-1}s^{-1}$)
10^6
10^5
NNN (E. coli)
QQQ (E. coli)
QQQ (P. pastoris)
NQQ (P. pastoris)
QNQ (P. pastoris)
QQN (P. pastoris)
NNQ (P. pastoris)
NQN (P. pastoris)
QNN (P. pastoris)
NNN (P. pastoris)
B
T_m (°C)
60
59
58
57
56
55
NNN (E. coli)
QQQ (E. coli)
QQQ (P. pastoris)
NQQ (P. pastoris)
QNQ (P. pastoris)
QQN (P. pastoris)
NNQ (P. pastoris)
NQN (P. pastoris)
QNN (P. pastoris)
NNN (P. pastoris)

Figure 2.4. (A) Ribonucleolytic activity of RNase 1 and its glycoforms. Values of k_{cat}/K_M were determined for the cleavage of 6-FAM–dArU$(dA)_2$–6-TAMRA at pH 7.5 and 25 °C. Each data point represents an individual measurement. (B) Thermostability of RNase 1 and its glycoforms. Values of T_m were determined were determined by using DSF in PBS containing SYPRO Orange (50×). Each data point represents an individual measurement.

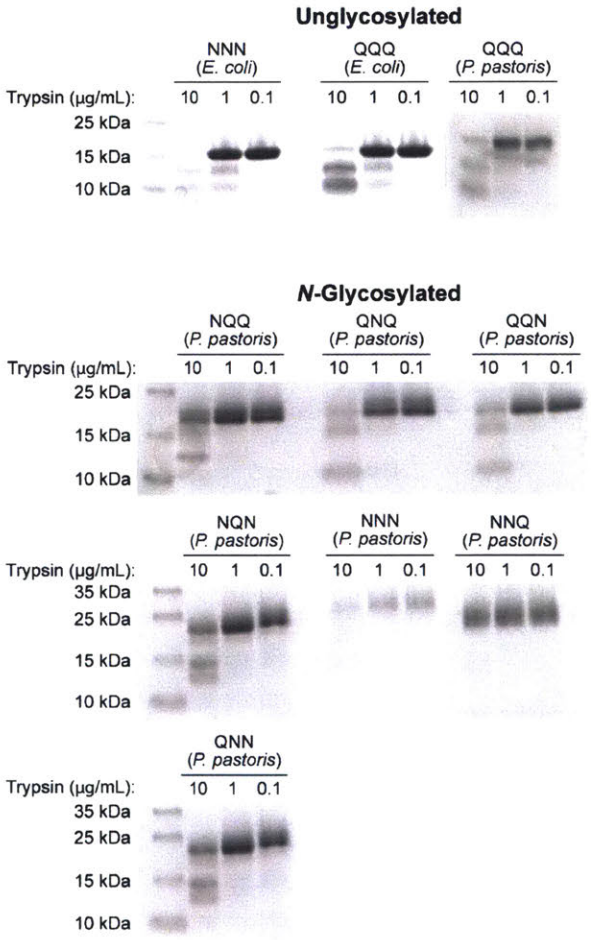
Unglycosylated
NNN (E. coli)
QQQ (E. coli)
QQQ (P. pastoris)
Trypsin (µg/mL):
10 1 0.1
25 kDa
15 kDa
10 kDa
N-Glycosylated
NQQ (P. pastoris)
QNQ (P. pastoris)
QQN (P. pastoris)
NQN (P. pastoris)
NNN (P. pastoris)
NNQ (P. pastoris)
QNN (P. pastoris)
35 kDa

Figure 2.5. SDS–PAGE gels showing the effect of trypsin on RNase 1 glycoforms. An RNase 1 glycoform (1 mg/mL) was incubated with trypsin (0.1, 1, or 10 μg/mL) at 37 °C for 1 h. The trypsin was inactivated with PMSF, and the products were subjected to electrophoresis in a 15% w/v gel and visualized by staining with Coomassie blue.

2.7 Supplementary information

NNN (*P. pastoris*): ATGAGATTTCCTTCAATTTTTACTGCTGTTTTATTCGCAGCATCCTCC
NNQ (*P. pastoris*): ATGAGATTTCCTTCAATTTTTACTGCTGTTTTATTCGCAGCATCCTCC
NQN (*P. pastoris*): ATGAGATTTCCTTCAATTTTTACTGCTGTTTTATTCGCAGCATCCTCC
QNN (*P. pastoris*): ATGAGATTTCCTTCAATTTTTACTGCTGTTTTATTCGCAGCATCCTCC
NQQ (*P. pastoris*): ATGAGATTTCCTTCAATTTTTACTGCTGTTTTATTCGCAGCATCCTCC
QNQ (*P. pastoris*): ATGAGATTTCCTTCAATTTTTACTGCTGTTTTATTCGCAGCATCCTCC
QQN (*P. pastoris*): ATGAGATTTCCTTCAATTTTTACTGCTGTTTTATTCGCAGCATCCTCC
QQQ (*P. pastoris*): ATGAGATTTCCTTCAATTTTTACTGCTGTTTTATTCGCAGCATCCTCC
NNN (*E. coli*):
QQQ (*E. coli*):

NNN (*P. pastoris*): GCATTAGCT**AAG**GAGAGTAGAGCTAAAAAGTTCCAACGTCAACATATG
NNQ (*P. pastoris*): GCATTAGCT**AAG**GAGAGTAGAGCTAAAAAGTTCCAACGTCAACATATG
NQN (*P. pastoris*): GCATTAGCT**AAG**GAGAGTAGAGCTAAAAAGTTCCAACGTCAACATATG
QNN (*P. pastoris*): GCATTAGCT**AAG**GAGAGTAGAGCTAAAAAGTTCCAACGTCAACATATG
NQQ (*P. pastoris*): GCATTAGCT**AAG**GAGAGTAGAGCTAAAAAGTTCCAACGTCAACATATG
QNQ (*P. pastoris*): GCATTAGCT**AAG**GAGAGTAGAGCTAAAAAGTTCCAACGTCAACATATG
QQN (*P. pastoris*): GCATTAGCT**AAG**GAGAGTAGAGCTAAAAAGTTCCAACGTCAACATATG
QQQ (*P. pastoris*): GCATTAGCT**AAG**GAGAGTAGAGCTAAAAAGTTCCAACGTCAACATATG
NNN (*E. coli*): **ATG**AAAGAATCTCGTGCTAAAAAATTCCAGCGTCAGCATATG
QQQ (*E. coli*): **ATG**AAAGAATCTCGTGCTAAAAAATTCCAGCGTCAGCATATG

NNN (*P. pastoris*): GATTCCGACTCCTCTCCATCTTCATCTTCCACATATTGTAATCAAATG
NNQ (*P. pastoris*): GATTCCGACTCCTCTCCATCTTCATCTTCCACATATTGTAATCAAATG
NQN (*P. pastoris*): GATTCCGACTCCTCTCCATCTTCATCTTCCACATATTGTAATCAAATG
QNN (*P. pastoris*): GATTCCGACTCCTCTCCATCTTCATCTTCCACATATTGTAATCAAATG
NQQ (*P. pastoris*): GATTCCGACTCCTCTCCATCTTCATCTTCCACATATTGTAATCAAATG
QNQ (*P. pastoris*): GATTCCGACTCCTCTCCATCTTCATCTTCCACATATTGTAATCAAATG
QQN (*P. pastoris*): GATTCCGACTCCTCTCCATCTTCATCTTCCACATATTGTAATCAAATG
QQQ (*P. pastoris*): GATTCCGACTCCTCTCCATCTTCATCTTCCACATATTGTAATCAAATG
NNN (*E. coli*): GACTCTGACTCTTCTCCGTCTTCTTCTTCTACTTACTGCAACCAGATG
QQQ (*E. coli*): GACTCTGACTCTTCTCCGTCTTCTTCTTCTACTTACTGCAACCAGATG

Aglycosylated Gln codons in red

NNN (*P. pastoris*): ATGAGAAGGAGAAATATGACCCAAGGTCGTTGTAAACCTGTTAATACG
NNQ (*P. pastoris*): ATGAGAAGGAGAAATATGACCCAAGGTCGTTGTAAACCTGTTAATACG
NQN (*P. pastoris*): ATGAGAAGGAGAAATATGACCCAAGGTCGTTGTAAACCTGTTAATACG
QNN (*P. pastoris*): ATGAGAAGGAGA**cag**ATGACCCAAGGTCGTTGTAAACCTGTTAATACG
NQQ (*P. pastoris*): ATGAGAAGGAGAAATATGACCCAAGGTCGTTGTAAACCTGTTAATACG
QNQ (*P. pastoris*): ATGAGAAGGAGA**cag**ATGACCCAAGGTCGTTGTAAACCTGTTAATACG
QQN (*P. pastoris*): ATGAGAAGGAGA**cag**ATGACCCAAGGTCGTTGTAAACCTGTTAATACG
QQQ (*P. pastoris*): ATGAGAAGGAGA**cag**ATGACCCAAGGTCGTTGTAAACCTGTTAATACG
NNN (*E. coli*): ATGCGTCGTCGTAACATGACTCAGGGTCGTTGCAAACCGGTTAACACT
QQQ (*E. coli*): ATGCGTCGTCGT**caa**ATGACTCAGGGTCGTTGCAAACCGGTTAACACT

NNN (*P. pastoris*): TTTGTGCACGAACCATTGGTGGACGTACAGAACGTTTGCTTCCAAGAG
NNQ (*P. pastoris*): TTTGTGCACGAACCATTGGTGGACGTACAGAACGTTTGCTTCCAAGAG
NQN (*P. pastoris*): TTTGTGCACGAACCATTGGTGGACGTACAGAACGTTTGCTTCCAAGAG
QNN (*P. pastoris*): TTTGTGCACGAACCATTGGTGGACGTACAGAACGTTTGCTTCCAAGAG
NQQ (*P. pastoris*): TTTGTGCACGAACCATTGGTGGACGTACAGAACGTTTGCTTCCAAGAG
QNQ (*P. pastoris*): TTTGTGCACGAACCATTGGTGGACGTACAGAACGTTTGCTTCCAAGAG
QQN (*P. pastoris*): TTTGTGCACGAACCATTGGTGGACGTACAGAACGTTTGCTTCCAAGAG
QQQ (*P. pastoris*): TTTGTGCACGAACCATTGGTGGACGTACAGAACGTTTGCTTCCAAGAG
NNN (*E. coli*): TTCGTTCATGAACCGCTGGTTGACGTTCAGAACGTTTGCTTCCAGGAA
QQQ (*E. coli*): TTCGTTCATGAACCGCTGGTTGACGTTCAGAACGTTTGCTTCCAGGAA

NNN (*P. pastoris*): AAAGTCACATGTAAAAATGGACAAGGTAATTGCTACAAGAGTAATTCC
NNQ (*P. pastoris*): AAAGTCACATGTAAAAATGGACAAGGTAATTGCTACAAGAGTAATTCC
NQN (*P. pastoris*): AAAGTCACATGTAAAAATGGACAAGGTAATTGCTACAAGAGTcaaTCC
QNN (*P. pastoris*): AAAGTCACATGTAAAAATGGACAAGGTAATTGCTACAAGAGTAATTCC
NQQ (*P. pastoris*): AAAGTCACATGTAAAAATGGACAAGGTAATTGCTACAAGAGTcaaTCC
QNQ (*P. pastoris*): AAAGTCACATGTAAAAATGGACAAGGTAATTGCTACAAGAGTAATTCC
QQN (*P. pastoris*): AAAGTCACATGTAAAAATGGACAAGGTAATTGCTACAAGAGTcaaTCC
QQQ (*P. pastoris*): AAAGTCACATGTAAAAATGGACAAGGTAATTGCTACAAGAGTcaaTCC
NNN (*E. coli*): AAAGTTACTTGCAAAAACGGTCAGGGTAACTGCTACAAATCTAACTCT
QQQ (*E. coli*): AAAGTTACTTGCAAAAACGGTCAGGGTAACTGCTACAAATCTcagTCT

NNN (*P. pastoris*): TCAATGCATATCACAGACTGTCGTCTGACTAATGGAAGCAGATACCCC
NNQ (*P. pastoris*): TCAATGCATATCACAGACTGTCGTCTGACTcagGGAAGCAGATACCCC
NQN (*P. pastoris*): TCAATGCATATCACAGACTGTCGTCTGACTAATGGAAGCAGATACCCC
QNN (*P. pastoris*): TCAATGCATATCACAGACTGTCGTCTGACTAATGGAAGCAGATACCCC
NQQ (*P. pastoris*): TCAATGCATATCACAGACTGTCGTCTGACTcagGGAAGCAGATACCCC
QNQ (*P. pastoris*): TCAATGCATATCACAGACTGTCGTCTGACTcagGGAAGCAGATACCCC
QQN (*P. pastoris*): TCAATGCATATCACAGACTGTCGTCTGACTAATGGAAGCAGATACCCC
QQQ (*P. pastoris*): TCAATGCATATCACAGACTGTCGTCTGACTcagGGAAGCAGATACCCC
NNN (*E. coli*): TCTATGCATATCACTGACTGCCGTCTGACTAACGGTTCTCGTTACCCG
QQQ (*E. coli*): TCTATGCATATCACTGACTGCCGTCTGACTcaaGGTTCTCGTTACCCG

NNN (*P. pastoris*): AACTGTGCATACAGAACTTCTCCAAAGGAAAGGCACATTATCGTTGCT
NNQ (*P. pastoris*): AACTGTGCATACAGAACTTCTCCAAAGGAAAGGCACATTATCGTTGCT
NQN (*P. pastoris*): AACTGTGCATACAGAACTTCTCCAAAGGAAAGGCACATTATCGTTGCT
QNN (*P. pastoris*): AACTGTGCATACAGAACTTCTCCAAAGGAAAGGCACATTATCGTTGCT
NQQ (*P. pastoris*): AACTGTGCATACAGAACTTCTCCAAAGGAAAGGCACATTATCGTTGCT
QNQ (*P. pastoris*): AACTGTGCATACAGAACTTCTCCAAAGGAAAGGCACATTATCGTTGCT
QQN (*P. pastoris*): AACTGTGCATACAGAACTTCTCCAAAGGAAAGGCACATTATCGTTGCT
QQQ (*P. pastoris*): AACTGTGCATACAGAACTTCTCCAAAGGAAAGGCACATTATCGTTGCT
NNN (*E. coli*): AACTGCGCTTACCGTACTTCTCCGAAAGAACGTCATATCATCGTTGCT
QQQ (*E. coli*): AACTGCGCTTACCGTACTTCTCCGAAAGAACGTCATATCATCGTTGCT

NNN (*P. pastoris*): TGTGAGGGTTCACCTTATGTCCCTGTTCATTTTGATGCCTCGGTGGAA
NNQ (*P. pastoris*): TGTGAGGGTTCACCTTATGTCCCTGTTCATTTTGATGCCTCGGTGGAA
NQN (*P. pastoris*): TGTGAGGGTTCACCTTATGTCCCTGTTCATTTTGATGCCTCGGTGGAA
QNN (*P. pastoris*): TGTGAGGGTTCACCTTATGTCCCTGTTCATTTTGATGCCTCGGTGGAA
NQQ (*P. pastoris*): TGTGAGGGTTCACCTTATGTCCCTGTTCATTTTGATGCCTCGGTGGAA
QNQ (*P. pastoris*): TGTGAGGGTTCACCTTATGTCCCTGTTCATTTTGATGCCTCGGTGGAA
QQN (*P. pastoris*): TGTGAGGGTTCACCTTATGTCCCTGTTCATTTTGATGCCTCGGTGGAA
QQQ (*P. pastoris*): TGTGAGGGTTCACCTTATGTCCCTGTTCATTTTGATGCCTCGGTGGAA
NNN (*E. coli*): TGCGAAGGTTCTCCGTACGTTCCGGTTCATTTCGACGCTTCTGTTGAA
QQQ (*E. coli*): TGCGAAGGTTCTCCGTACGTTCCGGTTCATTTCGACGCTTCTGTTGAA

NNN (*P. pastoris*): GATAGCACT
NNQ (*P. pastoris*): GATAGCACT
NQN (*P. pastoris*): GATAGCACT
QNN (*P. pastoris*): GATAGCACT
NQQ (*P. pastoris*): GATAGCACT
QNQ (*P. pastoris*): GATAGCACT
QQN (*P. pastoris*): GATAGCACT
QQQ (*P. pastoris*): GATAGCACT
NNN (*E. coli*): GACTCTACT
QQQ (*E. coli*): GACTCTACT

Figure 2.S1. DNA sequences that encode the proteins used in this work. DNA that encodes a leader sequence is in a gray box. The codon for the initial amino acid of each mature protein is in bold typeface.

Substitution	Forward (5′→3′)	Reverse (3′→5′)
Q34N	GAGAAATATGACCCAAGGTCGTTGTAAA	ACATTAGTTTACTACTCTTCCTCT**TTA**TACT
Q76N	GAGTAATTCCTCAATGCATATCACAGACTG	CCTGTTCCATTAACGATGTTCTCA**TTA**AGG
Q88N	TCGTCTGACTAATGGAAGCAGATACCCCAA CTGTGCATAC	GAGTTACGTATAGTGTCTGACAGCAGACTG A**TTA**CCTTCGTC

Figure 2.S2. Oligonucleotides used for site-directed mutagenesis. To effect the Q34N substitution, the CAG codon CAG codon of Gln34 was replaced with an AAT codon (underlined) of asparagine (reverse complement shown in bold). To effect the Q76N substitution, the CAA codon of Gln76 was replaced with an AAT codon (underlined) of asparagine (reverse complement shown in bold). To effect the Q88N substitution, the CAG codon of Gln88 was replaced with an AAT codon (underlined) of asparagine (reverse complement show in bold).

NNN (*P. pastoris*): MRFPSIFTAVLFAASSALAKESRAKKFQRQHMDSDSSPSSSSTYCNQ
NNQ (*P. pastoris*): MRFPSIFTAVLFAASSALAKESRAKKFQRQHMDSDSSPSSSSTYCNQ
NQN (*P. pastoris*): MRFPSIFTAVLFAASSALAKESRAKKFQRQHMDSDSSPSSSSTYCNQ
QNN (*P. pastoris*): MRFPSIFTAVLFAASSALAKESRAKKFQRQHMDSDSSPSSSSTYCNQ
NQQ (*P. pastoris*): MRFPSIFTAVLFAASSALAKESRAKKFQRQHMDSDSSPSSSSTYCNQ
QNQ (*P. pastoris*): MRFPSIFTAVLFAASSALAKESRAKKFQRQHMDSDSSPSSSSTYCNQ
QQN (*P. pastoris*): MRFPSIFTAVLFAASSALAKESRAKKFQRQHMDSDSSPSSSSTYCNQ
QQQ (*P. pastoris*): MRFPSIFTAVLFAASSALAKESRAKKFQRQHMDSDSSPSSSSTYCNQ
NNN (*E. coli*): MKESRAKKFQRQHMDSDSSPSSSSTYCNQ
QQQ (*E. coli*): MKESRAKKFQRQHMDSDSSPSSSSTYCNQ

NNN (*P. pastoris*): MMRRRNMTQGRCKPVNTFVHEPLVDVQNVCFQEKVTCKNGQGNCYKS
NNQ (*P. pastoris*): MMRRRNMTQGRCKPVNTFVHEPLVDVQNVCFQEKVTCKNGQGNCYKS
NQN (*P. pastoris*): MMRRRNMTQGRCKPVNTFVHEPLVDVQNVCFQEKVTCKNGQGNCYKS
QNN (*P. pastoris*): MMRRRQMTQGRCKPVNTFVHEPLVDVQNVCFQEKVTCKNGQGNCYKS
NQQ (*P. pastoris*): MMRRRNMTQGRCKPVNTFVHEPLVDVQNVCFQEKVTCKNGQGNCYKS
QNQ (*P. pastoris*): MMRRRQMTQGRCKPVNTFVHEPLVDVQNVCFQEKVTCKNGQGNCYKS
QQN (*P. pastoris*): MMRRRQMTQGRCKPVNTFVHEPLVDVQNVCFQEKVTCKNGQGNCYKS
QQQ (*P. pastoris*): MMRRRQMTQGRCKPVNTFVHEPLVDVQNVCFQEKVTCKNGQGNCYKS
NNN (*E. coli*): MMRRRNMTQGRCKPVNTFVHEPLVDVQNVCFQEKVTCKNGQGNCYKS
QQQ (*E. coli*): MMRRRQMTQGRCKPVNTFVHEPLVDVQNVCFQEKVTCKNGQGNCYKS

NNN (*P. pastoris*): NSSMHITDCRLTNGSRYPNCAYRTSPKERHIIVACEGSPYVPVHFDA
NNQ (*P. pastoris*): NSSMHITDCRLTQGSRYPNCAYRTSPKERHIIVACEGSPYVPVHFDA
NQN (*P. pastoris*): QSSMHITDCRLTNGSRYPNCAYRTSPKERHIIVACEGSPYVPVHFDA
QNN (*P. pastoris*): NSSMHITDCRLTNGSRYPNCAYRTSPKERHIIVACEGSPYVPVHFDA
NQQ (*P. pastoris*): QSSMHITDCRLTQGSRYPNCAYRTSPKERHIIVACEGSPYVPVHFDA
QNQ (*P. pastoris*): NSSMHITDCRLTQGSRYPNCAYRTSPKERHIIVACEGSPYVPVHFDA
QQN (*P. pastoris*): QSSMHITDCRLTNGSRYPNCAYRTSPKERHIIVACEGSPYVPVHFDA
QQQ (*P. pastoris*): QSSMHITDCRLTQGSRYPNCAYRTSPKERHIIVACEGSPYVPVHFDA
NNN (*E. coli*): NSSMHITDCRLTNGSRYPNCAYRTSPKERHIIVACEGSPYVPVHFDA
QQQ (*E. coli*): QSSMHITDCRLTQGSRYPNCAYRTSPKERHIIVACEGSPYVPVHFDA

NNN (*P. pastoris*): SVEDST
NNQ (*P. pastoris*): SVEDST
NQN (*P. pastoris*): SVEDST
QNN (*P. pastoris*): SVEDST
NQQ (*P. pastoris*): SVEDST
QNQ (*P. pastoris*): SVEDST
QQN (*P. pastoris*): SVEDST
QQQ (*P. pastoris*): SVEDST
NNN (*E. coli*): SVEDST
QQQ (*E. coli*): SVEDST

Figure 2.S3. Amino acid sequences of the proteins used in this work. Leader sequences are in a gray box. Asparagine→glutamine substitutions are indicated in red typeface.

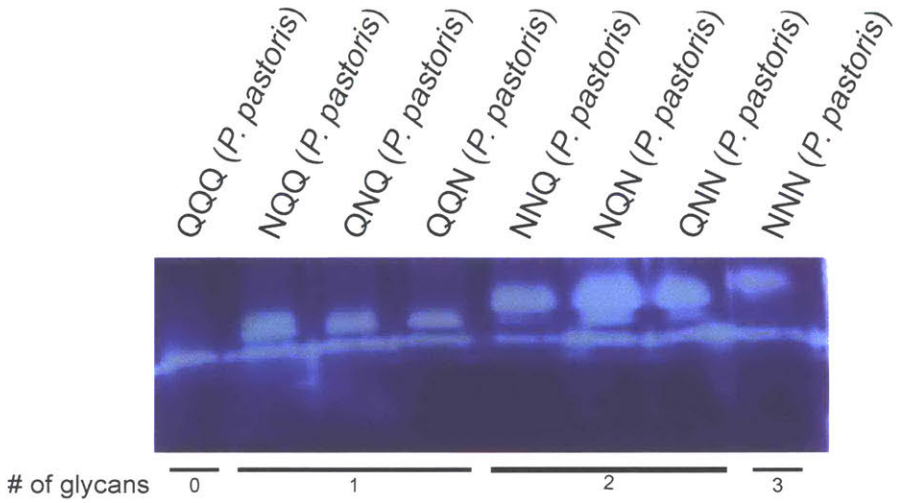
QQQ (P. pastoris)
NQQ (P. pastoris)
QNQ (P. pastoris)
QQN (P. pastoris)
NNQ (P. pastoris)
NQN (P. pastoris)
QNN (P. pastoris)
NNN (P. pastoris)
# of glycans
0
1
2
3

Figure 2.S4. Zymogram of secreted RNase 1 glycoforms. Conditioned medium samples from *P. pastoris* cultures were evaluated for ribonucleolytic activity. Inherent macroheterogeneity was observed in all glycosylated samples as multiple bands, including one with the same mobility as the aglycosylated control. The mobility shifts correspond to the addition of *N*-linked glycans.

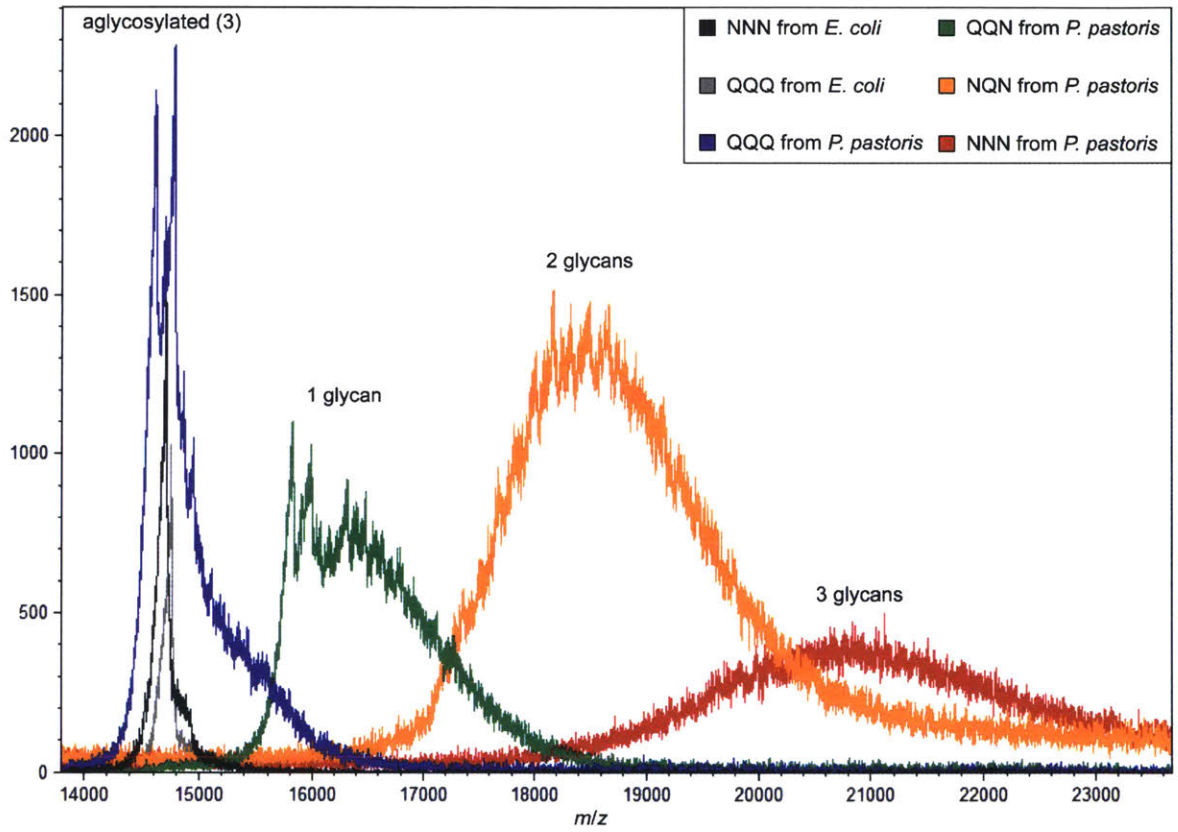
aglycosylated (3)
NNN from E. coli
QQN from P. pastoris
QQQ from E. coli
NQN from P. pastoris
QQQ from P. pastoris
NNN from P. pastoris
2 glycans
1 glycan
3 glycans
2000
1500
1000
500
0
14000
15000
16000
17000
18000
19000
20000
21000
22000
23000
m/z

Figure 2.S5. Representative MALDI–TOF mass spectra of human RNase 1 glycoforms.

NNN (*E. coli*)

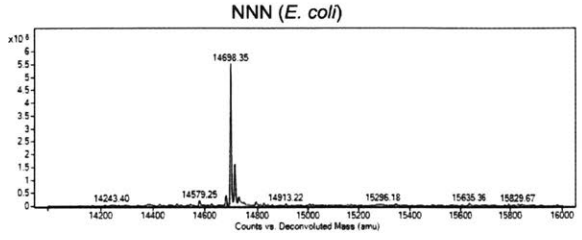

QQQ (*E. coli*)

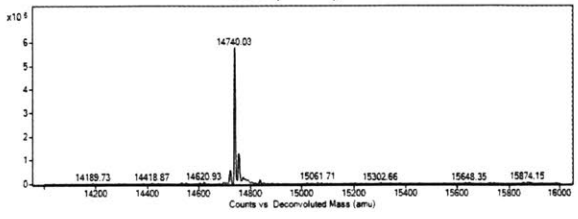

QQQ (*P. pastoris*)

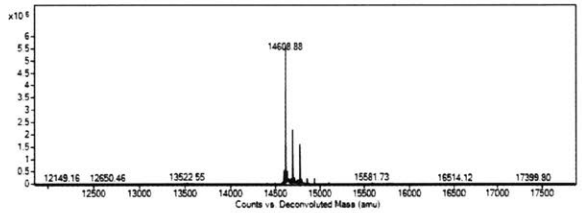

NQQ (*P. pastoris*)

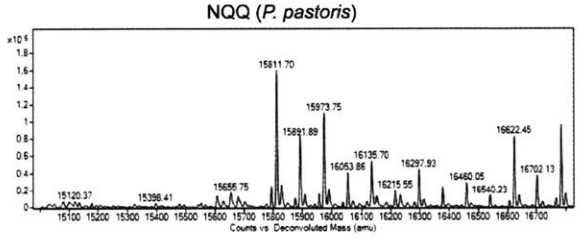

QNQ (*P. pastoris*)

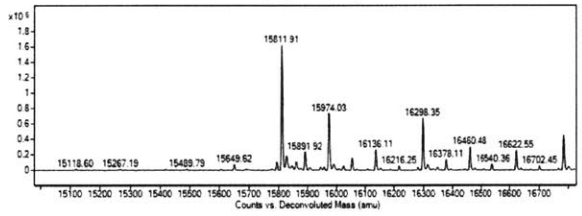

QQN (*P. pastoris*)

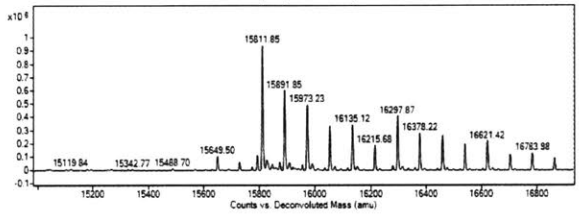

NNQ (*P. pastoris*)

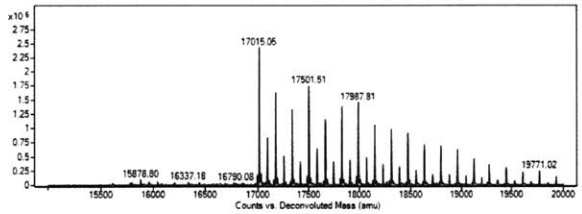

NQN (*P. pastoris*)

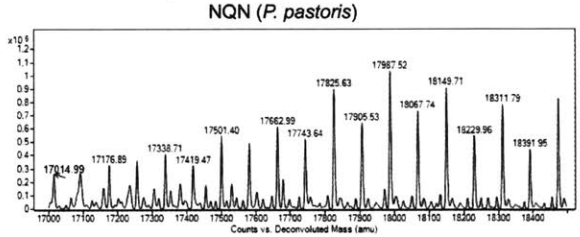

QNN (*P. pastoris*)

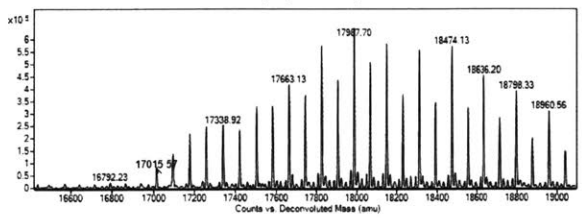

NNN (*P. pastoris*)

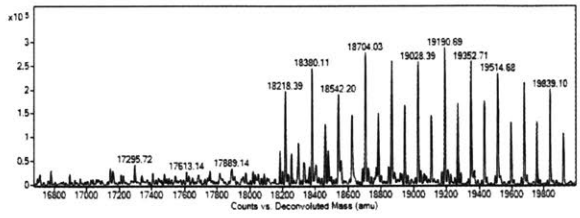

Figure 2.S6. Deconvoluted ESI mass spectra of human RNase 1 glycoforms. Each D-mannose unit has a mass of 162.05 Da. The mass of the lightest glycoform is listed in Table 2.1.

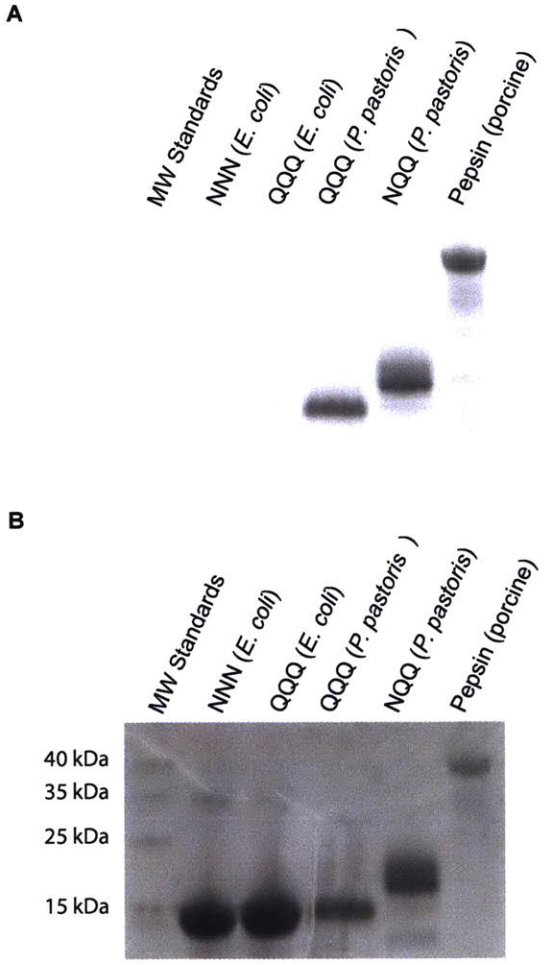
A
MW Standards
NNN (E. coli)
QQQ (E. coli)
QQQ (P. pastoris)
NQQ (P. pastoris)
Pepsin (porcine)
B
MW Standards
NNN (E. coli)
QQQ (E. coli)
QQQ (P. pastoris)
NQQ (P. pastoris)
Pepsin (porcine)
40 kDa
35 kDa
25 kDa
15 kDa

Figure 2.S7. SDS–PAGE gels showing phosphorylation of RNase 1 proteins from yeast. Representative RNase 1 variants as well as a phosphorylated pepsin standard from Sigma, were subjected to electrophoresis in a 15% (w/v) gel and visualized by staining for phosphorylated proteins with Pro–Q™ Diamond gel stain (A) or total proteins with Coomassie blue (B).

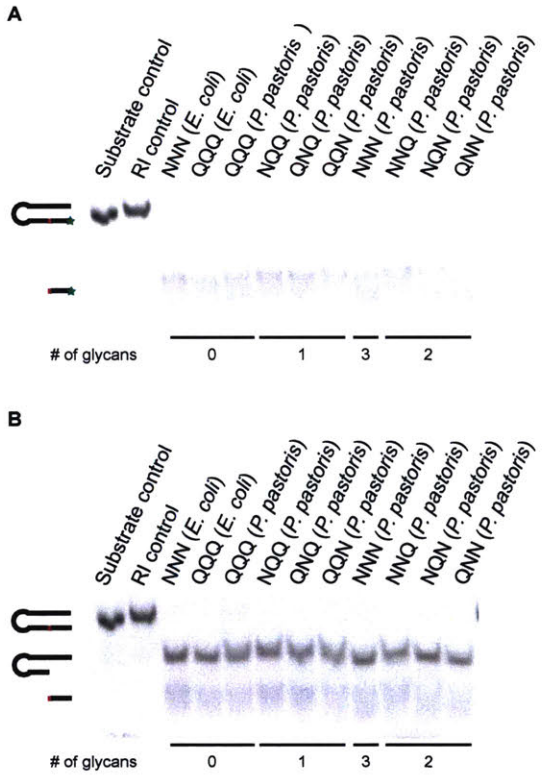
A
Substrate control
RI control
NNN (E. coli)
QQQ (E. coli)
QQQ (P. pastoris)
NQQ (P. pastoris)
QNQ (P. pastoris)
QQN (P. pastoris)
NNN (P. pastoris)
NNQ (P. pastoris)
NQN (P. pastoris)
QNN (P. pastoris)
# of glycans
0
1
3
2
B
Substrate control
RI control
NNN (E. coli)
QQQ (E. coli)
QQQ (P. pastoris)
NQQ (P. pastoris)
QNQ (P. pastoris)
QQN (P. pastoris)
NNN (P. pastoris)
NNQ (P. pastoris)
NQN (P. pastoris)
QNN (P. pastoris)
# of glycans
0
1
3
2

Figure 2S.8. Native gel demonstrating cleavage of a double-stranded substrate.[173] RNase 1 variants cleavage of a DNA hairpin containing a single RNA residue (red) and a fluorescent FAM (green) label at the 5' end. The gel was visualized for FAM products (A) and with SYBR Gold for total nucleic acids (B).

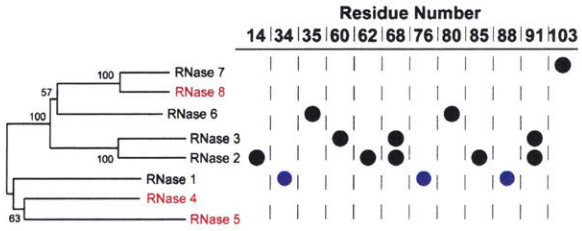
Residue Number
14 34 35 60 62 68 76 80 85 88 91 103
RNase 7
RNase 8
RNase 6
RNase 3
RNase 2
RNase 1
RNase 4
RNase 5
100
57
100
100
63

Figure 2.S9. Putative *N*-glycosylation sites in human ptRNases 1–8. Circles indicate an asparagine residue within an *N*-glycosylation sequon. The neighbor-joining phylogenetic tree is adapted from ref.[194] and shows bootstrap values >50. The sequon positions are adapted from ref. [153] and are aligned with the sequence for human RNase 1.

Chapter 3

Esterification Delivers a Functional Enzyme into a Human Cell

Contributions: I expressed and purified all ribonuclease 1 proteins, performed ribonucleolytic activity assays on all proteins, carried out esterification reactions, characterized proteins by mass spectrometry, and conducted all cell biology experiments. K. Mix and I worked jointly to design experiments. K. Mix provided early batches of diazo compound. I wrote the manuscript.

3.1 Abstract

A major hurdle in chemical biology is the delivery of native proteins into the cytosol of mammalian cells. Herein, we report that esterification of the carboxyl groups of an enzyme with a diazo compound enables not only its passage into the cytosol, but also the retention of its catalytic activity there. This scenario is demonstrated with human ribonuclease 1, which manifests ribonucleolytic activity that can be cytotoxic. After internalization, the nascent esters are hydrolyzed in situ by endogenous esterases, making the process traceless. This strategy provides unprecedented opportunities for the delivery of functional enzymes into human cells.

3.2 Introduction

Biologics are driving the growth of the modern pharmacopeia.[195] Still, nearly all of these biologics are antibodies and hormones that act on the cell surface.[100, 196] Virtually none are proteins that intervene beneficially in the cytosol or nucleus, despite incalculable opportunities there.

The translocation of a putative therapeutic agent across the plasma membrane is made difficult by the high anionicity of the glycocalyx and hydrophobicity of the lipid bilayer.[197] Any strategy for protein delivery must overcome these two obstacles. Medicinal chemists have done so by the bioreversible masking of anionic functional groups. The ensuing "prodrugs",[129-131] which are usually esters of carboxylic acids, constitute 20% of small-molecule drugs.[198] Recently, we demonstrated that the esterification of the carboxyl groups of the green fluorescent protein (GFP) with 2-diazo-2-(*p*-methylphenyl)-*N*,*N*-dimethylacetamide enables its passage across the plasma membrane, akin to a small-molecule prodrug (Scheme 3.1).[137] Importantly, the nascent esters are substrates for endogenous intracellular esterases.[129, 199] Thus, esterification can be a "traceless" delivery method that leaves no residual atoms attached to the cargo.

Upon cytosolic entry, esterified GFP retains its fluorescence,[137] consistent with the retention of its three-dimensional structure.[200] The catalytic activity of an enzyme is, however, the most sensitive indicator of proper conformation.[201] We sought to investigate the utility of esterification as a means to promote the delivery of a functional enzyme.

As a model enzyme, we chose human ribonuclease 1 (RNase 1; EC 3.1.27.5; UniProtKB P07998).[153] RNase 1 is an efficient catalyst of RNA cleavage, and its ribonucleolytic activity can be cytotoxic.[147, 202-203] To be cytotoxic, RNase 1 must not only enter the cytosol, but also evade the ribonuclease inhibitor protein (RI) that resides there.[84, 92] Wild-type RNase 1 forms a

complex with RI that has a K_d value of (at most[204]) 0.29 fM[193] and is not appreciably cytotoxic because of its sequestration by RI.[174]

RI is a highly anionic protein, and its evasion is best achieved by installing anionic groups into RNase 1. Indeed, the most evasive known variant is R39D/N67D/N88A/G89D/R91D RNase 1, which has 10^{10}-fold lower affinity for RI than does the wild-type enzyme.[76] The DDADD variant is, however, not appreciably cytotoxic because its anionicity deters cellular uptake.[76] Hence, the DDADD variant along with wild-type RNase 1 were ideal enzymes for the assessment of our approach, using cytotoxicity as a readout.

3.3 Methods

3.3.1 Materials

The BL21(DE3) strain of *Escherichia coli* was from Novagen (Madison, WI). Diazo compound **1** (2-diazo-*N*,*N*-dimethyl-2-(*p*-tolueyl)acetamide) was synthesized by Chicago Discovery Solutions (Plainfeld, IL) as described previously.[136] RNase A (bovine) was from Sigma–Aldrich (St. Louis, MO). A fluorogenic ribonuclease substrate (6-FAM–dArU(dA)$_2$–6-TAMRA) and DNA oligonucleotides were from Integrated DNA Technologies (Coralville, IA). A 50,000× solution of SYPRO Orange Protein Gel Stain was from Life Technologies (Grand Island, NY). All other chemicals and reagents were of commercial reagent grade or better and were used without further purification.

Aqueous solutions were made with water that was generated with an arium Pro water purification system from Sartorius (Bohemia, NY) and had resistivity ≥18 MΩ·cm^{-1}. Phosphate-buffered saline (PBS) contained Na_2HPO_4 (10 mM), KH_2PO_4 (1.8 mM), NaCl (137 mM), and KCl (2.7 mM) at pH 7.4. A Spectra Multicolor Broad Range Protein Ladder from Thermo Fisher Scientific (Waltham, MA) was used as a molecular mass standard for SDS–PAGE.

3.3.2 Instrumentation

Chromatography was performed with an ÄKTA Pure system from GE Healthcare Life Sciences (Piscataway, NJ), and the results were analyzed with the UNICORN Control System. HiTrap SPHP and HiLoad® 26/600 Superdex® 75 pg columns for protein purification were from GE Healthcare Life Sciences.

Protein concentrations were determined with a bicinchonic acid (BCA) assay kit from Thermo Fisher Scientific and measured with an infinite M1000 microplate reader from Tecan (Zürich, Switzerland).

Differential scanning fluorimetry (DSF), which requires thermal denaturation and the simultaneous monitoring of fluorescence, was performed with a ViiA Real-Time PCR system from Applied Biosystems (Foster City, CA). Denaturation data were obtained with ViiA 7 version 2.0 software and analyzed further by Protein Thermal Shift version 1.4 software, both from Applied Biosystems.

The intact molecular mass of RNase 1 variants was determined by ESI mass spectrometry using a 6530 Accurate-Mass Q-TOF LC/MS from Agilent (Santa Clara, CA) with a PLRP-S column (1000-Å pore size, 5-μM particle size, 50-mm length, and 2.1-mm ID).

3.3.3 Conditions

All procedures were performed in air at ambient temperature (~22 °C) and pressure (1.0 atm) unless indicated otherwise.

3.3.4 Plasmid preparation

cDNA that encodes Met(–1) RNase 1 in a pET22b(+) expression vector was used to generate wild-type RNase 1 in *E. coli* (Figure 3.S1). Two synthetic cDNAs encoding for either the R39D/N67D/N88A/G89D/R91D (DDADD) variant or the inactive H12A/K41A/H119A variant flanked by regions of homology near the T7 promoter and terminator of the pET22b vector were obtained from Integrated DNA Technologies (Figure 3.S1). Linear pET22b was prepared by PCR using primers that complement the DNA that encodes RNase 1 (5′-AAGCCCGAAAGGAAGCTGAGTTGGCTGCTG-3′ and 3′-AAACAAATTGAAATTCTTCCT CTATATGTA-5′). Each gene and plasmid fragment were combined with Gibson assembly for expression in *E. coli*. The corresponding amino acid sequence for each RNase 1 variant is shown in Figure 3.S2.

3.3.5 Enzyme production and purification

All enzymes, including wild-type RNase 1, DDADD RNase 1, H12/K41A/H119A RNase 1, and FLAG–RNase 1, were purified from inclusion bodies as described previously.[174] Briefly, induced cells were lysed with a benchtop cell disruptor from Constant Systems (Kennesaw, GA) at 19.0 kpsi. After centrifugation at 10,500 rpm for 45 min, the resulting inclusion bodies were dissolved in 20 mM Tris–HCl buffer, pH 8.0, containing guanidine–HCl (7 M), EDTA (10 mM), and DTT (100 mM). This solution was diluted 10-fold by the slow addition of degassed 20 mM acetic acid, then subjected to centrifugation at 10,500 rpm for 45 min. The resulting supernatant was then dialyzed using 3.5-kDa MWCO tubing from Spectrum Labs (Rancho Dominguez, CA) against 16 L of 20 mM acetic acid overnight. After centrifugation at 10,500 rpm for 40 min, the retentate was added dropwise to re-folding solution, which was 100 mM Tris–HCl buffer, pH

7.8, containing NaCl (100 mM), reduced glutathione (1.0 mM), and oxidized glutathione (0.2 mM), then allowed to re-fold at 4 °C for 5 days. The pH of the solution was adjusted to 5.0, and the resulting solution was concentrated to 10 mL with an Amicon® Stirred Cell concentrator from EMD Millipore (Billerica, MA) with Hydrostart® 10-kDa filters from Sartorius. The resulting protein solution was purified by chromatography on a HiLoad® 26/600 Superdex® 75 pg gel-filtration column from GE Healthcare Life Sciences with 50 mM sodium acetate buffer, pH 5.0, containing NaCl (100 mM) and sodium azide (0.05% w/v). The protein was purified further by passage through a HiTrap SP cation-exchange column from GE Healthcare Life Sciences before being dialyzed against PBS.

3.3.6 Enzyme esterification with diazo compound 1

Wild-type RNase 1 and its variants were esterified under identical reaction conditions. A solution of diazo compound **1** (2.8 mg, 14 μmol or 5.6 mg, 28 μmol) in 200 μL of acetonitrile was added to a solution of enzyme (0.14 μmol) in 200 μL of 10 mM MES–HCl buffer, pH 5.5. The reaction mixture was incubated for 4 h at 37 °C, then diluted by the addition of 40 mL of PBS. The solution was concentrated by using a Vivaspin filtration column (5-kDa MWCO) from GE Healthcare Life Sciences, and the extent of esterification was assessed with Q-TOF LC/MS.

3.3.7 Assays of ribonucleolytic activity

The ribonucleolytic activity of wild-type RNase 1 and its variants was determined by measuring the initial velocity of cleavage of ssRNA substrate in a 96-well plate (Corning) at 25 °C. A fluorogenic RNA substrate (0.2 μM of 6-FAM–dArU$(dA)_2$–6-TAMRA) in 100 mM Tris–HCl buffer, pH 7.5, containing NaCl (100 mM) was added to each well. After baseline fluorescent

readings were recorded, enzymes were added to a final concentration of 50 pM, and the initial velocity of substrate turnover was measured by the increase in fluorescence over time. After 8 min, substrate cleavage was saturated by the addition of RNase A to a final concentration of 5 μM. Values of k_{cat}/K_M were determined as described previously.[175] Values represent the mean of at least three independent experiments.

3.3.8 Mammalian cell culture

HeLa and NCI-H460 cells were obtained from American Type Culture Collection (Manassas, VA) and stored in vials immersed in $N_2(l)$. These cell lines were authenticated by morphology, karyotyping, and PCR-based methods, which included an assay to detect species specific variants of the cytochrome C oxidase I gene (to rule out interspecies contamination) and short tandem repeat profiling (to distinguish between individual human cell lines and rule out intraspecies contamination). To minimize genetic drift, a thawed vial was used for fewer than fifteen passages.

Cell culture medium and added components were the Gibco brand from Thermo Fisher Scientific. Cells were grown in flat-bottomed culture flasks in a cell culture incubator at 37 °C under $CO_2(g)$ (5%v/v). HeLa and NCI-H460 cells were cultured in Dulbecco's modified Eagle's medium (DMEM) or RPMI 1640 medium, respectively, each containing fetal bovine serum (FBS) (10% v/v) and penicillin–streptomycin solution (1% v/v).

3.3.9 Assays of cell viability

Cell viability was assessed with the CellTiter 96 AQueous One Solution Cell Proliferation Assay from Promega (Madison, WI), which is a tetrazolium dye-based assay for metabolic activity.

Cells were grown, treated, and assessed as described previously.[174] Briefly, cells were grown in the wells of a 96-well plate. After 24 h, the medium was replaced with FBS-free DMEM containing various concentrations of analyte proteins. Cells were then allowed to incubate for another 48 h before the addition of the MTS reagent and data collection. Data were analyzed with the program Prism from GraphPad (La Jolla, CA). Values of EC_{50}, which is the concentration of analyte that gives half-maximal cell viability, were calculated by using the equation:

$$y = y_{\min} + \frac{(y_{\max} - y_{\min})}{1+\left(\frac{EC_{50}}{x}\right)^{h}} \quad \text{(S1)}$$

where y is cell viability, x is the concentration of analyte, and h is the Hill coefficient. All values were the average of at least three biological replicates.

3.3.6 Reversibility of enzyme esterification in cellulo

Human RNase 1 is intact after incubation with a detergent-containing cell lysis kit and produces a well-resolved peak in a Q-TOF LC/MS spectrum. A FLAG-tagged variant of RNase 1 binds to a FLAG antibody with high affinity, thus allowing for recovery of this protein from treated cells. We used FLAG-tagged RNase 1 for an assessment of the bioreversibility of protein esterification *in cellulo*.

HeLa cells were plated at 500,000 cells in 10 mL of medium in a 10-cm^2 dish. After 24 h, cells were treated with FLAG–RNase 1 or esterified FLAG–RNase 1 (1 μg/mL) and incubated for 24 h. Then, cells were washed with PBS and lysed with 1.0 mL of M-PER mammalian protein extraction reagent (Pierce) containing a protease inhibitor cocktail (Thermo). After

centrifugation, the clarified lysate was incubated with α-FLAG magnetic beads (Sigma Chemical) for 1 h at room temperature. The beads were washed and then treated twice with 150 ng/μL of 3× FLAG peptide (APExBIO). The combined eluates were subjected to methanol/chloroform protein precipitation to remove detergents prior to further analysis. Briefly, protein eluate was treated with 4 volumes of methanol, then 1 volume of chloroform, and then 3 volumes of water. After centrifugation at 14,000*g* for 2 min, the upper aqueous layer was removed and 4 volumes of methanol were added to the solution. The precipitated protein was then pelleted by centrifugation at 14,000*g* for 2 min. The methanol solution was removed and the protein pellet was allowed to dry at room temperature for 5 min. After resuspension in PBS, protein samples were passed through a 0.2-μm filter from Thermo Fischer Scientific and analyzed by LC/MS.

3.4 Results

3.4.1 Esterification reduces ribonucleolytic activity

The mechanism of esterification with a diazo compound relies on a carboxyl group being in a protonated state.[205-206] To encourage protonation, we performed esterification reactions at pH 5.5 in aqueous acetonitrile (Scheme 3.1). These conditions were well-tolerated by RNase 1 and its variants, and enabled esterification of $^1/_3$–$^1/_2$ of enzymic carboxyl groups (Table 3.1). Esterification did reduce ribonucleolytic activity slightly (Table 3.1), but to a lesser extent than did the amidation of enzymic carboxyl groups.[207]

3.4.2 Cytotoxicity of esterified RNase variants towards HeLa

As observed previously,[174] wild-type RNase 1 had no detectable effect on the viability of HeLa cells, even at a concentration of 100 μM (Figure 3.2A). In contrast, esterification of wild-type RNase 1 engendered toxicity towards HeLa cells with an IC_{50} value of (10 ± 1) μM (Figure 3.2A). These data are consistent with esterified RNase 1 invading the cytosol and overwhelming RI, which is present at ~4 μM.[208]

Wild-type RNase 1 has a net charge of $Z = 5$.[209] The unmodified enzyme enters endosomes rapidly,[76] and a small fraction escapes into the cytosol.[210] In contrast, DDADD RNase 1 has a net charge of $Z = 0$ and enters endosomes slowly.[76] As expected, DDADD RNase 1 did not have an impact on the viability of HeLa cells (Figure 3.2B). In contrast, esterification made the DDADD variant cytotoxic with an IC_{50} value of (6 ± 1) μM (Figure 3.2B). This cytotoxicity is consistent with the esterified enzyme entering the cytosol directly and cleaving cellular RNA there.

3.4.3 Cytotoxicity of esterified RNases relies on ribonucleolytic activity

We were aware that the observed cytotoxicity of the esterified enzymes could be due to a property other than their catalytic activity. For example, some proteins and peptides are cytotoxic because of their ability to disrupt lipid bilayers.[211-212] To test this alternative mechanism, we employed H12A/K41A/H119A RNase 1, which has an eviscerated active site and no detectable ribonucleolytic activity (Table 3.1). We found that this variant is not cytotoxic, even upon esterification (Figure 3.2C). Accordingly, we conclude that the cytotoxicity of both esterified wild-type RNase 1 and esterified DDADD RNase 1 relies on the manifestation of their catalytic activity within cells. We note, too, that the toxicity of these esterified enzymes for HeLa cells

exceeds that of QBI-139 (IC_{50} = 18 ± 2 μM),[174] which is an RI-evasive variant of RNase 1 that is undergoing clinical trials as a cancer chemotherapeutic agent.[69-70]

3.4.4 Cytotoxicity of esterified RNases is maintained across cell lines

HeLa cells, which were derived from a cervical tumor, have numerous abnormalities.[213] Accordingly, we sought to reproduce our results in another cell line. We chose H460 cells, which were derived from a non-small-cell lung tumor. We also used this cell line to assess the effect of esterification level on cytotoxicity. Wild-type RNase 1 and its DDADD variant were treated with either 100 or 200 equiv of diazo compound **1**. We found that increasing the esters in wild-type RNase 1 from ~4 to ~6 reduced the IC_{50} value from (7 ± 1) μM to (5.1 ± 0.5) μM (Figure 3.3A). Wild-type RNase 1 has 13 carboxyl groups (Figure 3.1), whereas the DDADD variant has 17 carboxyl groups. The larger number of carboxyl groups amplified the effects. Specifically, we found that increasing the esters in DDADD RNase 1 from ~7 to ~11 reduced the IC_{50} value from (8.4 ± 0.5) μM to (1.0 ± 0.2) μM (Figure 3.3B).

3.4.4 Ester labels are fully removed in cellulo

Finally, we investigated the reversibility of enzymic esterification in living cells. To do so, we appended an 8-residue FLAG tag to the N-terminus of wild-type RNase 1 and esterified the resulting FLAG–RNase 1 by using diazo compound **1**. We treated HeLa cells with untreated or esterified FLAG–RNase 1 for 24 h, washed and lysed the cells, and recovered the FLAG–RNase 1 by using anti-FLAG magnetic beads. Mass spectrometry revealed complete removal of the labels (Figure 3.S6).[214] These data indicate that the esters installed by diazo compound **1** are hydrolyzed by esterases in human cells.

3.5 Discussion

In summary, we have used a diazo compound to esterify enzymic carboxyl groups and shown that the ensuing enzyme enters the cytosol of human cells and is functional there. Because the catalytic activity of an enzyme is fragile, its maintenance indicates that the delivery process is gentle. Notably, esterification can be performed without the need for mutagenesis,[215] and the modification is traceless, being removed by cellular esterases. This facile, versatile strategy provides new opportunities for delivering native, functional proteins to intracellular targets.

Table 3.1. Attributes of Untreated and Esterified RNase 1 Variants

RNase 1	Z^a	Carboxyl groups	**1** (equiv)[b]	Esters[c]	k_{cat}/K_M (10^7 $M^{-1}s^{-1}$)[d]	IC_{50} (μM)[e]	
						HeLa Cells	H460 Cells
Wild-type	+5	13	0	—	2.5 ± 0.1	>100	>100
Wild-type	+5	13	100	4	1.1 ± 0.5	10 ± 1	7 ± 1
Wild-type	+5	13	200	6	1.6 ± 0.1	ND[f]	5.1 ± 0.5
DDADD	0	17	0	—	0.022 ± 0.002	>100	>100
DDADD	0	17	100	7	0.023 ± 0.003	6 ± 1	8.4 ± 0.5
DDADD	0	17	200	11	0.025 ± 0.004	ND	1.0 ± 0.2
H12A/K41A/H119A	+4	13	0	—	$<1 \times 10^{-5}$	>100	>100
H12A/K41A/H119A	+4	13	100	4	$<1 \times 10^{-5}$	>100	>100
FLAG-labeled	+2	18	0	—	0.72 ± 0.07	ND	ND
FLAG-labeled	+2	18	100	5	0.35 ± 0.04	ND	ND

[a] The parameter Z is defined as the number of arginine + lysine – aspartate – glutamate residues.

[b]Reaction conditions: 200 μL of enzyme (0.14 μmol) in 10 mM MES–HCl buffer (pH 5.5) plus 200 μL of diazo compound **1** (14 or 28 μmol) in acetonitrile; 37 °C for 4 h. [c]Values are the most prevalent species apparent in the mass spectra of Figures 3.S3–S6.

[d]Values are the mean ± SD for the cleavage of 6-FAM-dArU$(dA)_2$–6-TAMRA in 100 mM Tris–HCl buffer (pH 7.5), containing NaCl (100 mM). Individual values are shown in Figure 3.S7. [e]Values are the mean ± SD from data in Figures 2 and 3. [f]ND, not determined.

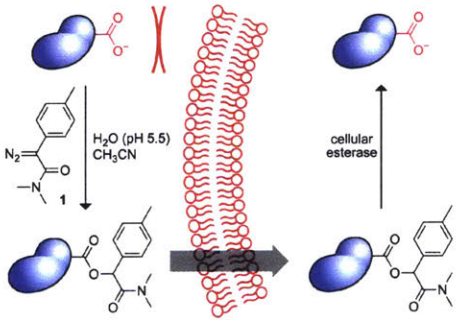
H2O (pH 5.5)
CH3CN
cellular
esterase
1

Scheme 3.1. Representation of diazo-mediated esterification strategy for enhanced delivery of RNase variants.

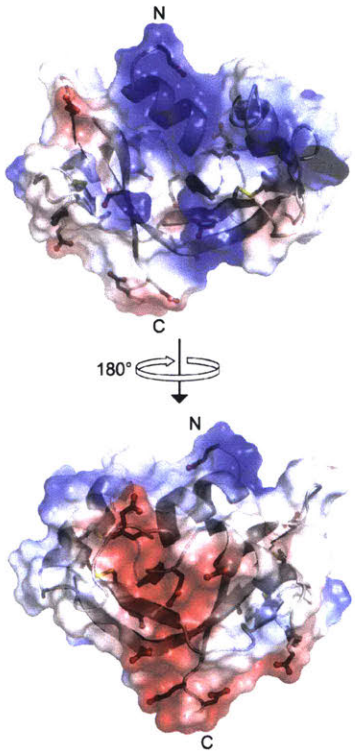
N
C
180°
N
C

Figure 3.1. Surface electrostatic potential of human RNase 1 (blue, positive; red, negative). The side chains of the 6 aspartate, 6 glutamate, and 4 cystine residues are shown explicitly. The image was created with the program PyMOL from Schrödinger (New York, NY) and Protein Data Bank entry 1z7x, chain X.[76]

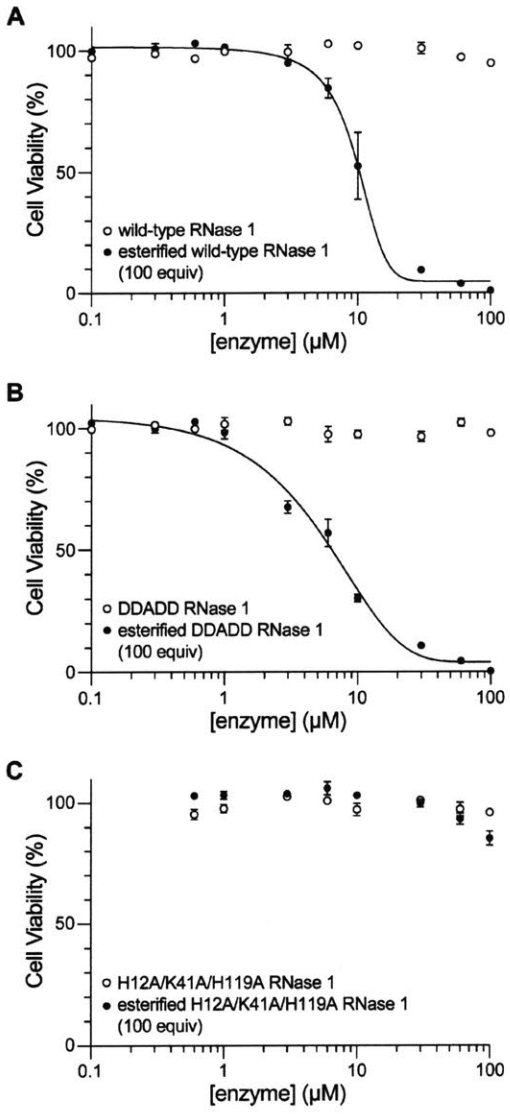
A
100
50
0
Cell Viability (%)
wild-type RNase 1
esterified wild-type RNase 1
(100 equiv)
0.1
1
10
100
[enzyme] (μM)
B
100
50
0
Cell Viability (%)
DDADD RNase 1
esterified DDADD RNase 1
(100 equiv)
0.1
1
10
100
[enzyme] (μM)
C
100
50
0
Cell Viability (%)
H12A/K41A/H119A RNase 1
esterified H12A/K41A/H119A RNase 1
(100 equiv)
0.1
1
10
100
[enzyme] (μM)

Figure 3.2. Effect of esterification of human RNase 1 (A) and its variants (B, C) on the viability of HeLa cells. Cell viability was measured with a tetrazolium dye-based assay for metabolic activity. Values of IC_{50} are listed in Table 3.1.

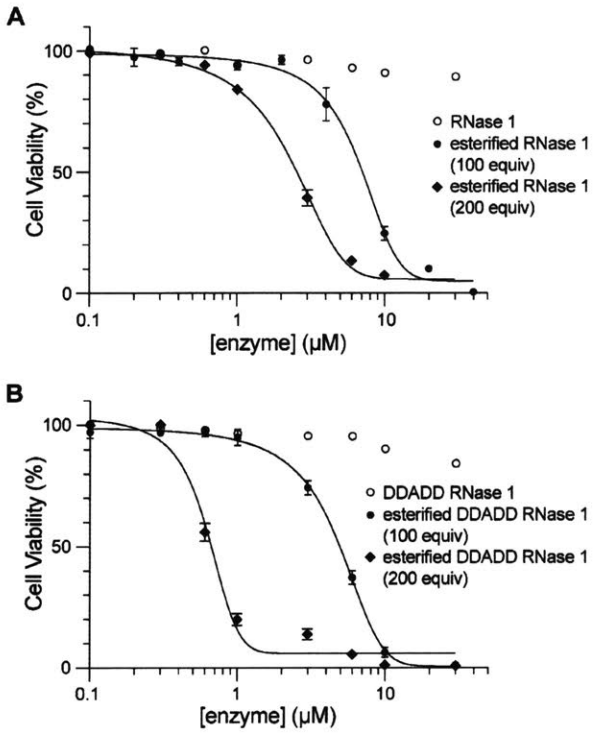
A
100
50
0
Cell Viability (%)
0.1
1
10
[enzyme] (μM)
RNase 1
esterified RNase 1 (100 equiv)
esterified RNase 1 (200 equiv)
B
100
50
0
Cell Viability (%)
0.1
1
10
[enzyme] (μM)
DDADD RNase 1
esterified DDADD RNase 1 (100 equiv)
esterified DDADD RNase 1 (200 equiv)

Figure 3.3. Impact of the extent of esterification of human RNase 1 (A) and its DDADD variant (B) on the viability of H460 cells. Cell viability was measured with a tetrazolium dye-based assay for metabolic activity. Values of IC_{50} are listed in Table 3.1.

3.6 Supplementary information

```
wild-type RNase 1:                                  ATGAAAGAATCTCGTGCTAAAAAATTCCAG
DDADD RNase 1:                                      ATGAAAGAATCTCGTGCTAAAAAATTCCAG
H12A/K41A/H119A:                                    ATGAAAGAATCTCGTGCTAAAAAATTCCAG
FLAG–RNase 1:       ATGGACTACAAAGACGATGACGACAAGAAAGAATCTCGTGCTAAAAAATTCCAG

wild-type RNase 1:  CGTCAGCATATGGACTCTGACTCTTCTCCGTCTTCTTCTTCTACTTACTGCAAC
DDADD RNase 1:      CGTCAGCATATGGACTCTGACTCTTCTCCGTCTTCTTCTTCTACTTACTGCAAC
H12A/K41A/H119A:    CGTCAGGCGATGGACTCTGACTCTTCTCCGTCTTCTTCTTCTACTTACTGCAAC
FLAG–RNase 1:       CGTCAGCATATGGACTCTGACTCTTCTCCGTCTTCTTCTTCTACTTACTGCAAC

wild-type RNase 1:  CAGATGATGCGTCGTCGTAACATGACTCAGGGTCGTTGCAAACCGGTTAACACT
DDADD RNase 1:      CAGATGATGCGTCGTCGTAACATGACTCAGGGTGATTGCAAACCGGTTAACACT
H12A/K41A/H119A:    CAGATGATGCGTCGTCGTAACATGACTCAGGGTCGTTGCGCACCGGTTAACACT
FLAG–RNase 1:       CAGATGATGCGTCGTCGTAACATGACTCAGGGTCGTTGCAAACCGGTTAACACT

wild-type RNase 1:  TTCGTTCATGAACCGCTGGTTGACGTTCAGAACGTTTGCTTCCAGGAAAAAGTT
DDADD RNase 1:      TTCGTTCATGAACCGCTGGTTGACGTTCAGAACGTTTGCTTCCAGGAAAAAGTT
H12A/K41A/H119A:    TTCGTTCATGAACCGCTGGTTGACGTTCAGAACGTTTGCTTCCAGGAAAAAGTT
FLAG–RNase 1:       TTCGTTCATGAACCGCTGGTTGACGTTCAGAACGTTTGCTTCCAGGAAAAAGTT

wild-type RNase 1:  ACTTGCAAAAACGGTCAGGGTAACTGCTACAAATCTAACTCTTCTATGCATATC
DDADD RNase 1:      ACTTGCAAAGACGGTCAGGGTAACTGCTACAAATCTAACTCTTCTATGCATATC
H12A/K41A/H119A:    ACTTGCAAAAACGGTCAGGGTAACTGCTACAAATCTAACTCTTCTATGCATATC
FLAG–RNase 1:       ACTTGCAAAAACGGTCAGGGTAACTGCTACAAATCTAACTCTTCTATGCATATC

wild-type RNase 1:  ACTGACTGCCGTCTGACTAACGGTTCTCGTTACCCGAACTGCGCTTACCGTACT
DDADD RNase 1:      ACTGACTGCCGTCTGACTGCGGATTCTGACTACCCGAACTGCGCTTACCGTACT
H12A/K41A/H119A:    ACTGACTGCCGTCTGACTAACGGTTCTCGTTACCCGAACTGCGCTTACCGTACT
FLAG–RNase 1:       ACTGACTGCCGTCTGACTAACGGTTCTCGTTACCCGAACTGCGCTTACCGTACT

wild-type RNase 1:  TCTCCGAAAGAACGTCATATCATCGTTGCTTGCGAAGGTTCTCCGTACGTTCCG
DDADD RNase 1:      TCTCCGAAAGAACGTCATATCATCGTTGCTTGCGAAGGTTCTCCGTACGTTCCG
H12A/K41A/H119A:    TCTCCGAAAGAACGTCATATCATCGTTGCTTGCGAAGGTTCTCCGTACGTTCCG
FLAG–RNase 1:       TCTCCGAAAGAACGTCATATCATCGTTGCTTGCGAAGGTTCTCCGTACGTTCCG

wild-type RNase 1:  GTTCATTTCGACGCTTCTGTTGAAGACTCTACT
DDADD RNase 1:      GTTCATTTCGACGCTTCTGTTGAAGACTCTACT
H12A/K41A/H119A:    GTTGCGTTCGACGCTTCTGTTGAAGACTCTACT
FLAG–RNase 1:       GTTCATTTCGACGCTTCTGTTGAAGACTCTACT
```

Figure 3.S1. DNA sequences that encode the proteins used this work. DDADD RNase 1 refers to the R39D/N67D/N88A/G89D/R91D variant. DNA that encodes a FLAG-tag sequence is in a gray box. The codon for the initial amino acid of each mature protein is in bold typeface. Red sequences indicate mutation sites.

```
wild-type RNase 1:          MKESRAKKFQRQHMDSDSSPSSSSTYCNQMMRRRNMTQGRCKPVNT
DDADD RNase 1:              MKESRAKKFQRQHMDSDSSPSSSSTYCNQMMRRRNMTQGDCKPVNT
H12A/K41A/H119A             MKESRAKKFQRQAMDSDSSPSSSSTYCNQMMRRRNMTQGRCAPVNT
FLAG–RNase 1:    MDYKDDDDKKESRAKKFQRQHMDSDSSPSSSSTYCNQMMRRRNMTQGRCKPVNT

wild-type RNase 1:    FVHEPLVDVQNVCFQEKVTCKNGQGNCYKSNSSMHITDCRLTNGSRYPNCAYRT
DDADD RNase 1:        FVHEPLVDVQNVCFQEKVTCKDGQGNCYKSNSSMHITDCRLTADSDYPNCAYRT
H12A/K41A/H119A:      FVHEPLVDVQNVCFQEKVTCKNGQGNCYKSNSSMHITDCRLTNGSRYPNCAYRT
FLAG–RNase 1:         FVHEPLVDVQNVCFQEKVTCKNGQGNCYKSNSSMHITDCRLTNGSRYPNCAYRT

wild-type RNase 1:    SPKERHIIVACEGSPYVPVHFDASVEDST
DDADD RNase 1:        SPKERHIIVACEGSPYVPVHFDASVEDST
H12A/K41A/H119A:      SPKERHIIVACEGSPYVPVAFDASVEDST
FLAG–RNase 1:         SPKERHIIVACEGSPYVPVHFDASVEDST
```

Figure 3.S2. Amino acid sequences of the proteins used in this work. DDADD RNase 1 refers to the R39D/N67D/N88A/G89D/R91D variant. FLAG-tag sequences are in a gray box. Substitutions from wild-type RNase 1 are indicated in red typeface.

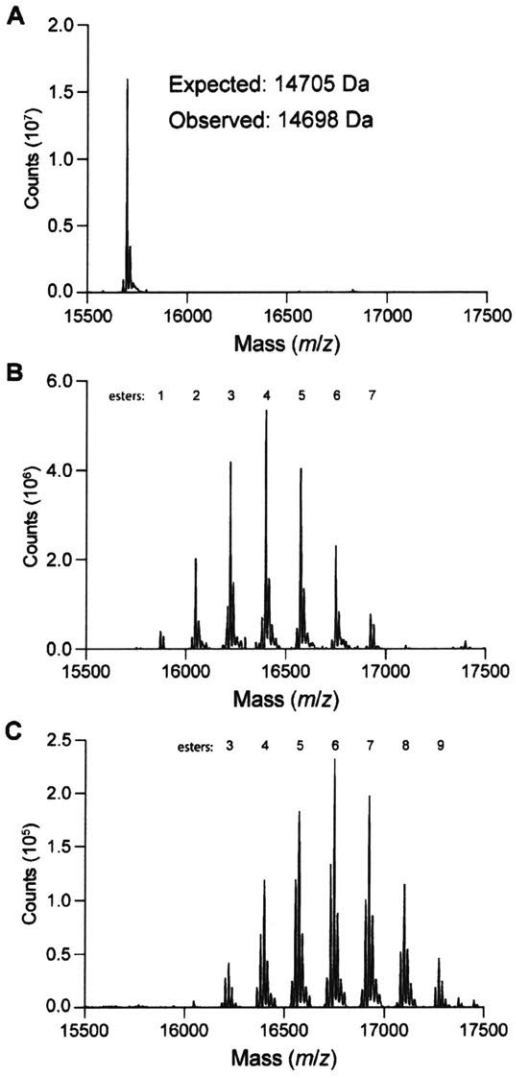
A
Expected: 14705 Da
Observed: 14698 Da
Counts (10^7)
Mass (m/z)
B
esters: 1 2 3 4 5 6 7
Counts (10^6)
Mass (m/z)
C
esters: 3 4 5 6 7 8 9
Counts (10^5)
Mass (m/z)

Figure 3.S3. Deconvoluted ESI mass spectra of wild-type RNase 1. (A) Untreated wild-type RNase 1. (B) Wild-type RNase 1 treated with 100 equiv of diazo compound **1**. (C) Wild-type RNase 1 treated with 200 equiv of diazo compound **1**. The numbers above the spectral peaks report the number of ester groups, each of which adds 175 Da. The most prevalent number of ester groups is listed in Table 3.1.

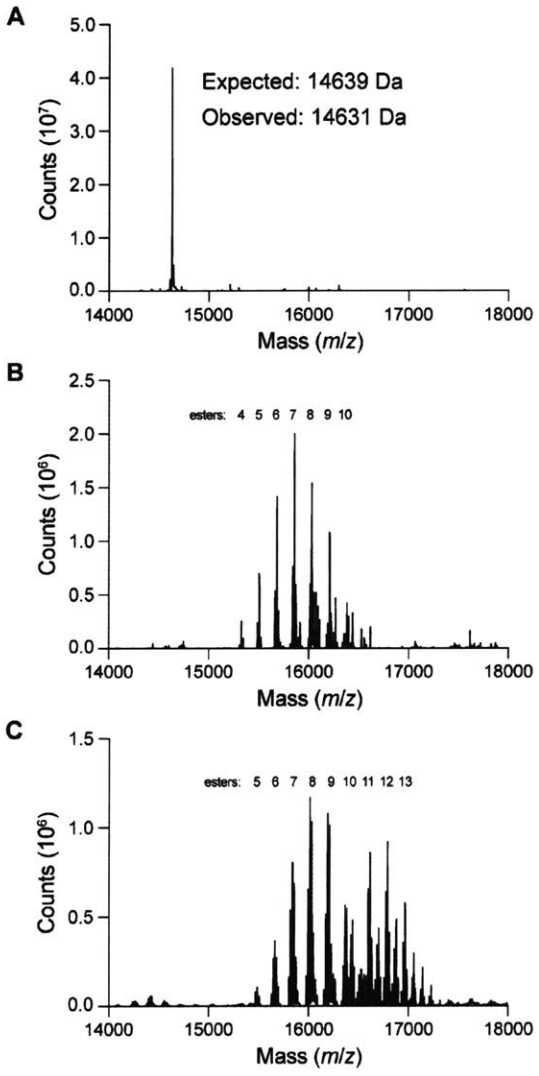
A
Expected: 14639 Da
Observed: 14631 Da
Counts (10^7)
Mass (m/z)
B
esters: 4 5 6 7 8 9 10
Counts (10^6)
Mass (m/z)
C
esters: 5 6 7 8 9 10 11 12 13
Counts (10^6)
Mass (m/z)

Figure 3.S4. Deconvoluted ESI mass spectra of DDADD RNase 1. (A) Untreated DDADD RNase 1. DDADD RNase 1 treated with 100 equiv of diazo compound **1**. (C) DDADD RNase 1 treated with 200 equiv of diazo compound **1**. DDADD RNase 1 refers to the R39D/N67D/N88A/G89D/R91D variant. The numbers above the spectral peaks report the number of ester groups, each of which adds 175 Da. The most prevalent number of ester groups is listed in Table 3.1.

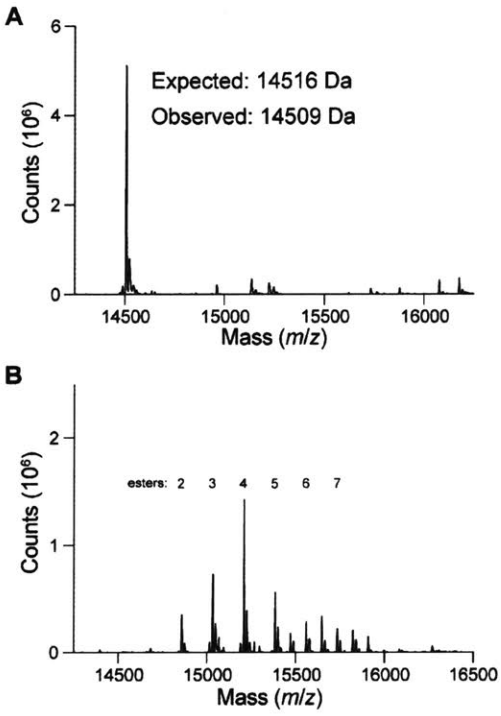
A
Expected: 14516 Da
Observed: 14509 Da
Counts (10^6)
Mass (m/z)
B
esters: 2 3 4 5 6 7
Counts (10^6)
Mass (m/z)

Figure 3.S5. Deconvoluted ESI mass spectra of H12A/K41A/H119A RNase 1. (A) Untreated H12A/K41A/H119A RNase 1. (B) H12A/K41A/H119A RNase 1 treated with 100 equiv of diazo compound **1**. The numbers above the spectral peaks report the number of ester groups, each of which adds 175 Da. The most prevalent number of ester groups is listed in Table 3.1.

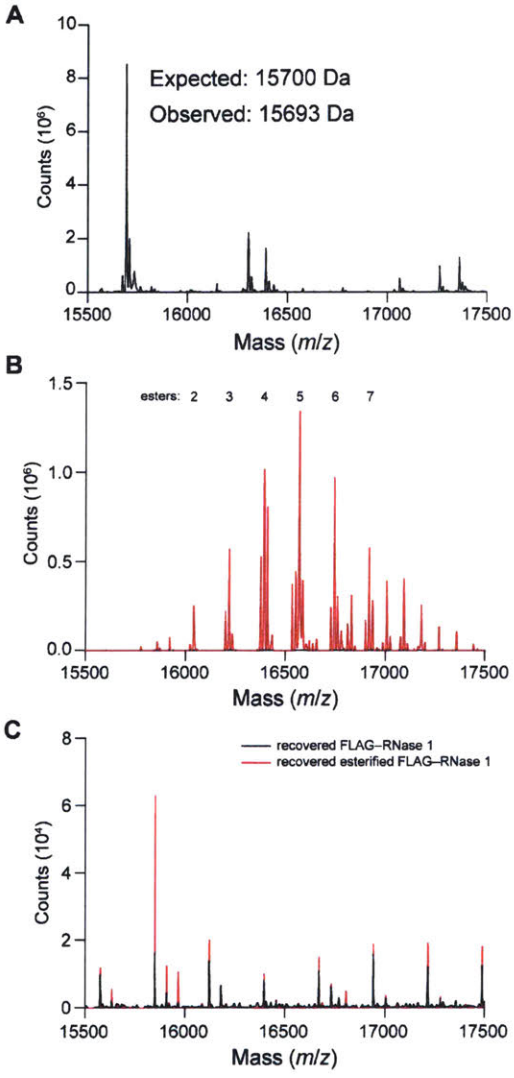
A
Expected: 15700 Da
Observed: 15693 Da
Counts (10^6)
Mass (m/z)
B
esters: 2 3 4 5 6 7
Counts (10^6)
Mass (m/z)
C
recovered FLAG–RNase 1
recovered esterified FLAG–RNase 1
Counts (10^4)
Mass (m/z)

Figure 3.S6. Deconvoluted ESI mass spectra of FLAG–RNase 1 before and after recovery from human cells. (A) Untreated FLAG–RNase 1. (B) FLAG–RNase 1 treated with 100 equiv of diazo compound **1**. (C). Overlay of untreated and treated FLAG–RNase 1 recovered from HeLa cells after a 24-h incubation. The numbers above the spectral peaks report the number of ester groups, each of which adds 175 Da. The most prevalent number of ester groups is listed in Table 3.1. Additional peaks observed in recovered samples correspond to detergents used in the cell lysis.

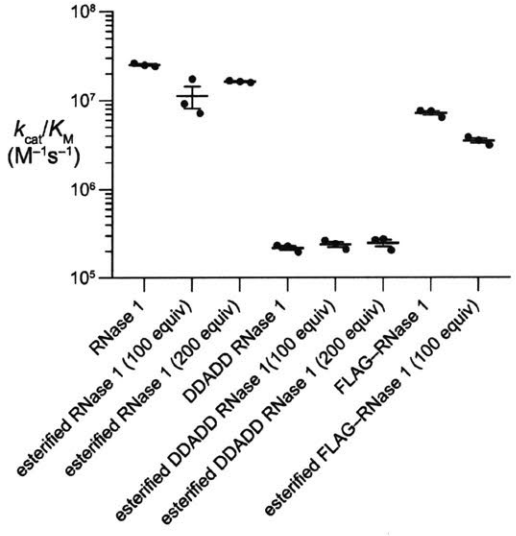
10^8
10^7
10^6
10^5
k_{cat}/K_M
$(M^{-1}s^{-1})$
RNase 1
esterified RNase 1 (100 equiv)
esterified RNase 1 (200 equiv)
DDADD RNase 1
esterified DDADD RNase 1(100 equiv)
esterified DDADD RNase 1 (200 equiv)
FLAG–RNase 1
esterified FLAG–RNase 1 (100 equiv)

Figure 3.S7. Graph of the values of k_{cat}/K_M for the enzymes used in this work, determined for the cleavage of 6-FAM–dArU(dA)$_2$–6-TAMRA at pH 7.5 and 25 °C.

Chapter 4

Conjugation to Dextran Enables a Protein to Enter the Cytosol

Contributions: I designed and conducted all cell biology experiments. H. Kilgore selected CytoC as a payload, then produced and characterized the CytoC-dextran conjugates.

4.1 Abstract

Glycosylation is the most common post-translational modification of proteins, altering both their physicochemical and biological properties. Glycosylation has been exploited as a strategy for enhancing the serum lifetime and thermodynamic stability of a protein. Here, we demonstrate that appending a polysaccharide endows a protein with access to the cytosol. Specifically, we use assays of cellular viability and caspase activity to show that cytochrome C, when functionalized with dextran, is cytotoxic and that its cytotoxicity results from the caspase-mediated intrinsic apoptosis pathway. These data demonstrate a new practical utility of protein glycosylation.

4.2 Introduction

Proteins have the capacity to effect significantly more complex and specific actions than do small molecules. Indeed, an increasing number of drugs are proteins, essentially all of which act upon extracellular targets.[216] The vast pool of intracellular therapeutic targets are beyond approach due to the intrinsic difficulty of gaining access to the cytosol and cellular organelles.[217] The past two decades have seen numerous methods developed for increasing cytosolic delivery.[218] Many of these methods induced undesirable responses in animal models or lead to inefficient cytosolic entry. Subsequently there is continued interest in developing technologies to endow cytosolic access.[100] An unexplored area in this landscape is conjugation to polysaccharides. Recently, we discovered 100-kDa monofunctionalized dextrans conjugated to a fluorogenic probe penetrate into cells.[144] This discovery prompted us to investigate whether dextrans can transport a protein into cells.

First described in the fermentation products of wine by Louis Pasteur,[219] dextrans are a widely employed class of polysaccharides with applications ranging from antithrombotics to biomolecular purifications.[138, 219-221] *Leuconostoc* and *Streptococcus*, among other bacterial and fungal genera are well-established sources of dextran polysaccharides.[222-223] Dextrans are synthesized through polymerization of glucose by glycosyl transfer from sucrose, forming a primarily α-1,6-linked polymer of glucose. Dextransucrases (EC 2.4.1.5) catalyze the glycosyl transfer reaction that yields dextrans, and can introduce occasional branches at the 3- and 4-positions of the constituent glucose monomers. The frequency and length of these branches on the polysaccharide core is dependent on the synthesizing dextransucrase.[222] A suite of degradative enzymes exist, facilitating the use of these polysaccharides by organisms as an energy storage mechanism and a method for producing an environment with ideal physical

properties.[224] The biological roles of dextrans have been sparsely studied by the higher resolution afforded with modern techniques. We sought a protein to conjugate with dextran which is impermeable to biological membranes, but readily adapted to assays for cytosolic delivery.

Cytochrome C (CytoC) is a critical element in both the homeostasis and apoptosis of a cell. In homeostasis, it affects electron transfer in the oxidative phosphorylation pathway facilitating the synthesis of adenosine triphosphate (ATP).[150] In apoptosis, pro-apoptotic stimuli induce the release of CytoC from the mitochrondrial intermembrane (MIM) space to the cytosol.[225] Liberated CytoC binds to apoptosome activating factor 1 (APAF1), which heptamerizes to form an apoptosome. Activation of caspase-8 by the apoptosome actuates caspase-3 and caspase-7, leading to apoptosis. Although CytoC is present in high concentrations in the MIM space, its lethality likely deters its spontaneous crossing of a membrane. Towards that end, CytoC has an exceptionally large dipole moment of μ = 320 D,[150,225,152] and has binding sites that actuate binding with phosphoryl and cardiolipin head groups.[226-230] These attributes render CytoC as a challenging target for cytosolic delivery and an ideal protein for our purpose (Figure 4.1A).

We chose a strategy to control the extent of labeling in order to conjugate CytoC to dextran. To install a site on CytoC for conjugation, we transferred diazo groups to a lysine side chain by using imidazole-*N*-sulfonyl azide and a Cu(II) catalyst in PBS, which avoids harsher conditions used previously.[231] Mass spectrometry indicated a yield of 45% with <10% of the protein reacting twice (Figure 4.1B, Figure 4.S2). We then employed a bifunctional linker strategy incorporating biorthogonal strain-promoted azide–alkyne cycloaddition (SPAAC) and maleimide conjugation techniques to prepare monofunctionalized 100 kDa CytoC–dextran conjugates (Figure 4.1B).

4.3 Methods

4.3.1. Materials

Monothiol dextran (100-kDa, **D1**) was from Fina Biosolutions (Rockville, MD). All other materials were from Sigma–Aldrich (St. Louis, MO), Fischer Scientific (Hampton, NH), or Alfa Aesar (Haverhill MA), and were used without further purification. Phosphate-buffered saline (PBS) contained Na_2HPO_4 (10 mM), KH_2PO_4 (1.8 mM), NaCl (137 mM), and KCl (2.7 mM) at pH 7.3.

4.3.2 Conditions

All procedures were performed at room temperature (~22 °C) and ambient pressure (1.0 atm) unless noted otherwise.

4.3.3 Mass spectrometry

Mass spectrometric analysis of compounds was performed with a 6530 Quadrupole time-of-flight mass spectrometer from Agilent (Santa Clara, CA) after separation by reversed-phase chromatography. Compounds were eluted from an Agilent PLRP-S 1000-Å 5-μm 2.1 × 50 mm column at 85 °C with an acetonitrile/water gradient containing formic acid (0.1% w/v) at 0.55 mL/min. The formic acid, water, and acetonitrile were Fisher Scientific Optima LC/MS grade. Charge envelopes from intact proteins were deconvoluted with Agilent Qualitative Analysis version B07 software. Protein digests were analyzed with the program BioConfirm version B08. Data were exported and plotted using Prism 7 software from GraphPad (San Diego, CA).

4.3.4 Protein concentrations

The concentration of aqueous solutions of CytoC and CytoC–dextran conjugates was determined by UV–Vis absorbance measurements using an extinction coefficient of ε_{max} = 106,000 $M^{-1} \cdot cm^{-1} \cdot$ at 410 nm.[232] Absorbance was measured with a Cary 60 UV–vis spectrophotometer from Agilent.

4.3.5 High performance liquid chromatography

Size-exclusion chromatography was performed with a reversed-phase 1200 system from Agilent that was equipped with refractive index and photodiode array detectors. Analytes were applied to an AdvanceBio SEC 130-Å 2.7-μm, 4.6 × 150 mm size-exclusion column from Agilent with 100 mM sodium phosphate buffer, pH 7.3, at a flow rate of 0.200 mL/min and a column temperature of 30 °C.

4.3.6 Mammalian cell culture

HeLa cells were obtained from American Type Culture Collection (Manassas, VA) and were maintained according to recommended instructions. Gibco brand Dulbecco's Modified Eagle Medium (DMEM), RPMI 1640 medium, (FBS), trypsin (0.25% w/v), OptiMEM, and Dulbecco's PBS were from Thermo Fisher Scientific (Waltham, MA). Cells were grown in DMEM containing fetal bovine serum (FBS) (10% v/v), penicillin (100 units/mL), and streptomycin (100 μg/mL) at 37 °C under 5% (v/v) CO_2(g).

4.3.7 Assays of cell viability

Cell viability assays were performed with the CellTiter 96 AQueous One Solution Cell Proliferation Assay from Promega (Madison, WI), which is a tetrazolium dye-based assay for metabolic activity. Cells were grown, treated, and assessed as described previously. Briefly, HeLa cells were plated at 50,000 cells per well in a 96-well plate. After 24 h, the medium was replaced with FBS-free DMEM containing various concentrations of proteins. All cells were then allowed to incubate for another 48 h before the addition of the MTS reagent and data collection. Data were analyzed with the program Prism from GraphPad (La Jolla, CA). Values of EC_{50}, which is the concentration of analyte that gives half-maximal cell viability, were calculated by using the equation:

$$y = y_{\min} + \frac{(y_{\max} - y_{\min})}{1+\left(\frac{EC_{50}}{x}\right)^{h}} \qquad (1)$$

where y is cell viability, x is the concentration of analyte, and h is the Hill coefficient. All values were the average of at least three biological replicates.

4.3.8 Assays of caspase activation

Activation of cellular caspases was confirmed with CellEvent™ Caspase-3/7 Green Detection Reagent from Thermo Fisher (Waltham, MA), which consists of a four-amino acid peptide (DEVD) conjugated to a nucleic acid-binding fluorescent dye. Cells were grown, treated, and assessed according to the manufacturer's protocol. Briefly, HeLa cells were plated at 50,000 cells per well in a 96-well, black plate. After 24 h, the medium was replaced with FBS-free DMEM containing detection reagent (final concentration: 5 μM) and various concentrations of

proteins. All cells were allowed to incubate for an additional 12 h. Then, fluorescence data was collected with a Tecan M1000 plate reader with excitation at 502 nm and emission at 530 nm. Data were analyzed with the program Prism from GraphPad (La Jolla, CA) and adjusted based on background fluorescence.

4.3.9 Synthesis of imidazole-N-sulfonyl-azide

Imidazole-*N*-sulfonyl azide was synthesized as described previously. H-NMR, (400 MHz, D_2O, δ): 9.42 (q, J = 1.2 Hz, 1H), 7.98 (t, J = 2.0 Hz, 1H), 7.61–7.55 (m, 1H). ^{13}C-NMR (100 MHz, D_2O, δ): 137.65, 122.90, 120.18. HRMS–ESI (*m/z*): $[M - Cl]^+$ calcd for 174.0086; found, 174.0062.

4.3.10 Diazo transfer reactions to proteins

A 10 mg/mL solution of bovine heart CytoC was prepared in PBS. A 150-μL aliquot of PBS was added to a 500-μL Eppendorf tube, followed by 50 μL of the solution of bovine heart cytochrome C. To this solution was added 20 μL of $CuSO_4 \cdot 5H_2O$ (1 mg/mL) in PBS, followed by 2 μL of aqueous imidazole-*N*-sulfonyl azide (100 mg/mL). The resulting solution was mixed by vortexing for 20 s, and then allowed to react overnight with nutation. A number of these aliquots were pooled and dialyzed (3×) against PBS to remove small-molecule reaction byproducts. The extent of labeling was characterized by LC–MS.

4.3.11 Deprotection of dextran monothiol

To 1.0 mL of PBS was added 100-kDa dextran monothiol (18.75 mg, 0.1875 μmol). The reaction mixture was mixed by vortexing and sonicated to dissolve the polysaccharide fully. To

the dissolved and protected polysaccharide was added dithiothreitol (0.375 μmol) from a 240 μM stock solution in PBS. The mixture was allowed to react overnight before desalting on a PD-10 column. The resulting deprotected monothiol-100kDa dextran was then used immediately.

4.3.12 Conjugation of monothiol dextran to protein

To 1.0 mL of PBS was added 100 μL of a 600 μM solution that contains CytoC azide (60 nmol), which is 45% of the total CytoC according to LC–MS, and the resulting solution was mixed by vortexing. To this solution was added 40 μL of a 1.5 mM solution of DBCO–PEG_4–maleimide (60 nmol) in PBS. To this mixture was added 0.1875 μmol of monothiol dextran. The resulting solution was mixed by vortexing for 30 s and then allowed to react overnight with nutation. Then, the reaction mixture was subjected to desalting on a PD-10 desalting column and concentrated with 10-kDa molecular weight cut-off spin-concentrator. The extent of labeling was measured by HPLC fitted with a size-exclusion column (*vide supra*).

4.4 Results

4.4.1 Dextran labeling approach

The robust reactivity of SPAAC and maleimide chemistry prompted us to utilize a dibenzyl cyclooctyne–PEG_4–maleimide linker (Figure 4.S3, 4.S5), resulting in the production of a heterogenous mixture of CytoC–dextran conjugate and unlabeled CytoC (Figure 4.S6). Comparisons of the CytoC–dextran conjugate solution to an equimolar mixture of CytoC and protected monothiol 100-kDa dextran demonstrate the completion of the reaction (Figure 4.S6, S7). Integration of peaks at t_R = 3.5 min and t_R = 5 min in 410 nm absorbance channel enabled us to estimate that the total population of CytoC–dextran conjugate in the mixture is 36% of the

total CytoC content. We proceeded to perform cytotoxicity assays with this mixture of CytoC–dextran and CytoC without further purification.

4.4.2 Conjugation of CytoC with dextran imbues cytotoxicity towards HeLa

We performed cytotoxicity assays with HeLa cells across a range of CytoC–dextran conjugate concentrations while controlling for the potential toxicity of free dextran or CytoC. Our measurements indicate that CytoC–dextran conjugates are cytotoxic with an IC_{50} of 10 μM (Figure 4.2A). This value is, however, an over-estimate, as the concentration is calculated from the molar absorptivity of CytoC at the isobestic point (410 nm) and only 35% of the CytoC in solution is conjugated to a dextran. We anticipate the true IC_{50} of our conjugate is in the low micromolar range. Treatment with dextran or CytoC alone did not lead to a loss in cell viability (Figures 4.2B and 4.2C). Likewise, treatment with CytoC and dextran mixed at equimolar concentrations did not elicit cytotoxicity (Figure 4.2D).

Literature comparisons on the cytotoxicity of CytoC–dextran are difficult to draw a direct comparison to the experiments performed here. Typical strategies for delivering CytoC into the cytosol require the formation of complexes with nanoparticles, which do not allow for a direct IC_{50} comparison with single protein methods.[233-235] A few examples of protein–protein conjugates in which CytoC is linked to a protein meant to enhance cytosolic delivery have been prepared, but the IC_{50} values are generally an order of magnitude greater. These studies do, though, confirm the recalcitrance of free CytoC to cytosolic delivery.[236-238]

4.4.3 CytoC–dextran conjugates trigger apoptosis in cytosol

Next, we sought to establish that the loss of cell viability was attributable to the activation of the intrinsic apoptosis pathway by our CytoC–dextran conjugates. To do so, we employed a fluorogenic Caspase3/7 probe, CellEvent Caspase-3/7, to demonstrate whether cells were in an apoptotic state. Activation of this probe occurs upon DEVD peptide cleavage by Caspase3/7, allowing a covalently bound fluorophore to bind to DNA, which alters its fluorescence. Treatment of HeLa cells with 100 μM resveratrol has been shown to evoke a pro-apoptotic response, serving as a positive control.[239-240] HeLa cells treated with CytoC–dextran conjugates at 30 μM experienced an 8-fold increase in fluorescence signal, relative to treatment with vehicle (PBS) (Figure 4.3). We did not observe a significant difference in fluorescence intensity between treatment with PBS, 30 μM CytoC, 30 μM dextran, or equimolar mixtures of CytoC and dextran at a concentration of 30 μM (Figure 4.3). These data show that CytoC is delivered into the cytosol when functionalized with a dextran, and there activates the intrinsic apoptosis pathway.

Our findings of dextran-conjugate internalization contradict observations made with endosomal tracking reagents, which often employ dextran polysaccharides. This discrepancy could be due to the type of dextran, and the number of labels on the polysaccharide. Typical reagents are prepared through reductive amination, accessing Maillard or Amadori pathways, or cyanoester-based conjugation. The aldehydes needed for reductive amination can impart significant perturbation to dextran structure.[241] Maillard and Amadori pathways lead to polysaccharide scission and yield heterogeneous products.[242] The monofunctionalized dextran conjugates employed herein represent a perturbation that is mild in comparison.

4.5 Discussion

The endosomal escape of large dextrans has been observed previously, but visualization indicated endosomally entrapped and cytosolically dispersed populations.[142,243,143] The results presented here demonstrate that monofunctionalization with dextran provides a far more efficient delivery strategy. In addition to cytosolic access, monofunctionalization of proteins by dextrans could endow several desirable attributes. For example, protein–dextran conjugates are likely to have improved serum half-life, thermodynamic and pH stability; albeit, at a slight cost in conjugate enzyme activity. In addition, a large covalently attached polysaccharide is likely beneficial for classes of drugs aimed at interrupting macromolecular interactions, an application unexplored by other dextran conjugates.

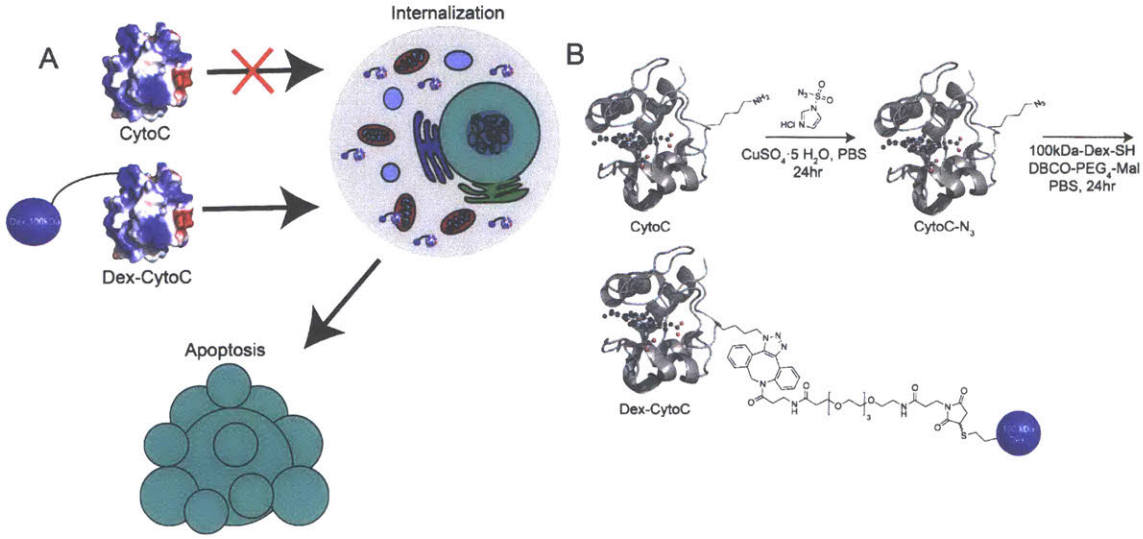
A
CytoC
Internalization
Dex-CytoC
Apoptosis
B
CytoC
CuSO4·5 H2O, PBS
24hr
CytoC-N3
100kDa-Dex-SH
DBCO-PEG4-Mal
PBS, 24hr
Dex-CytoC

Figure 4.1. Protein–dextran conjugates studied herein. (A) Schematic illustration of cytosolic access endowed by conjugation to dextrans. (B) Preparation of CytoC–dextran conjugates.

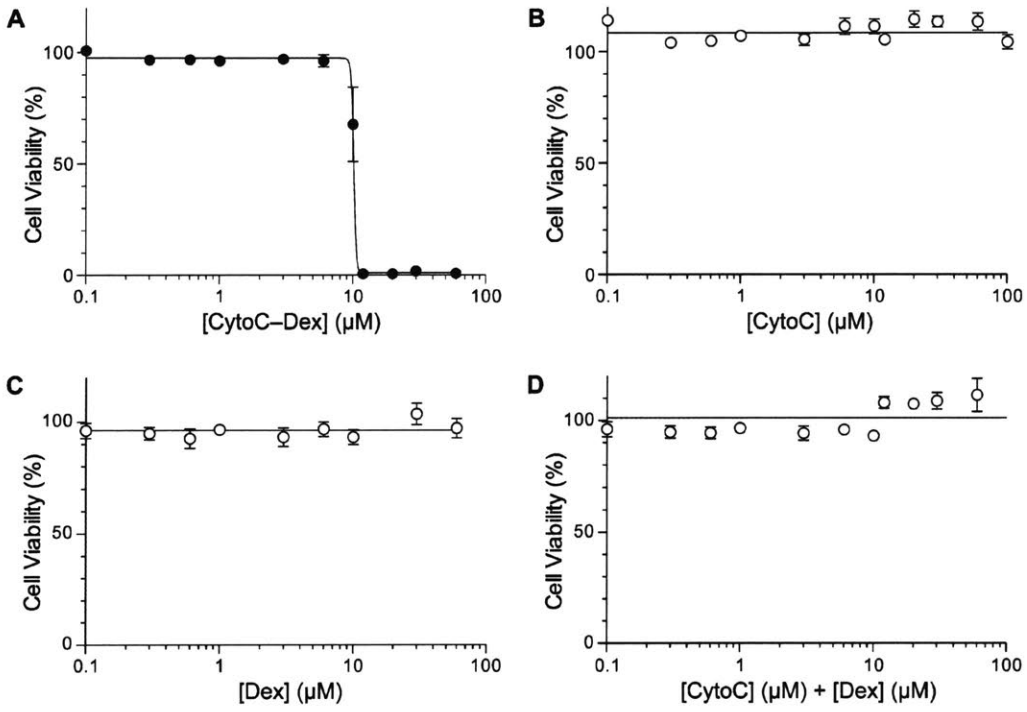
A
B
C
D
Cell Viability (%)
100
50
0
0.1
1
10
100
[CytoC–Dex] (μM)
[CytoC] (μM)
[Dex] (μM)
[CytoC] (μM) + [Dex] (μM)

Figure 4.2. HeLa cell viability after treatment for 48 h with (A) CytoC–dextran conjugate, (B) CytoC alone, (C) dextran alone, and (D) an equimolar mixture of CytoC plus dextran. Biological and technical replicates, $n = 3$.

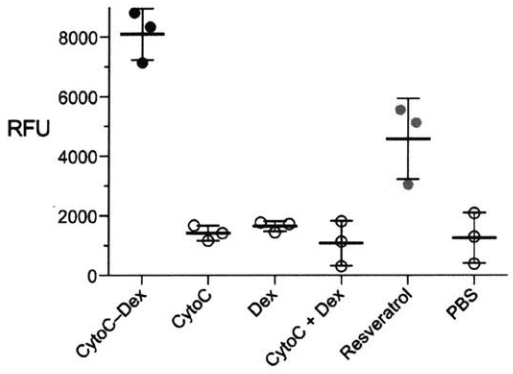
RFU
8000
6000
4000
2000
0
CytoC–Dex
CytoC
Dex
CytoC + Dex
Resveratrol
PBS

Figure 4.3. Relative activation of caspases-3/7 in HeLa cells after treatment for 12 h with CytoC–dextran conjugate (30 μM), CytoC alone (30 μM), dextran alone (30 μM), unconjugated CytoC plus dextran (30 μM each), resveratrol (100 μM), or vehicle (PBS). Technical replicates, $n = 3$; CytoC–dextran versus CytoC, $p = 0.0002$; CytoC–dextran versus resveratrol, $p = 0.0163$.

4.6 Supplemental information

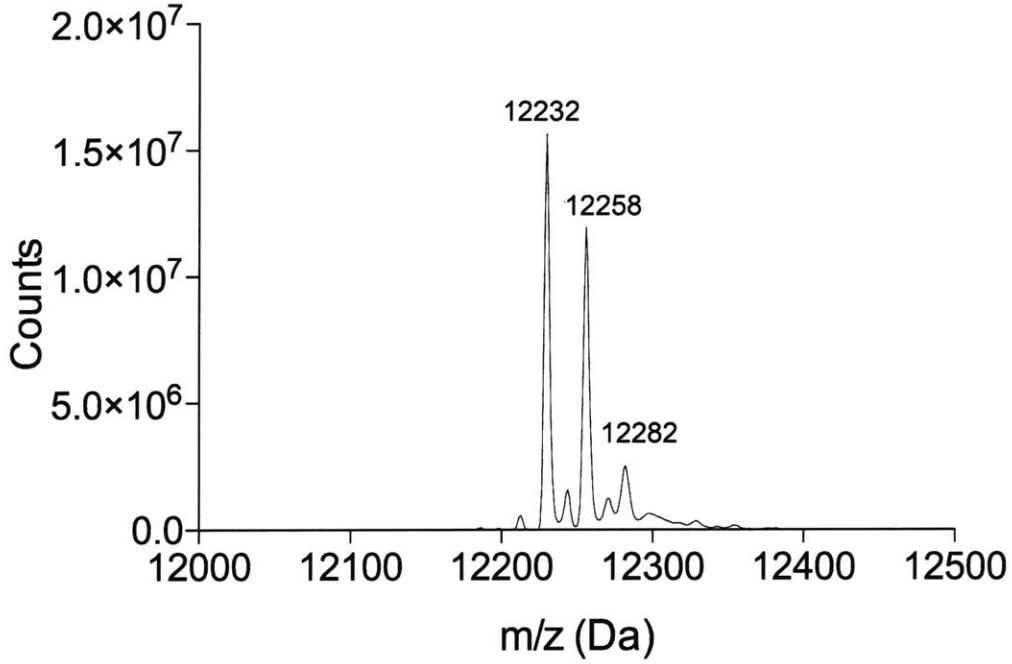

Figure 4.S1. Representative deconvoluted QTOF mass spectrum of CytoC azide.

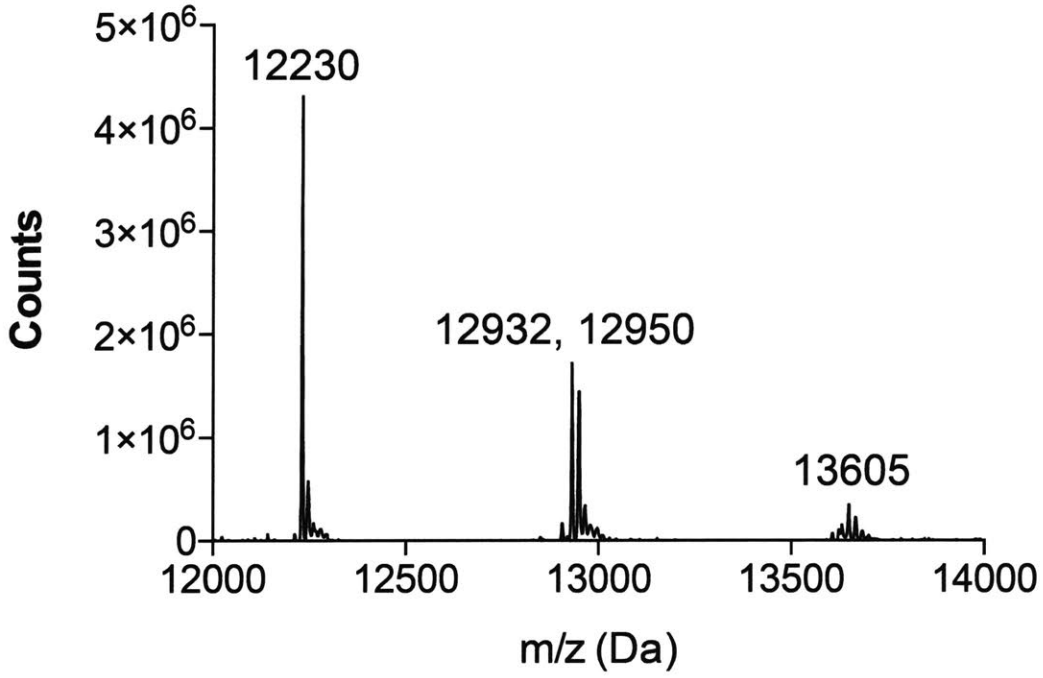
5×10^6
4×10^6
3×10^6
2×10^6
1×10^6
0
Counts
12230
12932, 12950
13605
12000
12500
13000
13500
14000
m/z (Da)

Figure 4.S2. Representative deconvoluted QTOF mass spectrum of Cyto C–DBCO–PEG_4–maleimide.

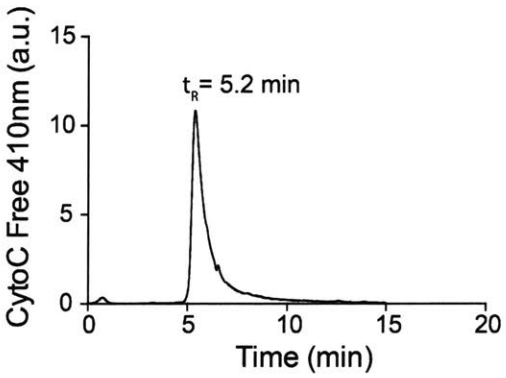
CytoC Free 410nm (a.u.)
15
10
5
0
t_R= 5.2 min
0
5
10
15
20
Time (min)

Figure 4.S3. Chromatogram from the size-exclusion chromatography of CytoC as eluted with 100 mM sodium phosphate buffer, pH 7.3, and monitored by absorbance at 410 nm.

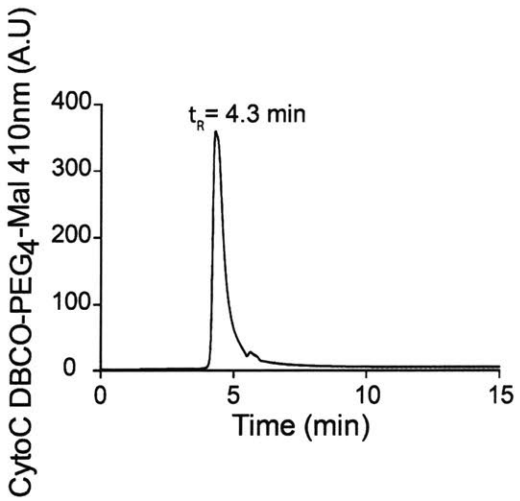
CytoC DBCO-PEG4-Mal 410nm (A.U)
400
300
200
100
0
0
5
10
15
Time (min)
tR= 4.3 min

Figure 4.S4. Chromatogram from the size-exclusion chromatography of CytoC–DBCO–PEG_4–maleimide as eluted with 100 mM sodium phosphate buffer, pH 7.3, and monitored by absorbance at 410 nm.

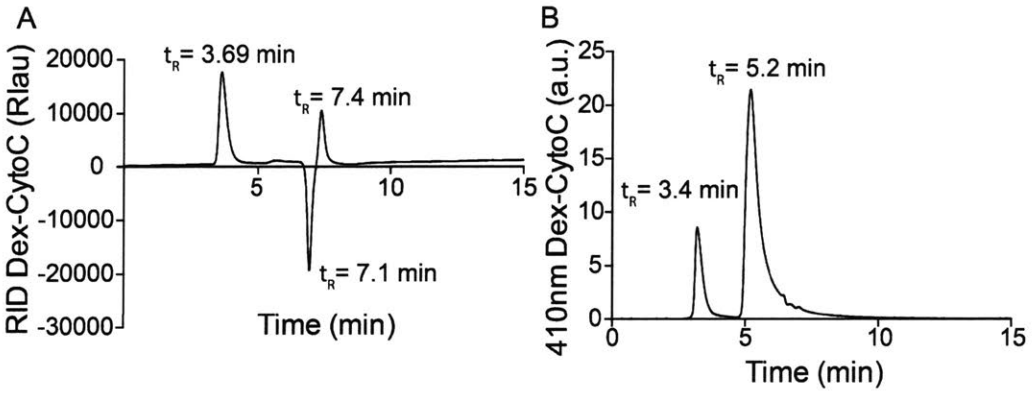
A
RID Dex-CytoC (Rlau)
20000
10000
0
-10000
-20000
-30000
t_R= 3.69 min
t_R= 7.4 min
t_R= 7.1 min
5
10
15
Time (min)
B
410nm Dex-CytoC (a.u.)
25
20
15
10
5
0
t_R= 5.2 min
t_R= 3.4 min
0
5
10
15
Time (min)

Figure 4.S5. Chromatograms from the size-exclusion chromatography of CytoC–dextran conjugate as eluted with 100 mM sodium phosphate buffer, pH 7.3, and monitored by refractive index (A) or absorbance at 410 nm (B).

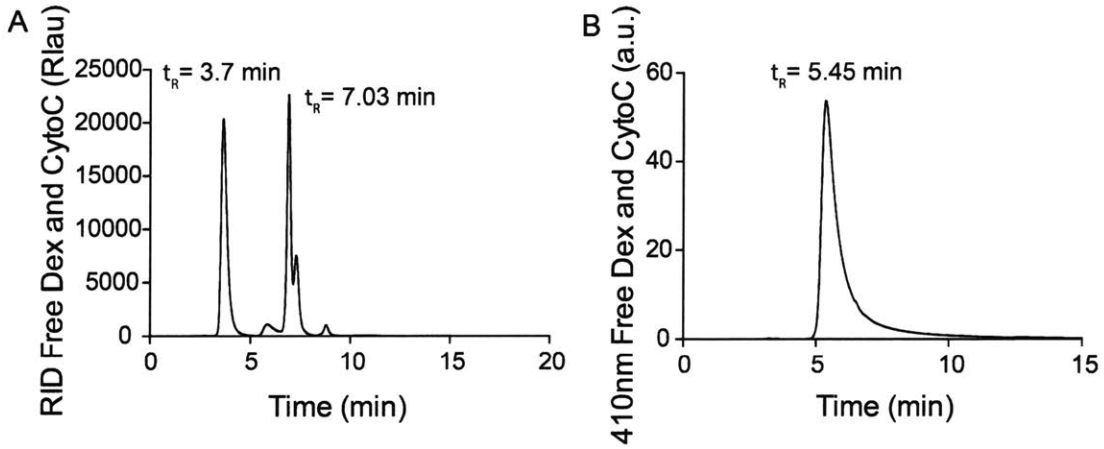
A
RID Free Dex and CytoC (Rlau)
25000
20000
15000
10000
5000
0
t_R= 3.7 min
t_R= 7.03 min
0
5
10
15
20
Time (min)
B
410nm Free Dex and CytoC (a.u.)
60
40
20
0
t_R= 5.45 min
0
5
10
15
Time (min)

Figure 4.S6. Chromatograms from the size-exclusion chromatography of equimolar free dextran and CytoC as eluted with 100 mM sodium phosphate buffer, pH 7.3, and monitored by refractive index (A) or absorbance at 410 nm (B).

^{1}H NMR (D_2O) and ^{13}C NMR (D_2O) Spectra of Imidazole-*N*-Sulfonyl Azide·HCl

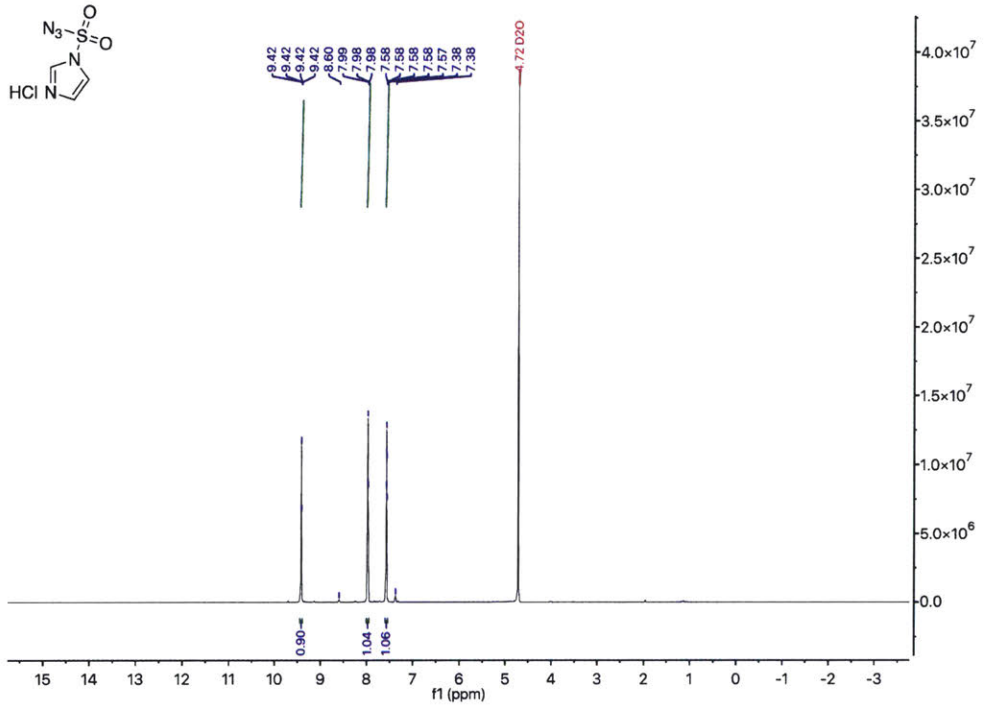

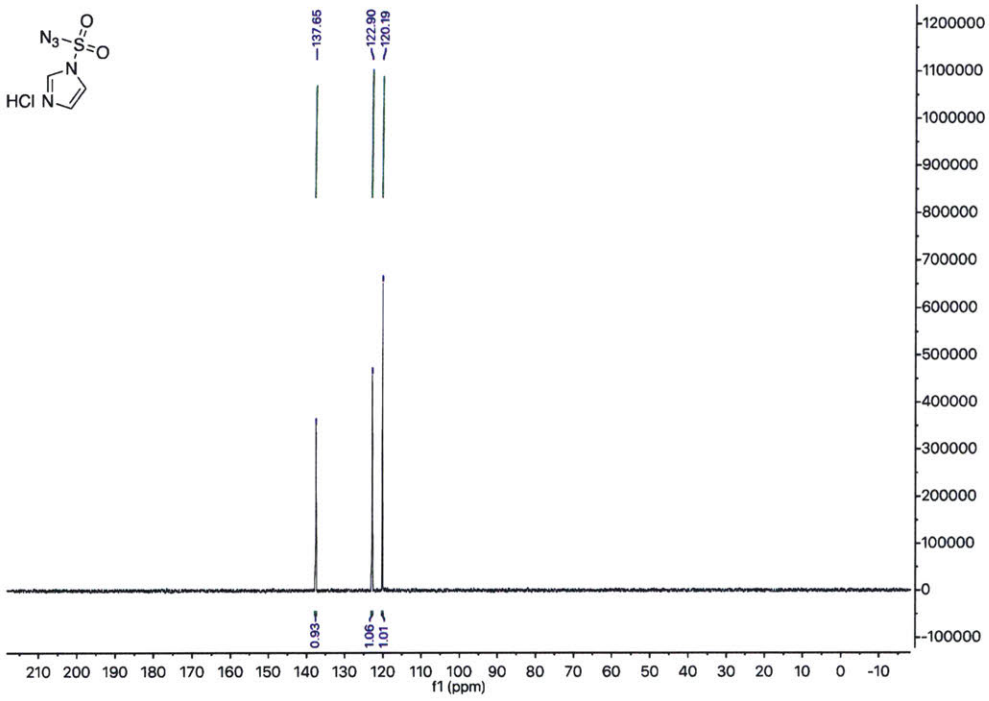

Chapter 5

Conclusions and Future Directions

5.1 Conclusions

Pancreatic-type ribonucleases (ptRNases), and RNase 1, in particular, have been extensively characterized and have demonstrated therapeutic potential against cancer as well as other conditions. Differential glycosylation of RNase 1 *in vivo* has been associated with certain disease states and pursued as a potential biomarker, yet many mysteries remain regarding the biochemical implications of RNase 1 glycosylation. Extensive efforts have focused on developing ptRNase-based therapeutics, but their effectiveness relies on accessing intracellular targets a common limitation for protein-based approaches. As a model protein and cytotoxin, RNase 1 is an ideal candidate for developing and evaluating cellular delivery strategies. The central aim of this thesis was to demonstrate the versatile biological potential of RNase 1 by showcasing its remarkable properties as a glycoprotein and a potent cytotoxin.

In Chapter 2, I described the first production and characterization of human RNase 1 glycoforms with all possible permutations of endogenous *N*-glycosylation. Previous studies have noted that protein glycosylation may significantly enhance pharmacokinetic properties,[179] such as stability,[244] and has inspired glycoengineering of therapeutically-relevant proteins.[146] My work confirms this trend extends to human RNase 1, with *N*-glycosylation enhancing stability towards thermal and proteolytic degradation, but reducing enzymatic activity. Interestingly, of the observed sequons of RNase 1, Asn34 has emerged as the most widely conserved across mammalian species[43, 169] and has displayed the highest glycan occupancy level in different biological samples.[42] I find that, of the different RNase 1 glycoforms, only glycosylation of Asn34 in human RNase 1 improves overall protein stability while maintaining robust catalytic activity.

In Chapter 3, I utilized a previously developed chemical biology tool[136] to deliver functional, native protein cytotoxins to the cellular cytosol. Proteins represent an expanding landscape within therapeutics, yet most do not cross the cellular membrane and are limited to targeting extracellular targets.[100, 196] Previous work has identified a diazo compound that readily masks protein carboxylates for improved cytosolic delivery[137]. I demonstrated the effectiveness of this masking strategy for the delivery of functional RNase 1 enzymes that act on cellular RNA substrates, thus triggering apoptosis.[202, 245] The cytotoxicity of wild-type RNase 1 and a previously impermeable RNase 1 variant[76] was drastically enhanced by diazo-based esterification of protein side chains. Recovery of a labeled RNase variant after cellular uptake confirmed the complete removal of the appended ester labels.

In Chapter 4, I presented conjugation of a dextran polysaccharide as an intracellular delivery system with a model protein, CytoC. Synthetic glycoengineering has gained traction for improvement of the serum-half life and thermodynamic stability of protein therapeutics.[246-247] Recent work demonstrated that a large monofunctionalized dextran conjugated with a fluorogenic probe displayed unusually high cytosolic entry[144] and could serve as an intracellular delivery platform for protein payloads. A model protein and known inducer of apoptosis[225], CytoC, was selected for delivery given its inability to penetrate cellular membranes[152] without further functionalization.[150, 234, 248] I reported that the covalent functionalization of CytoC with a unique dextran polysaccharide facilitated cytosolic delivery of the protein-conjugate, eliciting cell death through activation of the intrinsic apoptosis pathway. Cell viability measurements demonstrated that dextran–protein conjugation was critical for internalization and cytotoxicity. A caspase-specific assay confirmed that the dextran–protein conjugate activated the intrinsic apoptosis pathway, as expected based on other reports of CytoC delivery.[233]

5.2 Future directions

5.2.1: Biophysical implications of RNase 1 glycosylation

As described in Chapter 2, I identified biochemical differences between different human RNase 1 glycoforms, specifically in terms of protein stability and catalytic activity. These results indicate that the individual glycosylation sites of RNase 1 are unique from one another, inducing distinct alterations to the protein core. Further biophysical characterization of mono-glycosylated RNase 1 might aid in the interpretation of the observed biochemical attributes.

Glycosylation is one of the most common post-translational modifications in the human proteome yet glycoproteins remain a challenging target for structural studies.[171, 249] The inherent heterogeneity of most glycoprotein samples and the high degree of flexibility within glycans hinder glycoprotein structural determination, especially by X-ray crystallography.[250] To this end, small angle X-ray scattering (SAXS) has emerged as a powerful tool to examine disordered macromolecules in their native solution state.[251] I propose to use the well-defined structural data of RNase 1 to generate all-atoms models of each glycosylated protein to reveal the approximate spatial occupancy of each glycan chain in solution. Similar structural work with RNase A and its glycoform RNase B demonstrated that the single glycan chain attached at Asn34 is localized close to the protein surface.[244, 252] Position 34 is likewise *N*-glycosylated in human RNase 1, and I hypothesize that it might display similar interactions between the carbohydrate chain and the protein core. The remaining two glycosylation sites of human RNase 1, Asn76 and Asn88, evolved more recently in primates[43] and will provide new insights into the biophysical effects of glycosylation. SAXS data of RNase 1 glycoforms, combined with dynamic and static light scattering measurements, might elucidate protein structural changes related to glycosylation position and environment.

5.2.2: Role of glycosylation in RNase 1 secretion

I characterized the biochemical profiles of RNase 1 glycoforms *in vitro* after production in a yeast-based system, yet many unanswered questions remain regarding the biological role of glycosylation as RNase 1 traverses the protein secretory pathway. Protein glycosylation requires a highly orchestrated assembly line for glycan attachment and maturation from the endoplasmic reticulum (ER) through the Golgi.[3, 253] Growing evidence suggests that protein glycosylation might be crucial for biological recognition in the secretory pathway as the glycan structures influence protein folding,[254] serve as ligands for lectin chaperones,[255] aid in quality control surveillance, and mediate targeted secretion.[3]

Expression studies of human RNase 1 in CHO cells indicated rapid maturation and progression of all glycoforms through the secretory pathway.[57] These findings were consistent with observations from biological samples in which the three glycosylation sites of human RNase 1 were differentially occupied depending on tissue and cell-type.[41, 50, 166] I hypothesize that glycosylation of RNase 1 might improve the efficiency of its secretion into the extracellular matrix. To test this hypothesis, RNase 1 variants could be expressed in cells and analyzed for folding and secretion using pulse-chase methods, specifically the wild-type RNase 1 with three glycosylation sites (NNN) or an aglycosylated variant with all three sites removed by mutagenesis (QQQ). A human influenza hemagglutinin (HA) tag or a FLAG tag could be appended to human RNase 1 variants to distinguish these proteins from endogenous RNases and to aid in recovery after secretion.[256] The information gained from the pulse-chase analysis combined with our previously developed hypersensitive RNase substrate could provide valuable insight into the impact of glycosylation on RNase 1 processing and secretion.[175] The recovered tagged-RNase 1 variants could also be analyzed for additional modifications, such as the

unexpected phosphorylation pattern we observed in Chapter 2 with RNase 1 glycoforms expressed in yeast.

5.2.3: Probing the integrity of the protein secretory pathway

Protein secretion requires newly synthesized proteins to pass through multiple cellular compartments via transport vesicles. Whereas the secretory pathway appears to be tightly monitored and regulated,[257-258] unanswered questions remain regarding the integrity of this highly dynamic process. Secreted proteins such as RNase 1 might be able to escape into the cytosol during the secretion process, specifically when various stressors disrupt cellular homeostasis.[259-261] In the case of RNase 1 leaking into the cytosol, the endogenous RI would bind to the ptRNase with high affinity, thereby protecting the cell.[22]

I propose to examine the secretion of RNase 1 in cells lacking cytosolic RI as a means to probe the integrity of the secretory pathway. Previous work to characterize an RI knockout cell line demonstrated that it was especially susceptible to exogenous RNases.[174] The *ΔRNH1* cells express and secrete endogenous ptRNases, but the levels were insufficient to trigger apoptosis leading to no observable change in cell growth.[174] Increasing the production of RNase 1 through transient transfection might overwhelm the secretory system enough to cause protein leakage and trigger cell death. This work could reveal a previously unappreciated role for RI in protecting the cell not only from exogenous ptRNases, but also from ptRNases that escape the secretory pathway.

5.2.4: Investigating cellular internalization of esterified RNase

As described in Chapter 3, the bioreversible esterification of RNase 1 variants drastically enhanced cytotoxicity towards HeLa cells. Interestingly, esterification of wild-type RNase 1 carboxylates reduced cell viability even in the presence of the endogenous inhibitor protein, RI. Previous studies have identified RI as an intracellular "sentry" that readily binds ptRNases, thereby constraining their potency as cytotoxins.[208] I hypothesize that diazo-mediated esterification of RNase 1 might enhance internalization enough to overwhelm the endogenous levels of cellular RI. The appended labels might also confer some level of RI-evasiveness, depending on the kinetics of cellular esterase cleavage.

Fluorescently labeled ptRNases have served as adaptable tools for a variety of biological assays, including cellular internalization. To facilitate the attachment of a fluorophore, a cysteine residue can be installed at position 19 of RNase 1 using site-directed mutagenesis. Position 19 presents an optimal location for fluorescent labeling since this residue occurs in a solvated loop that is inconsequential for stability or catalytic activity.[262] The uptake of fluorescent RNase 1 conjugates into live cells can be visualized with fluorescence microscopy. The internalization rates for labeled and unlabeled RNase 1 can be quantified and compared with flow cytometry.

As mentioned in Chapter 3, ptRNases access the cytosol via multiple pathways that involve clathrin-coated vesicles and macropinosomes.[77] Esterification with a hydrophobic diazo-based compound might provide an alternate mechanism as seen by internalization of esterified GFP at 4 °C, indicating that uptake was driven by passing directly through the plasma membrane.[137] To probe the mechanism of entry for esterified RNases, uptake could be monitored by blocking specific components of endocytic pathways with pharmacological agents.[263] The uptake of labeled or unlabeled RNase 1 in the presence of endocytic inhibitors can be examined

qualitatively by confocal microscopy and quantitatively by using flow cytometry.[77] Increased cellular uptake of esterified RNase 1 relative to unlabeled protein in the presence of endocytic inhibitors would suggest that esterification with a diazo compound engenders delivery across the plasma membrane, similar to a prodrug.[264] Understanding the mechanism of esterified protein internalization would further expand the applications of this delivery strategy.

5.2.5: Probing dextran-based protein delivery

While synthetic glycosylation of proteins has been pursued as a strategy to enhance pharmacokinetic properties, we find that we can also exploit polysaccharide-protein conjugates to access intracellular targets. Using a previously anointed monofunctionalized dextran, we delivered therapeutically relevant, model proteins into cells.[144] The cytotoxicity associated with dextran-functionalized CytoC resulted from interactions in the cytosol that triggered the intrinsic apoptosis pathway, however previous work has demonstrated the ability of dextran-functionalized dyes to enter the nucleus as well.

I propose that dextran conjugation could enable nuclear delivery of a powerful, therapeutic payload such as RNase 1. The ability of human RNase 1 to degrade a variety of double-stranded RNA substrates makes it an ideal candidate for targeted delivery to the nucleus.[39] This strategy would mimic the endogenous actions of another human RNase, ANG, which uses an innate nuclear localization sequence (NLS) to target a nucleolar substrate.[20] Fluorescently labeled RNase 1 could be conjugated to dextran then monitored by confocal microscopy to confirm localization to the nucleus. Delivery of such a robust enzyme to the nucleus could induce cell death at sub-micromolar concentrations.

Appendix 1

Human Angiogenin is a Potent Cytotoxin in the Absence of Ribonuclease Inhibitor

*This chapter has been published in part, under the same title. Reference: Thomas, S.P.; Hoang, T.H.; Ressler, V.T.; and Raines, R.T. Human Angiogenin is a Potent Cytotoxin in the Absence of Ribonuclease Inhibitor. *RNA* **24**, 1018-1027.

Contributions: I performed control cell viability assays after transfections with phosphor-RNAs seen in Figure 6.4.

6.1 Abstract

Angiogenin (ANG) is a secretory ribonuclease that promotes the proliferation of endothelial cells, leading to angiogenesis. This function relies on its ribonucleolytic activity, which is low for simple RNA substrates. Upon entry into the cytosol, ANG is sequestered by the ribonuclease inhibitor protein (RNH1). We find that ANG is a potent cytotoxin for *RNH1*-knockout HeLa cells, belying its inefficiency as a nonspecific catalyst. The toxicity does, however, rely on the ribonucleolytic activity of ANG and a cytosolic localization, which lead to the accumulation of particular tRNA fragments (tRFs), such as tRF-5 Gly-GCC. These up-regulated tRFs are highly cytotoxic at physiological concentrations. Although ANG is well-known for its promotion of cell growth, our results reveal that ANG can also cause cell death.

6.2 Introduction

Angiogenin (ANG) is a protein in the pancreatic-type ribonuclease (ptRNase) superfamily. Early-on, ANG was identified as a promoter of neovascularization in human tumors [265]. For the past three decades, this ribonuclease has continued to be implicated in new biological processes, from reproduction to inflammation to neuroprotection [266-269]. Although the diversity of its roles is unique in the ptRNase superfamily, ANG does share many fundamental properties with other ptRNases, such as catalysis of RNA cleavage after pyrimidine residues and a high affinity for the cytosolic ribonuclease inhibitor protein (RNH1). Still, ANG is best described by its differences.[73, 270-271] Unlike other RNases, ANG has a cell-surface receptor, and is readily endocytosed into human cells [272-274]. ANG also contains a nuclear localization signal (NLS), and is known to act on both cytosolic and nuclear RNAs [20, 275-276]. Most strikingly, ANG exhibits 10^4-fold less activity than typical ptRNases towards simple RNA substrates [173, 277]. Thus, whereas most RNases degrade RNA efficiently and promiscuously in the extracellular matrix, ANG has adapted to perform specific, sensitive tasks inside the cell.

One of the recently discovered actions of ANG is to generate tRNA-derived small RNA fragments (tRFs) in stressed cells. Under normal growth conditions, ANG localizes in the nucleolus and promotes rDNA transcription by cleaving promoter-associated RNA [20]. In contrast, hypoxia and starvation cause ANG to localize to stress granules [278-279]. Within these granules, ANG cleaves the anticodon loop of tRNAs, producing tRFs [280-282]. These tRFs perform diverse cellular functions, such as participating in translational silencing or degrading specific mRNAs by an RNAi-like mechanism [281, 283-285], though a complete understanding is not at hand [269].

ANG function is regulated tightly *in cellulo*. RNH1 binds to ANG with femtomolar affinity, inactivating its ribonucleolytic activity [22, 279, 286]. RNH1 contains 32 cysteine residues, all of which must be reduced for RHN1 to retain its function [287-289]. Because RNH1 resides in the cytosol and most ptRNases carry out their functions in the extracellular matrix, RNH1 acts as an "intercellular sentry", protecting cellular RNA from degradation by endocytosed ptRNases [208]. This designation is apparent from the greatly increased toxicity of RNase 1, which is the most abundant ptRNase in humans, for RNH1 knockout cells [174]. Still, the sensitivity of RNH1 to oxidation and subsequent inactivation could play a role in its cellular function [279, 289].

Here, we demonstrate that—in the absence of RNH1 and despite its low enzymatic activity—ANG is a potent cytotoxin. Its toxicity is mediated by small tRNA fragments, which are upregulated upon ANG treatment in RNH-knockout cells. These tRFs, which induce cytotoxicity *in cellulo*, are not upregulated in RNase 1-treated cells. Thus, the degradation of specific cellular RNAs by ANG leads to greater cytotoxicity than does the nonspecific degradation of RNA by RNase 1. This work highlights the importance of ANG in tRF production, and provides insight into the biological roles of ANG and its inhibitor.

6.3 Methods

6.3.1 Materials

Reagents were from Sigma Chemical (St. Louis, MO), Invitrogen (Carlsbad, CA), or VWR (Radnor, PA), and were used without further purification. Synthetic tRFs and DNAs were from Integrated DNA Technologies (Coralville, IA). Aqueous solutions were made with water that was generated with an Atrium Pro water purification system from Sartorius (Bohemia, NY) and had resistivity $\geq$18 M$\Omega \cdot cm^{-1}$.

6.3.2 HeLa cell culture

HeLa cells were cultured in Dulbecco's modified Eagle's medium (DMEM) containing fetal bovine serum (FBS) (10% v/v) and penicillin–streptomycin solution (1% v/v). Cells were incubated at 37 °C in a humidified incubator under 5% v/v CO_2(g).

6.3.3 Generation of RNH1-knock-out HeLa cells

CRISPR–Cas9-mediated knock-out of *RNH1* in HeLa cells (Δ*RNH1*) and its subsequent validation by immunoblotting were performed as described previously [174].

6.3.4 Purification of ribonucleases

RNase 1, ANG, and their variants were purified as described previously [147, 174]. The Alexa Fluor 647–ANG conjugate was prepared from Q19C ANG and the Alexa Fluor 488–RNase 1 conjugate was prepared from P19C RNase 1 by *S*-alkylation of Cys19 using methods described previously [71, 290].

6.3.5 Assays of cell viability

Cell-viability assays were performed with the CellTiter 96 AQueous One Solution Cell Proliferation Assay from Promega (Madison, WI), which is a tetrazolium dye-based assay for metabolic activity. Cells were grown, treated, and assessed as described previously [174]. Briefly, cells were grown in the wells of a 96-well plate. After 24 h, the medium was replaced with FBS-free DMEM containing various concentrations of analyte proteins. In some assays, neomycin was added to a concentration of 100 μM. (This concentration of neomycin alone produced no detectable toxicity.) All cells were then allowed to incubate for another 48 h before the addition

of the MTS reagent and data collection. Data were analyzed with the program Prism from GraphPad (La Jolla, CA). Values of EC_{50}, which is the concentration of analyte that gives half-maximal cell viability, were calculated by using the equation:

$$y = y_{\min} + \frac{(y_{\max} - y_{\min})}{1+\left(\frac{EC_{50}}{x}\right)^{h}} \quad (1)$$

where y is cell viability, x is the concentration of analyte, and h is the Hill coefficient. All values were the average of at least three biological replicates.

6.3.6 Microscopy

Prior to experiments, HeLa cells were plated for 24 h at a density of 200,000 cells/mL in 0.2 mL of medium in the wells of an eight-well μ-chamber from Ibidi (Martinsried, Germany). On the day of an experiment, all cells were washed with serum-free DMEM (3 × 0.2 mL). Cells were incubated with either 5 μM of Alexa Fluor 488–RNase 1 conjugate or Alexa Fluor 647–ANG conjugate (or both) for 3 h at 37 °C under 5% v/v CO_2(g). Nuclear counterstaining was performed with Hoechst 33342 from Invitrogen for the final 5 min at 37 °C. Cells were washed with serum-free DMEM prior to imaging. Imaging was performed with an A1R+ resonant scanning confocal microscope from Nikon (Tokyo, Japan).

6.3.7 Flow cytometry

Cells were grown to a density of 200,000 cells/mL in 2.0 mL of complete growth medium in the wells of a flat-bottomed six-well plate. After 24 h, cells were washed with serum-free DMEM (3 × 2 mL). Cells were then incubated with 5 μM of Alexa Fluor 488–RNase 1 conjugate or Alexa

Fluor 647–ANG conjugate (or both) for 3 h at 37 °C under 5% v/v CO_2(g). Cells were then washed with PBS and treated with trypsin/EDTA (0.25% w/v) for 5 min at 37 °C under 5% v/v CO_2(g). The trypsin was diluted with DMEM containing 10% v/v FBS, and the cells were collected by centrifugation at 400*g* for 5 min. The supernatant was decanted, and the cell pellet was resuspended in 1 mL of medium. The suspension was strained through a 35-μm filter into a polystyrene flow cytometry test tube from BD Biosciences (Franklin Lakes, NJ). Fluorescence was measured with a FACSCalibur flow cytometer from BD Biosciences. The mean fluorescence per cell was determined in triplicate for 10,000 cells, and the data were analyzed with software from FlowJo (Ashland, OR).

6.3.8 Small RNA profiling

The small RNA profiles of RNase 1-treated, ANG-treated, and untreated cells were measured with the small RNA gel-electrophoresis chip from Agilent Technologies (Santa Clara, CA). Cells were grown to 80–100% confluency in DMEM containing FBS (10% v/v) and penicillin–streptomycin solution (1% v/v), then counted with a Coulter cell counter and seeded into a flat-bottomed 6-well plate at 100,000 cells per well. The cells were incubated for 24 h, after which the medium was replaced with FBS-free DMEM containing RNase 1 or ANG in PBS. Concentrations were chosen to produce ~75% and ~50% cell viability, which corresponded to 0.75 μM and 4 μM treatments of ANG and 1.5 μM and 18 μM treatments of RNase 1, respectively. After a 48-h incubation, RNA from each well was isolated with the miRCURY cell and plant RNA isolation kit from Exiqon (Woburn, MA) following the manufacturer's instructions. A small aliquot from each sample was then loaded onto a small RNA chip using the

small RNA analysis kit from Agilent Technologies. Samples were analyzed at the University of Wisconsin Biotechnology Center with a 2100 Bioanalyzer system from Agilent Technologies.

6.3.9 miRNA and tRNA sequence analysis

Analyses performed for both tRNA and miRNA sequences.

Data were checked for quality with FastQC and then loaded into iSMart, which allows access to a variety of small RNA analysis tools through a Virtual Box-based graphical user interface [291]. Fastq files were first loaded into Cutadapt to remove TruSeq small RNA adaptor sequences [292]. Reads aligning to rRNA sequences were filtered out, and then cut reads were aligned to hg19 miRNA and tRNA libraries using the recommended defaults for sRNABench [293]. The analysis of differential abundance from three biological replicates per condition was performed by using NOISeqBIO with Reads Per Million (RPM) normalization [294]. Normalized read-counts for each sample were exported into a spreadsheet and then loaded into Cluster3.0 for principal components analysis (PCA) [295]. Reads whose probability of having a differential abundance was ≥95%, which corresponds to $p \leq 0.05$, were compiled into a table for clustering analysis. This table was then loaded into Cluster 3.0 to perform hierarchical clustering using centroid linkages. Clusters were visualized with Java Treeview [296] or MATLAB.

Analyses performed only for tRNA sequences.

During sRNABench alignment, the minimum read-length for tRNA alignment was increased from 16 to 32 nt to filter-out any reads that should align to tRFs. These parameters did reduce substantially the number of tRNAs that were identified as having differential levels, from >500

with a 16-nt minimum to 306 with a 32-nt minimum. Nonetheless, fold-changes followed the same trends under both conditions.

Analyses performed only for miRNA sequences.

miRNA sequences from specific hierarchical clusters were loaded into the web-based tool miEAA and analyzed for enrichment using the default settings [297]. Significant GO annotations for sets of miRNAs with differential abundance were then loaded into the REVIGO web server for term reduction and analysis [298]. REVIGO reduction was performed using the Small Allowed Similarity setting. These lists were then loaded into Cytoscape 3.5.0 for network analysis [299]. Lastly, sequences were loaded into the DREME web server to perform motif analysis [300]. Upregulated miRNA sequences were compared to downregulated sequences to check for possible ANG binding motifs. In all cases, significant differences correspond to $p \leq 0.05$.

6.3.10 tRF sequence analysis

tRF analysis requires several processing steps to identify reads corresponding to full-length tRNAs and genomic tRNA transcripts. The tRF2Cancer web server was used for tRF analysis [301]. Briefly, cut reads from the CutAdapt tool on the iSMart Virtual Machine were collapsed using the FASTX-Toolkit developed by G. H. Hannon (Cold Spring Harbor Laboratory, NY). Reads were then loaded into the tRF2Cancer server and analyzed with default parameters except that the maximum read-length was increased to 32 to include as many tRF species as possible. The alignment score (which corresponds to RPM) was used as a normalized value for PCA with Cluster 3.0. Each biological replicate was then normalized by the total reads per replicate, and differential abundance was assessed by using NOISeqBIO. Only tRFs that were present in two of the three biological replicates were considered in this analysis. The filtering and analysis

(including motif analysis) of tRFs with differential abundance was then performed as described for miRNAs and tRNAs. Lastly, G-quadruplex structure was investigated by using the QGRS mapper web server [302].

6.3.11 Transfection of synthetic tRFs

tRFs with 5′-phosphate groups were obtained from IDT (Coralville, IA) as described previously [278]. The sequences were P-5′-tRF-Gly-GCC: GCAUGGGUGGUUCAGUGGUAGAAUUCUCGCCU, P-5′-tRF-Gln-CTG: GGUUCCAUGGUGUAAUGGUUAGCACUCUGGAC, and P-5′-tRF-Glu-CTC: UCCCUGGUGGUCUAGUGGUUAGGAUUCGGCGC. The single-stranded DNA analogs of these sequences were also obtained from IDT, as was a control DNA that did not vary in level across treatment conditions (5′-tRF-Lys-CTT: GCCCGGCTAGCTCAGTCGGTAGAGCATGAGAC). To assess tRF toxicity, each tRF and DNA analog was transfected into wild-type and Δ*RNH1* cells, which were then grown as described above for cell viability assays. jetPRIME transfection reagents from Polyplus Transfection (New York, NY) were used according to the manufacturer's instructions, and each tRF and DNA analog was incubated with the reagent for at least 10 min prior to its addition to cell culture medium. After a 1-h incubation, the medium was removed and replaced with FBS-free medium. Cells were then allowed to incubate for an additional 48 h before their viability was assayed as described above. Cells were also treated with transfection reagent alone to ensure that toxicity was not due to transfection conditions. All values were the compilation of at least three biological replicates. Significant differences were calculated by Student's paired t-test using the program Prism.

6.4 Results

6.4.1 Cytotoxicity of ANG

Recently, we reported on the toxicity of RNase 1 for Δ*RNH1* HeLa cells generated with CRISPR–Cas9 [303]. Remarkably, cell viability assays revealed that ANG is 3-fold more toxic to Δ*RNH1* HeLa cells than is RNase 1 (Table 1), despite having 10^4-fold less enzymatic activity [173, 277]. Assays with H114N ANG, which is an inactive catalyst [304], demonstrated that cytotoxicity relies on catalytic activity. Moreover, the cytotoxicity of ANG is unaffected by neomycin, which blocks its localization to the nucleolus [305-306], suggesting that ANG acts elsewhere.

6.4.2 Cellular uptake and localization of ANG

We began our investigation of this anomaly by using flow cytometry to measure the cellular uptake of ANG relative to that of RNase 1 (Figure 6.1A). We found that ANG uptake was 14-fold greater than that of RNase 1 in wild-type HeLa cells, and 20-fold greater in Δ*RNH1* HeLa cells. Increased uptake of ANG versus RNase 1 is expected, as ANG is known to bind a specific cell-surface receptor, whereas RNase 1 is endocytosed via a dynamin-independent pathway [73, 272-273]. Still, the greater uptake of ANG is not able to explain its anomalous cytotoxicity.

Next, we sought to discern the mode-of-action of ANG in Δ*RNH1* cells. The function of ANG is determined largely by its cellular localization. We visualized ANG uptake and localization using confocal microscopy (Figure 6.1B). Fluorophore-labeled ANG and RNase 1 exhibited punctate staining in both wild-type and Δ*RNH1* cells, which results from its localization to endocytic vesicles [173, 210]. This result is not surprising, as only a small fraction of endocytosed ptRNases escape from endocytic vesicles and enter the cytosol [210].

6.4.3 Effect of ANG on cellular tRF levels

Many functions of ANG are manifested in the nucleus, but under certain stress conditions ANG can relocate to the cytosol and produce tRFs [278, 280-281]. RNH1 plays an integral role in this process, and the partial knockdown of RNH1 leads to tRF production in unstressed cells [279-280]. To determine whether tRFs were upregulated after ANG treatment, we surveyed the small RNAs within ANG- and RNase 1-treated cells. The results revealed the accumulation of tRF-length fragments in ANG-treated Δ*RNH1* cells but not in wild-type cells (Figure 6.2). In contrast, RNase 1 produced random degradation in both cell lines. Hence, ANG-induced toxicity could be mediated by small RNAs.

To investigate further the production of small RNAs in ANG-treated cells, we determined the sequence of small RNAs in wild-type and Δ*RNH1* cells treated with ANG, RNase 1, or vehicle (PBS). This analysis, which included RNA species of the lengths of tRFs, full-length tRNAs, and miRNAs, provided a comprehensive profile of small RNA populations. A principal components analysis (PCA) revealed that ANG-treated Δ*RNH1* cells segregated from all other sample types and conditions (Figure 6.3A). This segregation is due to the abundance of particular tRFs (Table 6.S1).

We found that 124 tRFs were regulated differentially ($p \leq 0.05$) in ANG-treated Δ*RNH1* cells versus RNase 1-treated or untreated cells. In contrast, only 28 tRFs were regulated differentially in ANG-treated wild-type cells. A surprising number of tRFs were downregulated upon ANG treatment—between 70–80%. The 37 tRFs upregulated in ANG-treated Δ*RNH1* cells accounted for 92% of the total tRF population, whereas the 5 tRFs upregulated in ANG-treated wild-type cells made up only 26% of their total tRF population (Figure 6.3B and 6.3C).

Moreover, the vast majority of tRFs in Δ*RNH1* cells could be attributed to just five fragments from glycine, valine, or glutamine tRNAs. tRF-5 Gly-GCC was upregulated to an especially high level, constituting 66% of the tRFs in ANG-treated Δ*RNH1* cells and 25% in ANG-treated wild-type cells.

We investigated whether the upregulation of particular tRFs could account for ANG toxicity. To do so, we transfected synthetic tRFs, as well as their DNA analogs, into both wild-type and Δ*RNH1* cells. Cytotoxicity assays on transfected cells revealed that highly upregulated tRFs produced significant cell death at concentrations as low as ~1 μM (Figure 6.4A). At ~3 μM concentrations, Gly and Glu tRFs were highly cytotoxic, leading to cell viabilities as low as 15% (Figure 6.4B). Both of these concentrations are physiologically relevant [281]. Other tRFs did not elicit such a dramatic response. tRF-Gln-CTC, which was upregulated but not in high abundance in ANG-treated Δ*RNH1* cells, produced significant toxicity only in Δ*RNH1* cells, whereas tRF-Lys-CTT, which is of constant abundance, caused significantly less toxicity at all concentrations than did its highly upregulated counterparts. Thus, the upregulation of particular tRFs could be responsible for the cytotoxicity of ANG.

6.4.4 Effect of ANG on cellular tRNA levels

The results from our transfection experiment suggest that tRFs alone can mediate cellular toxicity. Still, it is important to investigate whether tRNA degradation also contributes to the toxicity [282]. For example, an increase in a specific tRF is coupled to a decrease in its corresponding tRNA. We surveyed our small RNA data for the corresponding mature tRNAs of differentially regulated tRFs. In all samples, there was a set of 85 tRNAs, which corresponded to 140 tRFs. Of these 85 tRNAs, 50 were produced differentially ($p \leq 0.05$), and 31 were

downregulated. Still, only 11 of these significantly downregulated tRNAs corresponded to upregulated tRFs (Table 6.S2). This number is a small fraction of the ~600 tRNAs encoded by the human genome. In addition, this set of 11 did not correspond to any highly abundant tRFs, and tRNAs corresponding to tRFs Gly-GCC, Glu-CTC, and Glu-TTC were slightly upregulated upon treatment with ANG. Another discrepancy between tRF levels and the levels of their corresponding tRNAs has been reported previously [280, 307].

Although specific tRNAs were not downregulated in ANG-treated samples, tRNAs were downregulated globally after ANG treatment (Figure 6.5A). Global tRNA downregulation has been reported previously in ANG-treated *Xenopus* oocytes, which lack RNH1, and was used to explain ANG toxicity in this system [308]. Our observation of tRNA downregulation in both wild-type and Δ*RNH1* cells indicates, however, that tRNA downregulation cannot fully explain ANG toxicity.

6.4.5 Effect of ANG on cellular miRNA levels

To complete our small RNA analysis, we investigated differences in miRNA levels in Δ*RNH1* cells. ANG has also been reported to cleave miRNAs [268, 309], and that cleavage could exacerbate the toxicity of ANG for Δ*RNH1* cells. We found differential levels in 48 mature miRNAs (Table 6.S3). Again, most of these miRNAs were downregulated—between 67–90% (Figure 6.4B). Still, unlike with tRFs, differentially regulated miRNAs did not constitute as large a part of the total miRNA population, with up- or down-regulated miRNAs constituting only 18–27%. miRNA enrichment analysis, semantic reduction, and network analysis provided several sets of unique GO terms in upregulated and downregulated miRNAs. Some of the GO terms enriched in upregulated miRNAs included acetyl- and methyl-transferase activities, as well as those for

protein folding and receptor binding, whereas downregulated miRNAs were enriched in oxidoreductase activity and transcription factor activation (Table 6.S4). Nonetheless, the large set of miRNA targets and biological processes lacked clear commonalities.

6.4.6 RNA motifs affected by ANG

Our small RNA analysis demonstrates differential small RNA levels in wild-type and Δ*RNH1* cells. To better understand why certain tRFs and miRNAs were upregulated in ANG-treated samples, we performed motif analysis on upregulated tRFs and miRNAs. This analysis did not reveal any significantly enriched motifs in differentially regulated sequences. We also investigated the presence of potential G-quadruplex structures, which have been reported to be important for tRF function [283-284]. Although upregulated tRFs in ANG-treated Δ*RNH1* cells lacked the G-quadruplex–forming terminal oligo-guanine (TOG) motif which has been studied previously, both Glu-TTC and Glu-CTC sequences contained GG-rich motifs that could form higher order structures (Figure 6.3D) [281]. Di-guanine motifs are, however, frequent in tRFs, complicating assignment of these structures as the main determinant of ANG binding and cleavage.

6.5 Discussion

ANG was the first substance shown to initiate the growth of a human organ [265]. We have uncovered a previously unknown action of ANG, one that leads to cytotoxicity rather than cell proliferation. When unchecked by RNH1, ANG is not only cytotoxic, but 3-fold more so than RNase 1. This toxicity is linked to the catalytic activity of ANG but not its ability to enter the

nucleus. Because ANG is a 10,000-fold less active catalyst than RNase 1 against simple substrates, these results are surprising.

To uncover the underlying basis for the cytotoxicity of ANG, we assessed its cellular uptake and localization. Flow cytometry revealed that ANG did enter cells more readily than did RNase 1 (Fig. 1A), though the increase was modest compared to the 30,000-fold difference in cytotoxic activity per unit of enzymatic activity. Likewise, confocal imaging revealed that the localization of RNase 1 and ANG were similar, and that ANG localization did not differ in wild-type and Δ*RNH1* cells (Fig. 1B). Together, these data suggested to us that ANG causes cell death in the cytosol by an unusual mechanism, perhaps based on the cleavage of particular RNAs.

Small RNA sequencing allowed us to pinpoint which RNAs are responsible for the cytotoxicity of ANG. tRFs were a logical candidate, as the regulation of tRFs by ANG in the cytosol was known [269, 280-282, 310]. Sequencing revealed that a subset of five tRFs were highly abundant in ANG-treated Δ*RNH1* cells, making up >90% of the total tRF population. Two of these five tRFs have known functions: one, tRF-Glu-CTC, targets apolipoprotein E receptor 2 during RSV infection [285, 311]. tRF-Gly-GCC has been shown to inhibit protein translation, regulate MERVL targets, and inhibit cell proliferation [281, 312-314]. It is upregulated after ischemic injury, and its expression is tied to the expression of ANG [314]. The dramatic upregulation of this tRF in our model, as well as these previous reports, suggest that tRF-Gly-GCC has a significant biological role that may be linked to ANG.

To understand this dichotomy, we investigated the cytotoxicity of upregulated tRFs in both wild-type and Δ*RNH1* cells. We found that the tRF species upregulated by ANG produced significant cytotoxicity, with tRF-Gly-GCC and tRF-Glu-CTC causing the highest levels of cell death in a dose-dependent fashion. Notably, these most toxic tRFs (Fig. 4) are the ones that are

most abundant in ANG-treated Δ*RNH1* cells (Fig. 3). Both RNA and DNA analogues of these tRFs caused toxicity, which agrees with previous reports [283].

It is important to note that tRNAs, and thus the tRfs from which they are derived, are heavily modified in the cell, while our transfected tRFs are unmodified. tRNA modifications can protect tRNAs from ANG cleavage, and could affect tRF function [315].

Although tRF sequences were the foci of our investigations, small RNA analysis also allowed us to measure tRNA levels. tRNA cleavage was used to explain ANG toxicity in *Xenopus* oocytes, which do not produce a homolog of RNH1 [308]. Our analysis did demonstrate a significant global decrease in tRNA levels upon treatment with ANG, but this decrease occurred in both wild-type and Δ*RNH1* cells. Thus, tRNA downregulation is unlikely to be responsible for the toxicity of ANG for Δ*RNH1* cells.

Finally, miRNAs were differentially regulated in ANG-treated cells, but did not produce the sharp contrast in abundance that occurred in the tRF population. GO-term enrichment and analysis followed the same theme; although unique GO terms did exist for upregulated and downregulated miRNAs, those terms did not reveal any underlying biological processes that could explain the toxicity of ANG for Δ*RNH1* cells. These data suggest that ANG might regulate certain miRNAs but without the consequences derived from the regulation of tRFs.

The differential regulation of tRFs and miRNAs by ANG provokes a question: why are certain sequences highly upregulated in Δ*RNH1* cells? The increase in specific tRFs and miRNAs suggests that ANG binds and cleaves certain RNAs efficiently. ANG is known to bind an angiogenin binding element (ABE) in genomic DNA [316], but this binding motif (which is a string of CTs) is not present in our small RNAs. Motif analysis also did not identify any significantly enriched motifs in upregulated versus downregulated small RNA sequences. We

also considered whether our small RNA sequences could form G-quadruplex structures, which are known to effect RNA stability and tRF function [281, 283]. Two of the highly upregulated tRFs did contain oligo-G motifs that could form G-quadruplex structures, but the tRF with the highest abundance, tRF-5 Gly-GCC, did not contain such a motif. Further structure–function analysis is necessary to reveal the basis for this substrate specificity.

6.6 Conclusions

Historically, ANG has been shown to contribute to a myriad of cellular processes linked by a common thread: ribonucleolytic activity that promotes cell survival and proliferation [268, 270]. Our data alter the perception of ANG. Specifically, we have discovered that ANG can be a potent cytotoxin. ANG induces cell death by a unique mechanism—the robust upregulation of cytotoxic tRFs. This finding contrasts with previous demonstrations of the ability of certain tRFs to arrest protein translation and encourage cell survival [278, 281, 283, 310]. Thus, under differing conditions, tRFs produced by ANG can lead to cell survival or cell death.

Table 6.1. Values of EC_{50} (μM) for the toxicity of ANG and related proteins for wild-type and Δ*RNH1* HeLa cells

	HeLa Cell	
ribonuclease	wild-type	Δ*RNH1*
ANG	>75	5 ± 4
ANG (+100 μM neomycin)	>75	3 ± 1
H114N ANG	>75	>75
RNase 1	>100	17 ± 4

Ribonucleases were incubated with cells for 48 h at 37 °C and 5% CO_2. Values are the average of at least three biological replicates (±95% confidence interval) as measured with a tetrazolium dye-based assay for metabolic activity. Lower limits indicate that the specified concentration resulted in <25% cell death.

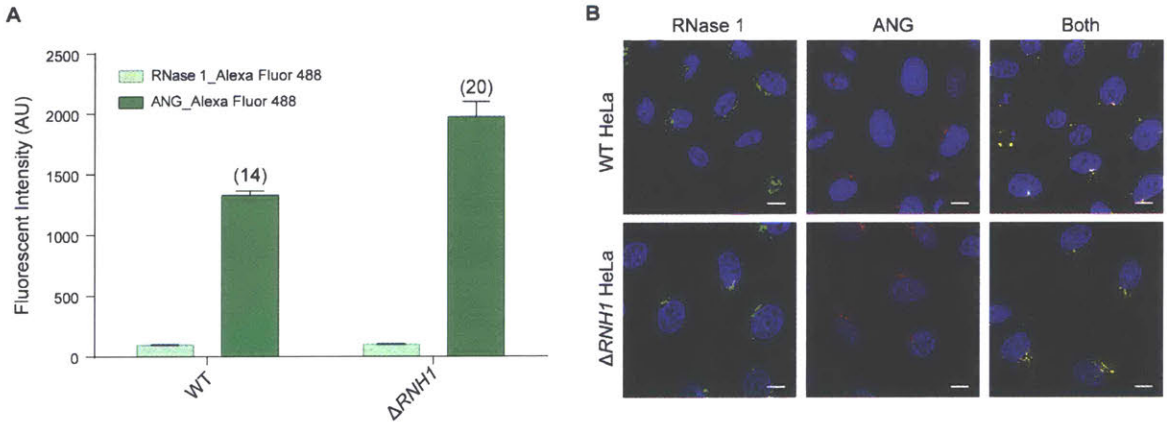
A
2500
2000
1500
1000
500
0
Fluorescent Intensity (AU)
RNase 1_Alexa Fluor 488
ANG_Alexa Fluor 488
(14)
(20)
WT
ΔRNH1
B
RNase 1
ANG
Both
WT HeLa
ΔRNH1 HeLa

Figure 6.1. Characterization of ANG uptake and localization in wild-type and Δ*RNH1* HeLa cells. (*A*) Bar graphs showing the cellular uptake of ANG and RNase 1. (*B*) Confocal microscopy images showing the cellular localization of fluorophore-labeled ANG and RNase 1. Scale bar: 10 μM.

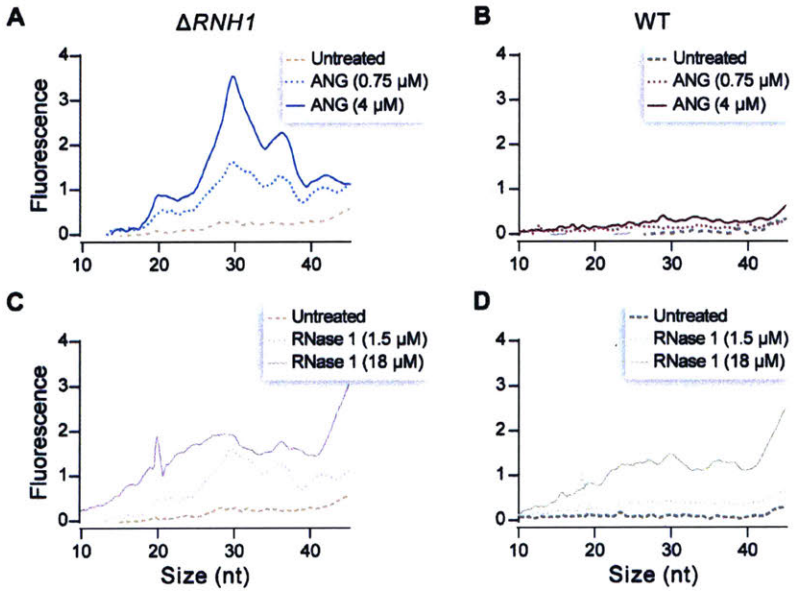
A
ΔRNH1
Untreated
ANG (0.75 μM)
ANG (4 μM)
Fluorescence
B
WT
Untreated
ANG (0.75 μM)
ANG (4 μM)
C
Untreated
RNase 1 (1.5 μM)
RNase 1 (18 μM)
Fluorescence
Size (nt)
D
Untreated
RNase 1 (1.5 μM)
RNase 1 (18 μM)
Size (nt)

Figure 6.2. Graphs showing the effect of ptRNase-treatment on small RNAs (10–50 nt) in wild-type and Δ*RNH1* HeLa cells. (*A*) ANG-treated Δ*RNH1* cells. (*B*) ANG-treated wild-type cells. (*C*) RNase 1-treated Δ*RNH1* cells. (*D*) RNase 1-treated wild-type cells.

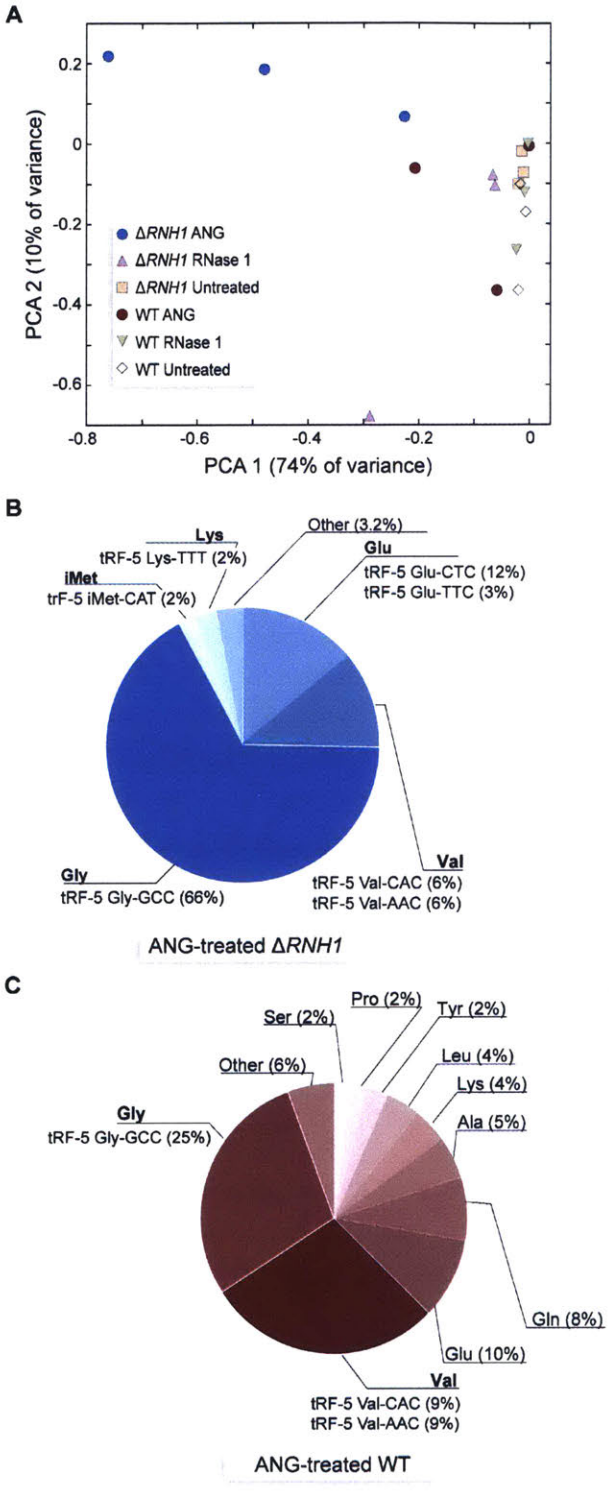
A
0.2
0
-0.2
-0.4
-0.6
PCA 2 (10% of variance)
ΔRNH1 ANG
ΔRNH1 RNase 1
ΔRNH1 Untreated
WT ANG
WT RNase 1
WT Untreated
-0.8
-0.6
-0.4
-0.2
0
PCA 1 (74% of variance)
B
Lys
tRF-5 Lys-TTT (2%)
iMet
trF-5 iMet-CAT (2%)
Other (3.2%)
Glu
tRF-5 Glu-CTC (12%)
tRF-5 Glu-TTC (3%)
Val
tRF-5 Val-CAC (6%)
tRF-5 Val-AAC (6%)
Gly
tRF-5 Gly-GCC (66%)
ANG-treated ΔRNH1
C
Pro (2%)
Ser (2%)
Tyr (2%)
Other (6%)
Leu (4%)
Lys (4%)
Gly
tRF-5 Gly-GCC (25%)
Ala (5%)
Gln (8%)
Glu (10%)
Val
tRF-5 Val-CAC (9%)
tRF-5 Val-AAC (9%)
ANG-treated WT
D
tRF-5 Glu-CTC TCCCTGGTGGTCTAGTGGTTAGGATTCGGCGC
tRF-5 Glu-TTC TCCCACATGGTCTAGCGGTTAGGATTCCTGGT
tRF-5 Gly-GCC GCATGGGTGGTTCAGTGGTAGAATTCTCGCCT

Figure 6.3. Effect of ptRNase-treatment on tRF levels in wild-type and Δ*RNH1* HeLa cells. (*A*) Principal component analysis of normalized tRF levels in ANG-, RNase 1-, or untreated cells. (*B*) Abundance of tRFs in ANG-treated Δ*RNH1* cells. Values are the average of three biological replicates. (*C*) Abundance of tRFs in ANG-treated wild-type cells. (*D*) Predicted G-quadruplex forming motifs in upregulated tRFs.

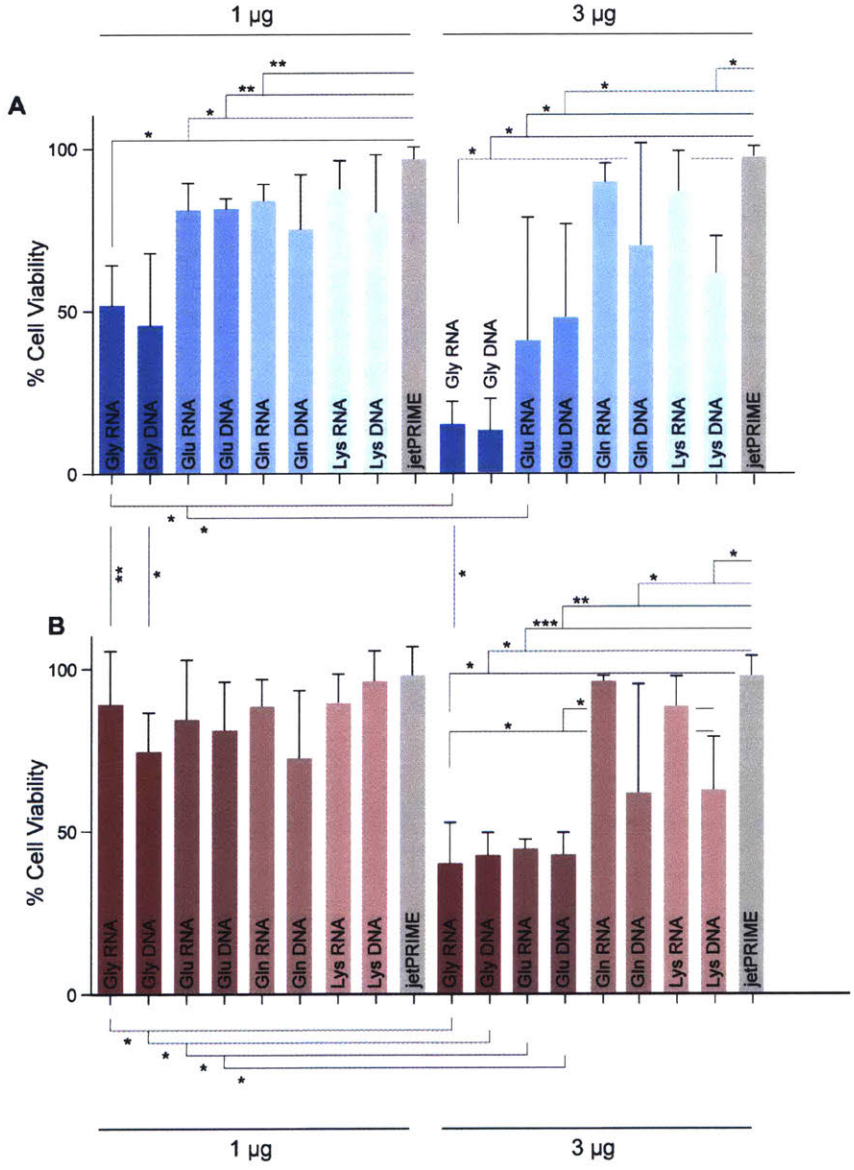
1 µg
3 µg
A
% Cell Viability
100
50
0
Gly RNA
Gly DNA
Glu RNA
Glu DNA
Gln RNA
Gln DNA
Lys RNA
Lys DNA
jetPRIME
B
% Cell Viability
100
50
0
Gly RNA
Gly DNA
Glu RNA
Glu DNA
Gln RNA
Gln DNA
Lys RNA
Lys DNA
jetPRIME
1 µg
3 µg

Figure 6.4. Bar graphs showing the effect of tRF transfection on the viability of wild-type and Δ*RNH1* HeLa cells. Cell viability (±95% confidence interval) after transfection of 1 μg (*A*) or 3 μg (*B*) of an RNA or DNA species. Significant cell death compared to transfection reagent (jetPRIME) are marked by asterisks, where * refers to $p \leq 0.05$; **, $p \leq 0.01$, and ***, $p \leq 0.001$. 1 μg or 3 μg transfection corresponds to ~1 or 3 μM RNA species in cell culture medium.

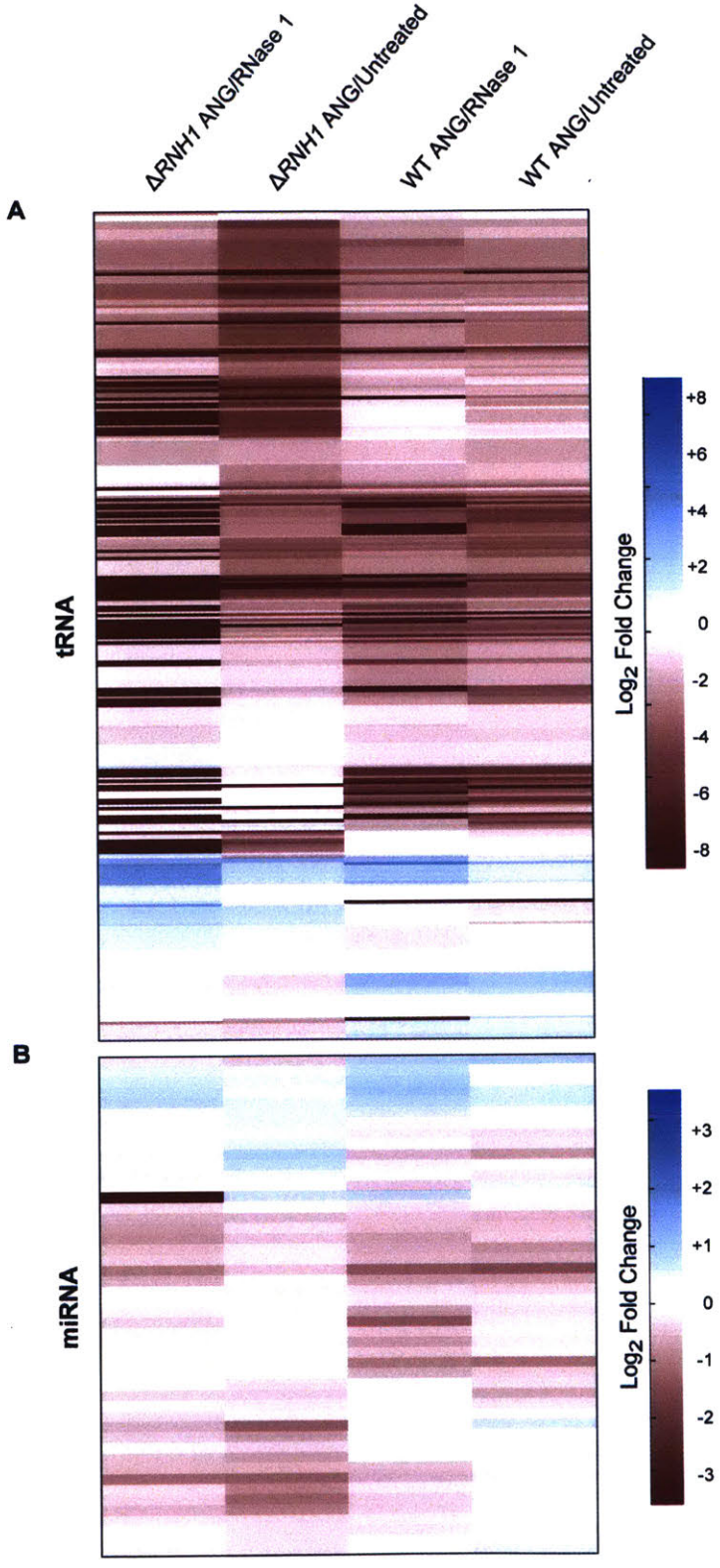
ΔRNH1 ANG/RNase 1
ΔRNH1 ANG/Untreated
WT ANG/RNase 1
WT ANG/Untreated
A
tRNA
Log2 Fold Change
+8
+6
+4
+2
0
-2
-4
-6
-8
B
miRNA
Log2 Fold Change
+3
+2
+1
0
-1
-2
-3

Figure 6.5. Heat maps showing the effect of ANG on tRNA and miRNA levels in wild-type and Δ*RNH1* cells. Log_2(fold change) in abundance from the indicated conditions are clustered hierarchically. (*A*) tRNA. (*B*) miRNA.

6.7 Supplemental information

Table 6.S1. tRFs with differential levels

			ΔRNH1		WT	
tRF Type	Precursor tRNA	Length	A/R	A/U	A/R	A/U
tRF-1	tRNA-Ala-CGC-2-1	18	-	-6.60901	-	-
tRF-1	tRNA-Arg-ACG-1-2	19	-	-6.38991	-	-
tRF-1	tRNA-Cys-GCA-2-4	23	-	-7.23496	-	-
tRF-1	tRNA-Glu-CTC-2-1	22	-6.32954	-	-	-
tRF-1	tRNA-Ile-AAT-2-1	17	-2.82046	-	-	-
tRF-1	tRNA-Ile-AAT-5-2	17	-	-1.19493	-	-
tRF-1	tRNA-Thr-CGT-3-1	17	-	-6.87521	7.345775	7.345775
tRF-1	tRNA-Thr-CGT-3-1	18	-	-	-	-8.01722
tRF-3	tRNA-Ala-AGC-2-1	18	-9.11937	-8.12528	-	-
tRF-3	tRNA-Ala-AGC-3-1	18	-9.10945	-8.12153	-	-
tRF-3	tRNA-Ala-CGC-1-1	22	-8.83571	-7.87502	-	-
tRF-3	tRNA-Ala-CGC-2-1	22	-8.84359	-7.93558	-	-
tRF-3	tRNA-Ala-CGC-3-1	17	-6.95579	-	-	-
tRF-3	tRNA-Ala-CGC-3-1	18	-	-7.45929	-	-
tRF-3	tRNA-Ala-TGC-1-1	18	-8.88495	-8.03046	-	-
tRF-3	tRNA-Ala-TGC-2-1	22	-8.83571	-7.87502	-	-
tRF-3	tRNA-Ala-TGC-3-1	22	-8.84359	-7.93905	-	-
tRF-3	tRNA-Ala-TGC-4-1	17	-6.9712	-	-	-
tRF-3	tRNA-Ala-TGC-4-1	18	-	-7.48218	-	-
tRF-3	tRNA-Ala-TGC-6-1	18	-8.88293	-8.02995	-	-
tRF-3	tRNA-Asp-GTC-3-1	22	-8.17931	-	-	-
tRF-3	tRNA-Gln-CTG-5-1	17	-6.57909	-	-7.50327	-6.88671
tRF-3	tRNA-Gln-TTG-1-1	17	-	-	-	-7.90913
tRF-3	tRNA-Gln-TTG-1-1	18	-	-6.82163	-	-
tRF-3	tRNA-Gln-TTG-2-1	17	-6.96012	-	-	-
tRF-3	tRNA-Gln-TTG-2-1	18	-	-6.86005	-	-
tRF-3	tRNA-Gln-TTG-3-1	17	-	-	-	-7.90913
tRF-3	tRNA-Gln-TTG-3-1	18	-	-6.82163	-	-
tRF-3	tRNA-Glu-TTC-4-2	26	-	-6.27829	-	-
tRF-3	tRNA-Gly-TCC-1-1	22	-8.65728	-7.48137	-	-
tRF-3	tRNA-Gly-TCC-2-2	22	-8.65945	-7.47978	-	-
tRF-3	tRNA-Gly-TCC-3-1	22	-8.65696	-7.47978	-	-
tRF-3	tRNA-Leu-CAA-1-2	22	-7.33432	-	-	-
tRF-3	tRNA-Leu-CAA-2-1	22	-7.33447	-	-	-
tRF-3	tRNA-Leu-CAA-3-1	22	-7.33351	-	-	-
tRF-3	tRNA-Leu-CAA-4-1	22	-7.43185	-	-	-
tRF-3	tRNA-Leu-CAG-2-2	22	-	-	-	7.263097

tRF-3	tRNA-Ser-GCT-3-1	18	-	-	-	-8.01918
tRF-3	tRNA-Ser-GCT-3-1	22	-7.70536	-6.41447	-	-
tRF-3	tRNA-Ser-GCT-4-1	18	-	-	-	-8.02338
tRF-3	tRNA-Ser-GCT-4-1	22	-7.70296	-6.40577	-	-
tRF-3	tRNA-Ser-GCT-5-1	18	-	-	-	-7.98299
tRF-3	tRNA-Ser-GCT-5-1	22	-7.6421	-6.37926	-	-
tRF-3	tRNA-Tyr-GTA-1-1	17	-7.00199	-6.40304	-	-
tRF-3	tRNA-Tyr-GTA-2-1	17	-3.93903	-3.56513	-	-
tRF-3	tRNA-Tyr-GTA-5-2	17	-3.93829	-3.56618	-	-
tRF-3	tRNA-Tyr-GTA-7-1	17	-8.89191	-8.55144	-	-
tRF-3	tRNA-Tyr-GTA-8-1	17	-7.00199	-6.40304	-	-
tRF-3	tRNA-Val-AAC-1-5	17	-	-9.92044	-	-
tRF-3	tRNA-Val-AAC-2-1	17	-2.12872	-1.81378	-	-
tRF-3	tRNA-Val-AAC-4-1	17	-	-9.92044	-	-
tRF-3	tRNA-Val-AAC-chr6-84	17	-2.08343	-1.84565	-	-
tRF-3	tRNA-Val-CAC-1-6	17	-	-9.91421	-	-
tRF-3	tRNA-Val-CAC-2-1	17	-	-	-7.59934	-7.5042
tRF-3	tRNA-Val-CAC-5-1	17	-	-9.91421	-	-
tRF-3	tRNA-Val-TAC-1-2	22	-	-6.90067	-	-
tRF-3	tRNA-Val-TAC-2-1	22	-	-6.90215	-	-
tRF-5	nm-tRNA-Tyr-GTA-chr1-125	32	-7.51067	-6.55985	-	-
tRF-5	nm-tRNA-Tyr-GTA-chr14-8	32	-7.51067	-6.55985	-	-
tRF-5	tRNA-Ala-CGC-1-1	22	-	-	-	-6.4567
tRF-5	tRNA-Ala-CGC-2-1	22	-	-	-	-6.44222
tRF-5	tRNA-Ala-TGC-2-1	22	-	-	-	-6.4567
tRF-5	tRNA-Ala-TGC-3-1	22	-	-	-	-6.44222
tRF-5	tRNA-Asp-GTC-2-7	32	7.053691	7.053691	-	-
tRF-5	tRNA-Gln-CTG-1-3	32	8.333066	8.333066	-	-
tRF-5	tRNA-Gln-CTG-2-1	32	8.333066	8.333066	-	-
tRF-5	tRNA-Gln-CTG-5-1	32	8.320425	8.320425	-	-
tRF-5	tRNA-Gln-TTG-1-1	32	7.239105	7.239105	-	-
tRF-5	tRNA-Gln-TTG-2-1	32	7.234099	7.234099	-	-
tRF-5	tRNA-Glu-CTC-1-7	32	-	4.881728	11.62415	-
tRF-5	tRNA-Glu-CTC-2-1	32	-	4.881728	-	-
tRF-5	tRNA-Glu-TTC-1-1	32	6.878194	6.878194	-	-
tRF-5	tRNA-Glu-TTC-2-2	32	9.322567	9.322567	-	-
tRF-5	tRNA-Glu-TTC-3-1	32	-	10.53981	-	-
tRF-5	tRNA-Glu-TTC-4-2	32	-	10.53981	-	-
tRF-5	tRNA-Glu-TTC-8-1	32	-	10.53871	-	-
tRF-5	tRNA-Gly-GCC-1-4	32	1.872016	5.046968	2.992051	2.844319
tRF-5	tRNA-His-GTG-1-6	29	-3.58386	-2.07641	-	-
tRF-5	tRNA-iMet-CAT-1-2	31	-	3.295521	-	-
tRF-5	tRNA-iMet-CAT-2-1	31	-	3.275267	-	-
tRF-5	tRNA-Leu-CAG-1-7	26	-2.31893	-	-	-
tRF-5	tRNA-Leu-CAG-2-2	26	-2.31893	-	-	-

tRF-5	tRNA-Lys-TTT-3-3	32	-	10.00184	-	-
tRF-5	tRNA-Lys-TTT-5-1	32	-	10.00173	-	-
tRF-5	tRNA-Ser-AGA-1-1	24	-8.1955	-	-	-
tRF-5	tRNA-Ser-AGA-2-5	24	-8.1955	-	-	-
tRF-5	tRNA-Ser-AGA-3-1	24	-8.1955	-	-	-
tRF-5	tRNA-Ser-AGA-4-1	24	-8.00873	-	-	-
tRF-5	tRNA-Ser-TGA-2-1	24	-8.19605	-	-	-
tRF-5	tRNA-Ser-TGA-3-1	24	-8.19605	-	-	-
tRF-5	tRNA-Ser-TGA-4-1	24	-8.19605	-	-	-
tRF-5	tRNA-Val-AAC-1-5	32	-	2.327097	-	-
tRF-5	tRNA-Val-AAC-2-1	23	-	-6.47054	-	-
tRF-5	tRNA-Val-AAC-3-1	32	-	2.326959	-	-
tRF-5	tRNA-Val-AAC-4-1	32	-	2.327097	-	-
tRF-5	tRNA-Val-CAC-1-6	32	-	2.421139	-	-
tRF-5	tRNA-Val-CAC-2-1	32	-	9.375315	-	-
tRF-5	tRNA-Val-CAC-4-1	32	-	2.421139	-	-
tRF-5	tRNA-Val-CAC-5-1	32	-	2.421798	-	-
tRF-5	tRNA-Val-TAC-1-2	31	-7.24136	-	-	-
tRF-novel	tRNA-Asp-GTC-1-1	22	-7.37095	-	-8.22546	-
tRF-novel	tRNA-Asp-GTC-4-1	22	-7.36367	-	-8.18307	-
tRF-novel	tRNA-Gln-CTG-1-3	20	-10.5867	-9.74629	-	-
tRF-novel	tRNA-Gln-CTG-2-1	20	-10.5785	-9.74427	-	-
tRF-novel	tRNA-Gln-CTG-3-2	19	8.286773	8.286773	-	-
tRF-novel	tRNA-Gln-CTG-3-2	20	-10.3677	-9.35586	-	-
tRF-novel	tRNA-Gln-CTG-4-1	19	8.268581	8.268581	-	-
tRF-novel	tRNA-Gln-CTG-4-1	20	-10.3646	-9.33409	-	-
tRF-novel	tRNA-Gln-CTG-5-1	23	-	-6.87336	-	-
tRF-novel	tRNA-Gln-CTG-6-1	19	8.340874	8.340874	-	-
tRF-novel	tRNA-Gln-CTG-6-1	20	-10.4435	-9.40049	-	-
tRF-novel	tRNA-Gln-TTG-1-1	19	-2.33615	-	-	-
tRF-novel	tRNA-Gln-TTG-1-1	22	-	-	-	-8.60587
tRF-novel	tRNA-Gln-TTG-2-1	18	-7.59813	-7.22741	-	-7.61075
tRF-novel	tRNA-Gln-TTG-3-1	19	-1.60189	-	-	-
tRF-novel	tRNA-Gln-TTG-3-1	22	-	-	-	-8.60004
tRF-novel	tRNA-Glu-CTC-1-7	32	-	-9.18982	-	-
tRF-novel	tRNA-Glu-CTC-2-1	32	-	-9.18975	-	-
tRF-novel	tRNA-Gly-GCC-2-3	20	-	-8.6265	-	-
tRF-novel	tRNA-Gly-GCC-2-3	22	-8.09251	-	-	-
tRF-novel	tRNA-Gly-GCC-2-3	24	7.974491	7.974491	-	-
tRF-novel	tRNA-Gly-GCC-3-1	20	-	-8.63753	-	-
tRF-novel	tRNA-Gly-GCC-3-1	22	-8.09099	-	-	-
tRF-novel	tRNA-Gly-GCC-3-1	24	7.972827	7.972827	-	-
tRF-novel	tRNA-Gly-GCC-5-1	20	-	-	-	-8.09935
tRF-novel	tRNA-Gly-GCC-5-1	21	-	-	8.753506	8.753506
tRF-novel	tRNA-Gly-GCC-5-1	22	-7.1036	-	-	-

tRF-novel	tRNA-Gly-GCC-5-1	24	8.115772	8.115772	-	-
tRF-novel	tRNA-Lys-CTT-6-1	17	-8.49978	-7.72247	-	-
tRF-novel	tRNA-Lys-CTT-6-1	21	7.886144	7.886144	-	-
tRF-novel	tRNA-Lys-TTT-3-3	20	-	-7.73279	-	-8.99114
tRF-novel	tRNA-Lys-TTT-4-1	20	-2.46976	-	-	-
tRF-novel	tRNA-Lys-TTT-4-1	21	9.269641	9.269641	-	-
tRF-novel	tRNA-Lys-TTT-5-1	20	-	-7.73234	-	-9.01546
tRF-novel	tRNA-Lys-TTT-6-1	21	9.196438	9.196438	-	-
tRF-novel	tRNA-Val-CAC-2-1	18	-	-7.89089	-	-7.32793
tRF-novel	tRNA-Val-CAC-6-1	18	-7.09901	-7.3726	-6.97705	-7.47379
tRF-novel	tRNA-Val-CAC-6-1	20	8.749814	8.749814	8.375619	8.375619
tRF-novel	tRNA-Val-TAC-1-2	21	9.312739	9.312739	-	-
tRF-novel	tRNA-Val-TAC-2-1	17	7.129901	7.129901	-	-

Values are for $\log_2$(fold change) in tRNA levels as calculated with NOISeqBIO. Treatments: A/R, $\log_2$(ANG/RNase 1); A/U, $\log_2$(ANG/untreated). All values of $\log_2$(fold change) have $p \leq 0.05$.

Table 6.S2. tRNAs with differential levels

tRNA Name	Δ*RNH1* A/R	Δ*RNH1* A/U	WT A/R	WT A/U
Tyr-GTA-chr10-3	-	-	-	-4.87133
Tyr-GTA-chr1-125	-2.84739	-5.87496	-2.7248	-2.92902
Tyr-GTA-chr14-8	-2.88621	-5.91918	-2.74293	-2.94326
Tyr-GTA-chr21-2	-2.84739	-5.87496	-2.7248	-2.92902
Tyr-GTA-chr2-12	-	-	-5.33511	-
Tyr-GTA-chr9-10	-	-6.21221	-	-
Tyr-GTA-chr9-4	-	-4.9163	-6.25643	-5.54804
Gln-TTG-6-1	-4.03757	-5.81164	-2.97997	-2.52093
Gln-TTG-9-1	-	0	-	-6.5197
Leu-TAA-1-1	-	-5.83236	-	-
Leu-TAA-4-1	-3.3889	-6.27025	-	-1.74909
Ala-AGC-1-1	-	-	-	-5.4994
Ala-AGC-4-1	-	-	-	-3.75695
Ala-AGC-8-1	-3.16365	-	-	-
Ala-AGC-8-2	-3.16365	-	-	-
Ala-CGC-3-1	-	-3.70617	-2.81208	-
Ala-CGC-4-1	-	-	-	-3.91345
Ala-CGC-5-1	-	0	-	-4.80576
Ala-TGC-3-1	-	-	-	-4.88762
Ala-TGC-3-2	-	-	-	-4.88762
Ala-TGC-4-1	-	-2.8163	-3.84068	-5.38585
Ala-TGC-5-1	-	-	-	-3.64791
Ala-TGC-6-1	-	-3.18095	-3.80565	-5.40732
Ala-TGC-7-1	-	-	-	-3.64791
Arg-ACG-1-1	-2.74799	-4.94213	-3.85961	-2.70908
Arg-ACG-1-2	-2.74799	-4.94213	-3.85961	-2.70908
Arg-ACG-1-3	-2.74799	-4.94213	-3.85961	-2.70908
Arg-ACG-2-1	-1.66102	-4.02698	-	-
Arg-ACG-2-2	-1.66102	-4.02698	-	-
Arg-ACG-2-3	-1.66102	-4.02698	-	-
Arg-ACG-2-4	-1.66102	-4.02698	-	-
Arg-CCG-1-1	-	-	-6.49877	-6.04571
Arg-CCG-1-2	-	-	-6.49877	-6.04571
Arg-CCG-1-3	-	-	-6.49877	-6.04571
Arg-CCG-2-1	-3.57593	-2.71029	-	-
Arg-CCT-1-1	-2.97442	-3.38158	-4.2399	-5.01787
Arg-CCT-2-1	-2.90074	-2.93241	-4.08597	-5.27897
Arg-CCT-3-1	-2.72708	-4.7063	-4.7801	-3.63992
Arg-CCT-4-1	-2.914	-3.7982	-4.92207	-3.64284
Arg-TCT-2-1	-1.353	-	-	-
Arg-TCT-3-1	-2.30423	-3.98003	-2.38368	-2.46517
Arg-TCT-5-1	-2.83725	-4.02529	-2.69144	-2.52392

Asn-GTT-10-1	-3.38862	-5.21624	-	-
Asn-GTT-1-1	-2.38239	-4.33996	-	-
Asn-GTT-17-1	-	-4.01939	0	0
Asn-GTT-2-1	-3.14037	-4.63759	-2.94271	-2.83827
Asn-GTT-2-2	-3.14037	-4.63759	-2.94271	-2.83827
Asn-GTT-2-3	-3.14037	-4.63759	-2.94271	-2.83827
Asn-GTT-2-4	-3.14037	-4.63759	-2.94271	-2.83827
Asn-GTT-2-5	-3.14037	-4.63759	-2.94271	-2.83827
Asn-GTT-2-6	-3.14037	-4.63759	-2.94271	-2.83827
Asn-GTT-3-1	-2.41427	-4.53507	-2.49934	-
Asn-GTT-3-2	-2.41427	-4.53507	-2.49934	-
Asn-GTT-4-1	-	-3.86388	-	-
Asn-GTT-6-1	-3.93791	-5.12842	-	-2.84623
Asp-GTC-3-1	-	-	-2.87834	-2.28779
Cys-GCA-1-1	2.087495	-	-	-
Cys-GCA-11-1	-	-4.87899	-	-
Cys-GCA-17-1	-	-5.23799	-	-
Cys-GCA-20-1	-	0	-	-4.14926
Cys-GCA-2-1	-1.01681	-	-	-
Cys-GCA-21-1	-	-5.89673	-	-
Cys-GCA-2-2	-1.01681	-	-	-
Cys-GCA-2-3	-1.01681	-	-	-
Cys-GCA-23-1	-	-5.43444	-	-
Cys-GCA-2-4	-1.01681	-	-	-
Cys-GCA-24-1	-	-5.6477	-	-
Cys-GCA-25-1	-	-5.94361	-	-
Cys-GCA-4-1	-0.99468	-	-	-
Cys-GCA-5-1	-1.89197	-2.60543	-	-
Cys-GCA-7-1	-	-3.99027	-	-
Cys-GCA-8-1	-	-2.42271	-	-
Gln-CTG-1-1	-	-2.47142	-1.72353	-1.57616
Gln-CTG-1-2	-	-2.47142	-1.72353	-1.57616
Gln-CTG-1-3	-	-2.47142	-1.72353	-1.57616
Gln-CTG-1-4	-	-2.47142	-1.72353	-1.57616
Gln-CTG-1-5	-	-2.47142	-1.72353	-1.57616
Gln-CTG-2-1	-	-2.47849	-1.72093	-1.56977
Gln-CTG-3-1	-4.1867	-6.77468	-2.70031	-2.8208
Gln-CTG-3-2	-4.1867	-6.77468	-2.70031	-2.8208
Gln-CTG-4-1	-1.77264	-4.5221	-2.449	-2.59942
Gln-CTG-4-2	-1.77264	-4.5221	-2.449	-2.59942
Gln-CTG-6-1	-3.94191	-6.56684	-2.50382	-2.70527
Gln-CTG-7-1	3.807028	-	-	-
Gln-CTG-chr19-4	-	-5.8547	-	-5.24018
Gln-TTG-1-1	-	-3.4299	-2.23288	-2.21515
Gln-TTG-2-1	-	-2.48766	-2.47785	-2.54207

Gln-TTG-3-1	-2.50934	-5.41082	-2.22001	-2.24104
Gln-TTG-3-2	-2.50934	-5.41082	-2.22001	-2.24104
Gln-TTG-3-3	-2.50934	-5.41082	-2.22001	-2.24104
Glu-CTC-1-1	0.526727	-	-0.55372	-0.63347
Glu-CTC-1-2	0.526727	-	-0.55372	-0.63347
Glu-CTC-1-3	0.526727	-	-0.55372	-0.63347
Glu-CTC-1-4	0.526727	-	-0.55372	-0.63347
Glu-CTC-1-5	0.526727	-	-0.55372	-0.63347
Glu-CTC-1-6	0.526727	-	-0.55372	-0.63347
Glu-CTC-1-7	0.526727	-	-0.55372	-0.63347
Glu-CTC-2-1	0.527545	-	-0.54934	-0.62824
Glu-CTC-5-1	-	-	-4.56486	-4.73422
Glu-TTC-10-1	-	-2.90076	-3.23469	-2.61027
Glu-TTC-1-1	-	-	-1.80243	-
Glu-TTC-1-2	-	-	-1.80243	-
Glu-TTC-2-1	1.405875	-	-	-
Glu-TTC-2-2	1.405875	-	-	-
Glu-TTC-3-1	1.734595	1.528142	-	-
Glu-TTC-4-1	1.715924	1.474512	-	-
Glu-TTC-4-2	1.715924	1.474512	-	-
Glu-TTC-8-1	1.751555	1.573552	-	-
Glu-TTC-9-1	-	-	-3.61911	-2.70689
Gly-CCC-1-1	-	-	-0.711	-
Gly-CCC-1-2	-	-	-0.711	-
Gly-CCC-2-1	-1.57105	-2.30654	-	-
Gly-CCC-2-2	-1.57105	-2.30654	-	-
Gly-CCC-5-1	-	-	-2.61238	-
Gly-CCC-6-1	-4.52526	-7.67051	-2.64083	-2.14447
Gly-CCC-7-1	-	-4.26859	-	-4.3871
Gly-GCC-1-1	0.595762	-	-	-
Gly-GCC-1-2	0.595762	-	-	-
Gly-GCC-1-3	0.595762	-	-	-
Gly-GCC-1-4	0.595762	-	-	-
Gly-GCC-1-5	0.595762	-	-	-
Gly-GCC-2-1	-	-0.29743	-	-
Gly-GCC-2-2	-	-0.29743	-	-
Gly-GCC-2-3	-	-0.29743	-	-
Gly-GCC-2-4	-	-0.29743	-	-
Gly-GCC-2-5	-	-0.29743	-	-
Gly-GCC-2-6	-	-0.29743	-	-
Gly-GCC-3-1	-	-0.29507	-	-
Gly-GCC-5-1	-	-	0.411541	-
Gly-TCC-1-1	-	-	-2.45662	-
Gly-TCC-2-1	-1.05364	-3.0875	-2.2854	-2.43261
Gly-TCC-2-2	-1.05364	-3.0875	-2.2854	-2.43261

Gly-TCC-2-3	-1.05364	-3.0875	-2.2854	-2.43261
Gly-TCC-2-4	-1.05364	-3.0875	-2.2854	-2.43261
Gly-TCC-2-5	-1.05364	-3.0875	-2.2854	-2.43261
Gly-TCC-2-6	-1.05364	-3.0875	-2.2854	-2.43261
Gly-TCC-3-1	-	-1.87289	-	-
Gly-TCC-4-1	-	-5.67056	-	-
His-GTG-1-1	-	-	-0.9771	-
His-GTG-1-2	-	-	-0.9771	-
His-GTG-1-3	-	-	-0.9771	-
His-GTG-1-4	-	-	-0.9771	-
His-GTG-1-5	-	-	-0.9771	-
His-GTG-1-6	-	-	-0.9771	-
His-GTG-1-7	-	-	-0.9771	-
His-GTG-1-8	-	-	-0.9771	-
His-GTG-1-9	-	-	-0.9771	-
His-GTG-2-1	-	-3.05468	-	-
Ile-AAT-2-1	-	-5.6513	-	-
Ile-AAT-3-1	-	-5.6513	-	-
Ile-AAT-4-1	-	-4.78252	-3.73081	-5.04677
Ile-AAT-5-1	-	-5.78252	-	-
Ile-AAT-5-2	-	-5.78252	-	-
Ile-AAT-5-3	-	-5.78252	-	-
Ile-AAT-5-4	-	-5.78252	-	-
Ile-AAT-5-5	-	-5.78252	-	-
Ile-AAT-6-1	-	0	-4.77731	-5.31357
Ile-AAT-8-1	-3.03752	-5.42197	-	-
Ile-AAT-9-1	-	-	-	-4.56285
Ile-TAT-1-1	-	-3.53551	-	0
Ile-TAT-2-3	-	-3.53551	-	0
Leu-AAG-1-1	-1.97216	-	-	-
Leu-AAG-1-2	-1.97216	-	-	-
Leu-AAG-1-3	-1.97216	-	-	-
Leu-AAG-2-1	-1.96557	-	-	-
Leu-AAG-2-2	-1.96557	-	-	-
Leu-AAG-2-3	-1.96557	-	-	-
Leu-AAG-2-4	-1.96557	-	-	-
Leu-AAG-3-1	-1.96557	-	-	-
Leu-CAA-1-1	-2.08231	-3.8873	-3.56686	-4.32631
Leu-CAA-1-2	-2.12699	-3.94946	-3.16643	-4.1876
Leu-CAA-2-1	-2.13368	-4.01688	-2.49639	-3.90116
Leu-CAA-3-1	-2.06275	-3.83784	-	-3.45589
Leu-CAA-4-1	-2.00092	-4.06073	-3.2061	-4.31379
Leu-TAA-1-1	1.534311	-	-	-
Leu-TAA-3-1	-	-3.54277	-4.3062	-5.48883
Leu-TAA-4-1	1.892357	-	0	0

Leu-TAG-1-1	-1.90925	-	-	-
Leu-TAG-2-1	1.184648	-	-	-
Leu-TAG-3-1	-	-	-3.39643	-3.49197
Lys-CTT-10-1	-	-	-4.77731	-
Lys-CTT-1-1	-	-0.9831	1.494161	1.715847
Lys-CTT-11-1	-3.73159	-6.07767	-4.64839	-4.39485
Lys-CTT-1-2	-	-0.9831	1.494161	1.715847
Lys-CTT-2-1	-	-1.16184	2.685364	2.172222
Lys-CTT-2-2	-	-1.16184	2.685364	2.172222
Lys-CTT-2-3	-	-1.16184	2.685364	2.172222
Lys-CTT-2-4	-	-1.16184	2.685364	2.172222
Lys-CTT-2-5	-	-1.16184	2.685364	2.172222
Lys-CTT-3-1	-2.99274	-3.27634	-2.29151	-
Lys-CTT-4-1	-	-0.92587	1.747432	1.943258
Lys-CTT-5-1	-	-2.53749	-	-
Lys-CTT-6-1	-4.34442	-7.53133	-3.95648	-4.23472
Lys-CTT-7-1	-	-2.73505	-	-
Lys-CTT-8-1	-	-2.16739	-	-
Lys-CTT-chr15-5	0	0	-5.87359	-4.64518
Lys-CTT-chr7-30	-	-5.40885	-8.55701	-7.28096
Lys-TTT-1-1	-	-3.06257	-	-
Lys-TTT-14-1	-	-	-7.00079	-6.16658
Lys-TTT-2-1	-	-3.06928	-	-
Lys-TTT-3-1	-1.1947	-	-	-
Lys-TTT-3-2	-1.1947	-	-	-
Lys-TTT-3-3	-1.1947	-	-	-
Lys-TTT-3-4	-1.1947	-	-	-
Lys-TTT-3-5	-1.1947	-	-	-
Lys-TTT-4-1	-1.20819	-2.152	-2.50242	-3.01758
Lys-TTT-5-1	-1.20138	-	-	-
Lys-TTT-6-1	-	-	-2.56562	-2.48742
Lys-TTT-7-1	-1.59498	-	-2.76709	-4.59281
Lys-TTT-8-1	1.527709	-	-	-
Lys-TTT-9-1	-	-4.67056	-7.11426	-7.00816
Met-CAT-1-1	-2.39592	-3.52847	-2.68089	-2.72254
Met-CAT-2-1	-	-	-	-4.02769
Met-CAT-4-1	-	-	-	-4.02769
Met-CAT-4-2	-	-	-	-4.02769
Met-CAT-4-3	-	-	-	-4.02769
Met-CAT-5-1	-	-	-	-3.99376
Met-CAT-6-1	-2.30853	-3.21335	-	-
Phe-GAA-1-1	-2.9256	-4.97001	-	-2.92443
Phe-GAA-1-2	-2.9256	-4.97001	-	-2.92443
Phe-GAA-1-3	-2.9256	-4.97001	-	-2.92443
Phe-GAA-1-4	-2.9256	-4.97001	-	-2.92443

Phe-GAA-1-5	-2.9256	-4.97001	-	-2.92443
Phe-GAA-1-6	-2.9256	-4.97001	-	-2.92443
Phe-GAA-2-1	-2.89596	-5.13445	-	-2.95498
Phe-GAA-3-1	-	-4.64224	-3.2557	-3.29209
Phe-GAA-5-1	-	-5.77334	-5.16742	-6.47032
Pro-AGG-2-1	-	-	-2.25965	-
Pro-AGG-2-2	-	-	-2.25965	-
Pro-AGG-2-3	-	-	-2.25965	-
Pro-AGG-2-4	-	-	-2.25965	-
Pro-AGG-2-5	-	-	-2.25965	-
Pro-AGG-2-6	-	-	-2.25965	-
Pro-AGG-2-7	-	-	-2.25965	-
Pro-AGG-2-8	-	-	-2.25965	-
Pro-TGG-1-1	-3.96671	-5.46154	-3.06563	-2.98239
Pro-TGG-3-1	-	-	-2.26255	-
Pro-TGG-3-2	-	-	-2.26255	-
Pro-TGG-3-3	-	-	-2.26255	-
Pro-TGG-3-4	-	-	-2.26255	-
Pro-TGG-3-5	-	-	-2.26255	-
SeC-TCA-2-1	-	-	-	-3.04198
Ser-AGA-4-1	-2.55139	-4.37715	-3.73567	-4.61312
Ser-CGA-1-1	3.287595	-	-	-
Ser-CGA-2-1	3.285537	-	-	-
Ser-CGA-3-1	4.411013	-	-	-
Ser-CGA-4-1	-	-	-3.69289	-3.38046
Ser-GCT-1-1	3.896844	-	-	-
Ser-GCT-2-1	3.897154	-	-	-
Ser-GCT-3-1	3.789298	-	-	-
Ser-GCT-4-1	3.743573	-	-	-
Ser-GCT-4-2	3.743573	-	-	-
Ser-GCT-4-3	3.743573	-	-	-
Ser-GCT-5-1	3.934759	-	-	-
Ser-GCT-6-1	-2.00766	-4.93301	-	-
Ser-TGA-1-1	-	-	-3.77731	-3.96542
Sup-TTA-1-1	-2.56782	-5.51812	-	-
Thr-AGT-2-1	-	-5.45035	-4.88888	-4.6536
Thr-AGT-2-2	-	-5.45035	-4.88888	-4.6536
Thr-AGT-3-1	-	-4.57914	-4.52735	-4.19873
Thr-AGT-4-1	-	-	-5.70601	-6.29743
Thr-AGT-5-1	-	-	-6.8131	-6.08453
Thr-AGT-6-1	-	-5.45035	-4.77174	-4.6536
Thr-CGT-3-1	-	-5.45035	-4.28061	-4.12851
Thr-TGT-2-1	-	-	-3.19235	-
Thr-TGT-3-1	-	-	-	-3.96542
Thr-TGT-4-1	-	-2.89558	-	-

Thr-TGT-5-1	-2.27964	-3.31719	-	-
Thr-TGT-6-1	-	-2.24326	-	-
Trp-CCA-1-1	-	-	-	-4.33418
Trp-CCA-3-1	-	-	-	-3.59722
Trp-CCA-3-2	-	-	-	-3.59722
Trp-CCA-3-3	-	-	-	-3.59722
Tyr-GTA-1-1	-	-6.46733	-7.23661	-6.54804
Tyr-GTA-3-1	-5.74764	-7.63914	-5.16308	-5.93971
Tyr-GTA-4-1	-	-	-5.37052	-3.67405
Tyr-GTA-5-1	-	-2.78282	-5.33387	-4.22301
Tyr-GTA-5-2	-	-4.65906	-	-
Tyr-GTA-5-3	-	-2.87439	-5.24219	-
Tyr-GTA-5-4	-	-2.87439	-4.66195	-
Tyr-GTA-5-5	-	-2.87439	-5.03428	-4.93234
Tyr-GTA-6-1	-	-2.50943	-4.95075	-4.662
Tyr-GTA-7-1	-	-	-5.37052	-3.30521
Tyr-GTA-8-1	-	-3.53551	-4.83117	-5.61011
Val-AAC-1-1	-0.5647	0.604749	-0.6896	-0.8064
Val-AAC-1-2	-0.5647	0.604749	-0.6896	-0.8064
Val-AAC-1-3	-0.5647	0.604749	-0.6896	-0.8064
Val-AAC-1-4	-0.5647	0.604749	-0.6896	-0.8064
Val-AAC-1-5	-0.5647	0.604749	-0.6896	-0.8064
Val-AAC-2-1	-1.52364	-	-1.33314	-
Val-AAC-3-1	-0.5647	0.605364	-0.6891	-0.80594
Val-AAC-4-1	-0.56466	0.606216	-0.68901	-0.80599
Val-CAC-10-1	-	-	-4.83456	-4.14926
Val-CAC-1-1	-0.35309	-	0.339328	-
Val-CAC-11-1	-	-	-	-4.73422
Val-CAC-11-2	-	-	-	-4.73422
Val-CAC-1-2	-0.35309	-	0.339328	-
Val-CAC-1-3	-0.35309	-	0.339328	-
Val-CAC-1-4	-0.35309	-	0.339328	-
Val-CAC-1-5	-0.35309	-	0.339328	-
Val-CAC-1-6	-0.35309	-	0.339328	-
Val-CAC-2-1	-	0.956561	-	-
Val-CAC-4-1	-0.35309	-	0.339975	-
Val-CAC-5-1	-0.35217	-	0.358185	-
Val-TAC-2-1	-1.28588	-3.23338	-2.32199	-2.43273

Values are for $\log_2$(fold change) in tRNA levels as calculated with NOISeqBIO. Treatments: A/R, $\log_2$(ANG/RNase 1); A/U, $\log_2$(ANG/untreated). All values of $\log_2$(fold change) have $p \leq 0.05$.

Table 6.S3. miRNA with differential levels

miRNA Name	Δ*RNH1* A/R	Δ*RNH1* A/U	WT A/R	WT A/U
hsa-miR-92b-3p	0.637961	-	0.917395	-
hsa-miR-21-5p	0.23454	0.391549	-0.28297	-
hsa-miR-1246	-3.48241	-	-	-
hsa-miR-181b-5p	0.398107	0.309214	-	-
hsa-miR-192-5p	-0.34387	-	-	-
hsa-let-7i-5p	-0.56144	-	-0.72627	-
hsa-miR-196a-5p	-0.81072	-	-	-
hsa-miR-183-5p	-	-	-1.52403	-
hsa-miR-16-5p	-	-	-0.55057	-
hsa-miR-423-3p	0.46394	-	-	-
hsa-miR-98-5p	-0.70656	-	-0.54702	-
hsa-miR-10a-5p	-	-0.56752	-	-
hsa-let-7b-5p	-0.44477	-	-0.55481	-
hsa-miR-92a-3p	0.696078	-	0.685252	-
hsa-miR-191-5p	-0.61775	-0.58719	-0.6549	-
hsa-let-7c-5p	-0.88866	-	-0.76867	-
hsa-miR-27b-3p	-	-0.38275	-	-
hsa-miR-148b-3p	-	-0.358	-	-
hsa-miR-30a-5p	-	0.377059	-	-
hsa-miR-93-5p	-0.31718	-	-0.78504	-
hsa-miR-99b-5p	-	-1.48949	-	-
hsa-miR-100-5p	-	-0.94423	-	-
hsa-miR-21-3p	-	-0.53326	-	-
hsa-miR-24-3p	-	-	-1.15176	-
hsa-miR-320a	-0.67418	-	-0.79949	-
hsa-miR-99a-5p	-	-1.06808	-	-
hsa-miR-22-3p	-	-0.26951	-	-
hsa-miR-30d-5p	-	0.303704	-	-
hsa-miR-423-5p	0.306335	-	-	-
hsa-miR-186-5p	-0.35832	-	-	-
hsa-miR-193b-3p	-1.1136	-	-1.49097	-
hsa-miR-17-5p	-	-	-0.78964	-
hsa-miR-148a-3p	-	-0.39106	-0.40573	-
hsa-miR-374a-3p	-	-0.86105	-	-
hsa-miR-181a-5p	-	0.36722	-	-
hsa-miR-27a-3p	-	-0.26946	-	-
hsa-miR-106b-3p	-	0.848428	-	-
hsa-miR-126-5p	-	-1.2177	-	-
hsa-miR-30c-5p	-	-0.41851	-	-
hsa-let-7e-5p	-	-0.39318	-	-
hsa-miR-30a-3p	-	-0.39102	-	-
hsa-miR-182-5p	-	0.630049	-	-

hsa-miR-20a-5p	-	-	-0.54094	-
hsa-miR-331-3p	-	-1.33843	-	-
hsa-miR-484	-	-0.81671	-	-
hsa-miR-31-5p	-	-	-0.51893	-
hsa-miR-221-3p	-	-	-0.66057	-
hsa-miR-103a-3p	-	-	-0.27398	-

Values are for $\log_2$(fold change) in tRNA levels as calculated with NOISeqBIO. Treatments: A/R, $\log_2$(ANG/RNase 1); A/U, $\log_2$(ANG/untreated). All values of $\log_2$(fold change) have $p \leq 0.05$.

Table 6.S4. Enriched GO terms for miRNAs

Upregulated miRNAs	Downregulated miRNAs
hsa-miR-181b-5p, hsa-miR-423-3p, hsa-miR-92b-3p, hsa-miR-92a-3p, hsa-miR-181a-5p	hsa-miR-192-5p, hsa-miR-98-5p, hsa-miR-196a-5p, hsa-let-7c-5p, hsa-let-7i-5p, hsa-let-7b-5p, hsa-miR-193b-3p, hsa-miR-320a, hsa-miR-22-3p, hsa-miR-103a-3p, hsa-miR-93-5p, hsa-miR-183-5p, hsa-miR-31-5p, hsa-miR-17-5p, hsa-miR-20a-5p hsa-miR-24-3p, hsa-miR-221-3p, hsa-miR-192-5p

Unique enriched GO terms in miRNAs upregulated after ANG treatment	
Name	Log size
U6 snRNA binding	3.114
RNA polymerase II repressing transcription factor binding	2.976
6-phosphofructo-2-kinase activity	3.356
glutathione transferase activity	3.671
microtubule binding	4.557
NADP binding	4.917
protein binding involved in protein folding	3.250
hydrogen ion transmembrane transporter activity	5.115
axon guidance receptor activity	2.220
modified amino acid binding	4.368
calcium-dependent phospholipase A2 activity	1.908
deacetylase activity	4.212
polyubiquitin binding	3.321
translation initiation factor activity	4.762
NAD^+ ADP-ribosyltransferase activity	3.663
steroid hormone receptor activity	3.829
cyclin-dependent protein serine/threonine kinase inhibitor activity	3.104
phosphatidylinositol-3-phosphatase activity	2.768
protein deacetylase activity	3.833
lyase activity	5.704
transcription coactivator activity	4.105
centromeric DNA binding	2.906
eukaryotic translation initiation factor 2α kinase activity	2.639
NADPH binding	3.704
single-stranded RNA binding	3.899
MAP kinase activity	3.725
ATP-dependent DNA helicase activity	4.659
phosphotyrosine binding	3.104
poly(A) binding	3.024
MHC class I receptor activity	1.771
signal recognition particle binding	3.274
fructose binding	2.053
Y-form DNA binding	2.377

acetyltransferase activity	5.239
methyltransferase activity	5.593
transferase activity	6.472
fructose-2,6-bisphosphate 2-phosphatase activity	2.413
S-methyl-5-thioribose-1-phosphate isomerase activity	3.355
bisphosphoglycerate 2-phosphatase activity	1.708
bisphosphoglycerate mutase activity	2.468
transferase activity, transferring acyl groups	5.610
LRR domain binding	2.515
scavenger receptor activity	3.761
insulin receptor substrate binding	2.528
translation initiation factor binding	3.625
insulin-like growth factor binding	3.297
protein homodimerization activity	4.493
α-2A adrenergic receptor binding	2.004
threonine-type endopeptidase activity	4.253
androgen receptor binding	2.808
insulin-like growth factor-activated receptor activity	1.505
peroxiredoxin activity	4.348

Unique enriched GO terms in miRNAs downregulated after ANG treatment

Name	Log size
cofactor binding	5.897
protein disulfide oxidoreductase activity	4.634
peroxidase activity	4.725
cyclin binding	3.226
hydrolase activity	6.497
chemoattractant activity	2.815
cell adhesion molecule binding	4.095
protein serine/threonine/tyrosine kinase activity	3.596
protein tyrosine kinase activity	4.288
non-membrane spanning protein tyrosine kinase activity	3.768
electron carrier activity	5.254
NAD binding	5.129
L-ascorbic acid binding	3.938
Hsp90 protein binding	2.934
protein self-association	3.279
translation factor activity, RNA binding	5.107
protein tyrosine phosphatase activity	4.515
transcription factor activity, protein binding	5.074
phosphatidylinositol 3-kinase binding	2.873
Wnt-protein binding	3.083
sequence-specific DNA binding	5.495
oxidoreductase activity, acting on single donors with incorporation of molecular oxygen, incorporation of two atoms of oxygen	4.399
thiol-dependent ubiquitin-specific protease activity	4.040

protein transporter activity	4.863
growth factor binding	3.677
peptide binding	4.098
calcium-dependent protein binding	3.176
DNA-directed DNA polymerase activity	4.808
catalytic activity	6.967
helicase activity	5.236
microtubule motor activity	4.487
histone acetyltransferase activity	3.966
manganese ion binding	4.557
4 iron, 4 sulfur cluster binding	5.152
PDZ domain binding	3.259
peptidase activity	5.756
transcription corepressor activity	3.847
protein kinase inhibitor activity	3.627
RNA binding	5.871
core promoter binding	3.798
receptor activity	5.579
mRNA 3'-UTR binding	3.365
double-stranded RNA binding	4.071
DNA binding	6.247
p53 binding	3.276
ion channel binding	3.388
chaperone binding	4.155
histone-lysine *N*-methyltransferase activity	3.995
single-stranded DNA binding	4.490
vitamin D receptor binding	2.217
methylated histone binding	3.331
transforming growth factor β-activated receptor activity	2.529
lamin binding	2.493
transforming growth factor β binding	2.667
RNA polymerase II carboxy-terminal domain kinase activity	3.175

Enriched Molecular Function GO terms for miRNAs up- or downregulated after ANG treatment. Lists of differentially regulated miRNAs were chosen from hierarchical clusters of fold-change data generated with NOISeqBIO (see: Table 6.S3). The GO terms listed are semantically reduced, and then analyzed for uniqueness using network analysis (see: Materials and Methods section). "Log size" refers to the extent of enrichment for a particular term.

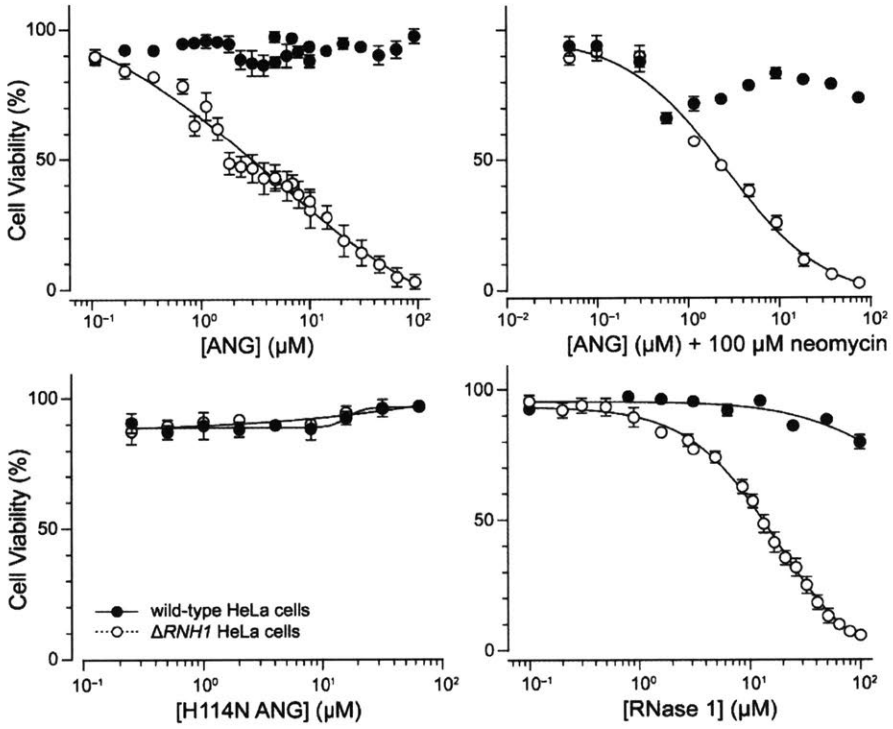
Cell Viability (%)
100
50
0
10^{-1}
10^{0}
10^{1}
10^{2}
[ANG] (μM)
10^{-2}
[ANG] (μM) + 100 μM neomycin
wild-type HeLa cells
ΔRNH1 HeLa cells
[H114N ANG] (μM)
[RNase 1] (μM)

Figure 6.S1. Toxicity of ANG and related proteins for wild-type and Δ*RNH1* HeLa cells. Ribonucleases were incubated with cells for 48 h at 37 °C and 5% CO_2. Data points are the average of at least three biological replicates as measured with a tetrazolium dye-based assay for metabolic activity. Values of EC_{50} were calculated by fitting the data to Eq. 1 and are listed in Table 6.1.

References

1. Walsh, C., *Posttranslational Modification of Proteins: Expanding Nature's Inventory.* Englewood, CO.: Roberts and Co.: 2006.
2. Apweiler, R.; Hermjakob, H.; Sharon, N., On the frequency of protein glycosylation, as deduced from analysis of the SWISS-PROT database. *Biochim. Biophysi. Acta* **1999,** *1473* (1), 4-8.
3. Moremen, K. W.; Tiemeyer, M.; Nairn, A. V., Vertebrate protein glycosylation: Diversity, synthesis and function. *Nat. Rev. Mol. Cell Biol.* **2012,** *13* (7), 448-462.
4. Hart, G. W.; Slawson, C.; Ramirez-Correa, G.; Lagerlof, O., Cross talk between O-GlcNAcylation and phosphorylation: Roles in signaling, transcription, and chronic disease. *Annu. Rev. Biochem.* **2011,** *80*, 825-858.
5. Varki, A., Biological roles of oligosaccharides: All of the theories are correct. *Glycobiology* **1993,** *3* (2), 97-130.
6. Spicer, C. D.; Davis, B. G., Selective chemical protein modification. *Nat. Commun.* **2014,** *5*, 4740.
7. Bertozzi, C. R.; Kiessling, L. L., Chemical glycobiology. *Science* **2001,** *291* (5512), 2357-2364.
8. Beintema, J. J.; Schüller, C.; Irie, M.; Carsana, A., Molecular evolution of the ribonuclease superfamily. *Prog. Biophys. Mol. Biol.* **1988,** *51* (3), 165-192.
9. Raines, R. T., Ribonuclease A. *Chem. Rev.* **1998,** *98* (3), 1045-1066.
10. Neurath, H., The golden years of protein science. *Protein Sci.* **1995,** *4* (9), 1939-1943.
11. Kartha, G.; Bello, J.; Harker, D., Tertiary structure of ribonuclease. *Nature* **1967,** *213*, 862.
12. Anfinsen, C. B., Principles that govern the folding of protein chains. *Science* **1973,** *181* (4096), 223-230.
13. Moore, S.; Stein, W. H., Chemical structures of pancreatic ribonuclease and deoxyribonuclease. *Science* **1973,** *180* (4085), 458-464.
14. Merrifield, R. B., Solid phase synthesis. *Science* **1986,** *232*, 341-348.
15. Rodríguez, M.; Moussaoui, M.; Benito, A.; Cuchillo, C. M.; Nogués, M. V.; Vilanova, M., Human pancreatic ribonuclease presents higher endonucleolytic activity than ribonuclease A. *Arch. Biochem. Biophys.* **2008,** *471* (2), 191-197.
16. Sorrentino, S.; Naddeo, M.; Russo, A.; D'Alessio, G., Degradation of double-stranded RNA by human pancreatic ribonuclease: crucial role of noncatalytic basic amino acid residues. *Biochemistry* **2003,** *42* (34), 10182-10190.
17. Rosenberg, H. F., Eosinophil-derived neurotoxin / RNase 2: connecting the past, the present and the future. *Curr. Pharm. Biotechnol.* **2008,** *9* (3), 135-140.
18. Boix, E.; Torrent, M.; Sanchez, D.; Nogues, M. V., The antipathogen activities of eosinophil cationic protein. *Curr. Pharm. Biotechnol.* **2008,** *9* (3), 141-152.
19. de Oliveira, P. C.; de Lima, P. O.; Oliveira, D. T.; Pereira, M. C., Eosinophil cationic protein: Overview of biological and genetic features. *DNA Cell Biol.* **2012,** *31* (9), 1442-1446.
20. Hoang, T. T.; Raines, R. T., Molecular basis for the autonomous promotion of cell proliferation by angiogenin. *Nucleic Acids Res.* **2017,** *45* (2), 818-831.
21. Li, S.; Sheng, J.; Hu, J. K.; Yu, W.; Kishikawa, H.; Hu, M. G.; Shima, K.; Wu, D.; Xu, Z.; Xin, W.; Sims, K. B.; Landers, J. E.; Brown, R. H., Jr.; Hu, G. F., Ribonuclease 4 protects neuron degeneration by promoting angiogenesis, neurogenesis, and neuronal survival under stress. *Angiogenesis* **2013,** *16* (2), 387-404.

22. Dickson, K. A.; Haigis, M. C.; Raines, R. T., Ribonuclease inhibitor: Structure and function. *Prog. Nucleic Acids Res. Mol. Biol.* **2005,** *80*, 349-374.
23. Braakman, I.; Hebert, D. N., Protein folding in the endoplasmic reticulum. *Cold Spring Harb. Perspect. Biol.* **2013,** *5* (5).
24. Araki, K.; Nagata, K., Protein folding and quality control in the ER. *Cold Spring Harb. Perspect. Biol.* **2011,** *3* (11).
25. Medus, M. L.; Gomez, G. E.; Zacchi, L. F.; Couto, P. M.; Labriola, C. A.; Labanda, M. S.; Bielsa, R. C.; Clérico, E. M.; Schulz, B. L.; Caramelo, J. J., N-Glycosylation triggers a dual selection pressure in eukaryotic secretory proteins. *Sci. Rep.* **2017,** *7* (1), 8788-8788.
26. Lizak, C.; Gerber, S.; Numao, S.; Aebi, M.; Locher, K. P., X-ray structure of a bacterial oligosaccharyltransferase. *Nature* **2011,** *474* (7351), 350-355.
27. Ruiz-Canada, C.; Kelleher, D. J.; Gilmore, R., Cotranslational and posttranslational N-glycosylation of polypeptides by distinct mammalian OST isoforms. *Cell* **2009,** *136* (2), 272-283.
28. Petrescu, A.-J.; Milac, A.-L.; Petrescu, S. M.; Dwek, R. A.; Wormald, M. R., Statistical analysis of the protein environment of N-glycosylation sites: implications for occupancy, structure, and folding. *Glycobiology* **2004,** *14* (2), 103-114.
29. Mohorko, E.; Glockshuber, R.; Aebi, M., Oligosaccharyltransferase: the central enzyme of N-linked protein glycosylation. *J. Inherit. Metab. Dis.* **2011,** *34* (4), 869-878.
30. Bieberich, E., Synthesis, processing, and function of N-glycans in N-glycoproteins. *Adv. Neurobiol.* **2014,** *9*, 47-70.
31. Durand, G.; Seta, N., Protein glycosylation and diseases: Blood and urinary oligosaccharides as markers for diagnosis and therapeutic monitoring. *Clin. Chem.* **2000,** *46* (6), 795.
32. Rudd, P. M.; Dwek, R. A., Glycosylation: Heterogeneity and the 3D structure of proteins. *Criti. Rev. Biochem. Mol. Biol.* **1997,** *32* (1), 1-100.
33. An, H. J.; Froehlich, J. W.; Lebrilla, C. B., Determination of glycosylation sites and site-specific heterogeneity in glycoproteins. *Curr. Opin. Chem. Biol.* **2009,** *13* (4), 421-426.
34. Martin, A. J. P.; Porter, R. R., The chromatographic fractionation of ribonuclease. *Biochem. J.* **1951,** *49* (2), 215-218.
35. Hirs, C. H.; Moore, S.; Stein, W. H., A chromatographic investigation of pancreatic ribonuclease. *J. Biol. Chem.* **1953,** *200* (2), 493-506.
36. Plummer, T. H., Jr., Glycoproteins of bovine pancreatic juice. Isolation of ribonucleases C and D. *J. Biol. Chem.* **1968,** *243*, 5961-5966.
37. Plummer, T. H.; Hirs, C. H. W., On the Structure of Bovine Pancreatic Ribonuclease B: Isolation of a glycopeptide. *J. Biol. Chem.* **1964,** *239* (8), 2530-2538.
38. Marshall, G. R.; Feng, J. A.; Kuster, D. J., Back to the future: Ribonuclease A. *Biopolymers* **2008,** *90* (3), 259-277.
39. Lomax, J. E.; Eller, C. H.; Raines, R. T., Comparative functional analysis of ribonuclease 1 homologs: molecular insights into evolving vertebrate physiology. *Biochem. J.* **2017,** *474* (13), 2219-2233.
40. Futami, J.; Tsushima, Y.; Murato, Y.; Tada, H.; Sasaki, J.; Seno, M.; Yamada, H., Tissue-specific expression of pancreatic-type RNases and RNase inhibitor in humans. *DNA Cell Biol.* **1997,** *16* (4), 413-419.
41. Barrabés, S.; Pagès-Pons, L.; Radcliffe, C. M.; Tabarés, G.; Fort, E.; Royle, L.; Harvey, D. J.; Moenner, M.; Dwek, R. A.; Rudd, P. M.; De Llorens, R.; Peracaula, R., Glycosylation of serum

ribonuclease 1 indicates a major endothelial origin and reveals an increase in core fucosylation in pancreatic cancer. *Glycobiology* **2007,** *17*, 388-400.
42. Ribó, M.; Beintema, J. J.; Osset, M.; Fernández, E.; Bravo, J.; de Llorens, R.; Cuchillo, C. M., Heterogeneity in the glycosylation pattern of human pancreatic ribonuclease. *Biol. Chem. Hoppe-Seyler* **1994,** *375*, 357-363.
43. Beintema, J. J.; Breukelman, H. J.; Carsana, A.; Furia, A., Evolution of vertebrate ribonucleases: Ribonuclease A superfamily. In *Ribonucleases: Structures and Functions*, D'Alessio, G.; Riordan, J. F., Eds. Academic Press: New York, 1997; pp 245-269.
44. Gautschi, M.; Beintema, J. J., Selection against glycosylation in ruminant pancreatic ribonucleases by replacements in the ancestral carbohydrate attachment site. *Biochem. Genet.* **2008,** *46* (7-8), 446-450.
45. Weickmann, J. L.; Olson, E. M.; Glitz, D. G., Immunological assay of pancreatic ribonuclease in serum as an indicator of pancreatic cancer. *Cancer Res.* **1984,** *44*, 1682-1687.
46. Fischer, S.; Nishio, M.; Dadkhahi, S.; Gansler, J.; Saffarzadeh, M.; Shibamiyama, A.; Kral, N.; Baal, N.; Koyama, T.; Deindl, E.; Preissner, K. T., Expression and localisation of vascular ribonucleases in endothelial cells. *Thromb. Haemost.* **2011,** *105* (2), 345-355.
47. Su, A. I.; Wiltshire, T.; Batalo, S.; Lapp, H.; Ching, K. A.; Block, D.; Zhang, J.; Soden, R.; Hayakawa, M.; Kreiman, G.; Cooke, M. P.; Walker, J. R.; Hogenesch, J. B., A gene atlas of the mouse and human protein-encoding transcriptomes. *Proc. Natl. Acad. Sci. U.S.A.* **2004,** *101*, 6062-6067.
48. Morita, T.; Niwata, Y.; Ohgi, K.; Ogawa, M.; Irie, M., Distribution of two urinary ribonuclease-like enzymes in human organs and body fluids. *Biochem. J.* **1986,** *99* (1), 17-25.
49. Yasuda, T.; Nadano, D.; Takeshita, H.; Kishi, K., Two distinct secretory ribonucleases from human cerebrum: Purification, characterization and relationships to other ribonucleases. *Biochem. J.* **1993,** *296 (Pt 3)* (Pt 3), 617-625.
50. Beintema, J. J.; Blank, A.; Schieven, G. L.; Dekker, C. A.; Sorrentino, S.; Libonati, M., Differences in glycosylation pattern of human secretory ribonucleases. *Biochem. J.* **1988,** *255* (2), 501-505.
51. Reddi, K. K.; Holland, J. F., Elevated serum ribonuclease in patients with pancreatic cancer. *Proc. Natl. Acad. Sci. U.S.A.* **1976,** *73* (7), 2308-2310.
52. Doran, G.; Allen-Mersh, T. G.; Reynolds, K. W., Ribonuclease as a tumour marker for pancreatic carcinoma. *J. Clin. Pathol.* **1980,** *33* (12), 1212-1213.
53. Fabris, C.; Farini, R.; del Favero, G.; Piccoli, A.; Naccarato, R., "Plasma"-type ribonuclease in pancreatic cancer diagnosis: A critical appraisal. *Hepatogastroenterology* **1981,** *28* (6), 316-318.
54. Peterson, L. M., Serum RNase in the diagnosis of pancreatic carcinoma. *Proc. Natl. Acad. Sci. U.S.A.* **1979,** *76* (6), 2630-2634.
55. Nakata, D., Increased N-glycosylation of Asn88 in serum pancreatic ribonuclease 1 is a novel diagnostic marker for pancreatic cancer. *Sci. Rep.* **2014,** *4*, 6715.
56. Ribo, M.; delCardayre, S. B.; Raines, R. T.; de Llorens, R.; Cuchillo, C. M., Production of human pancreatic ribonuclease in Saccharomyces cerevisiae and Escherichia coli. *Protein Expr. Purif.* **1996,** *7* (3), 253-261.
57. Geiger, R.; Gautschi, M.; Thor, F.; Hayer, A.; Helenius, A., Folding, quality control, and secretion of pancreatic ribonuclease in live cells. *J. Biol. Chem.* **2011,** *286* (7), 5813-5822.
58. Tang, H.; Wang, S.; Wang, J.; Song, M.; Xu, M.; Zhang, M.; Shen, Y.; Hou, J.; Bao, X., *N*-Hypermannose glycosylation disruption enhances recombinant protein production by regulating

secretory pathway and cell wall integrity in Saccharomyces cerevisiae. *Sci. Rep.* **2016,** *6*, 25654-25654.
59. Irani, Z. A.; Kerkhoven, E. J.; Shojaosadati, S. A.; Nielsen, J., Genome-scale metabolic model of Pichia pastoris with native and humanized glycosylation of recombinant proteins. *Biotechnol. Bioeng.* **2016,** *113* (5), 961-969.
60. Gemmill, T. R.; Trimble, R. B., Overview of N- and O-linked oligosaccharide structures found in various yeast species. *Biochim. Biophys. Acta* **1999,** *1426* (2), 227-237.
61. Daly, R.; Hearn, M. T., Expression of heterologous proteins in Pichia pastoris: a useful experimental tool in protein engineering and production. *J. Mol. Recognit.* **2005,** *18* (2), 119-138.
62. Cregg, J. M.; Cereghino, J. L.; Shi, J.; Higgins, D. R., Recombinant protein expression in Pichia pastoris. *Mol. Biotechnol.* **2000,** *16* (1), 23-52.
63. Laukens, B.; De Wachter, C.; Callewaert, N., Engineering the Pichia pastoris N-glycosylation pathway using the GlycoSwitch Technology. *Methods Mol. Biol.* **2015,** *1321*, 103-122.
64. Hamilton, S. R.; Davidson, R. C.; Sethuraman, N.; Nett, J. H.; Jiang, Y.; Rios, S.; Bobrowicz, P.; Stadheim, T. A.; Li, H.; Choi, B. K.; Hopkins, D.; Wischnewski, H.; Roser, J.; Mitchell, T.; Strawbridge, R. R.; Hoopes, J.; Wildt, S.; Gerngross, T. U., Humanization of yeast to produce complex terminally sialylated glycoproteins. *Science* **2006,** *313* (5792), 1441-1443.
65. Bretthauer, R. K., Genetic engineering of Pichia pastoris to humanize N-glycosylation of proteins. *Trends Biotechnol.* **2003,** *21* (11), 459-462.
66. Chiba, Y.; Akeboshi, H., Glycan engineering and production of 'humanized' glycoprotein in yeast cells. *Biol. Pharm. Bull.* **2009,** *32* (5), 786-795.
67. Vervecken, W.; Callewaert, N.; Kaigorodov, V.; Geysens, S.; Contreras, R., Modification of the N-glycosylation pathway to produce homogeneous, human-like glycans using GlycoSwitch plasmids. In *Pichia Protocols*, Cregg, J. M., Ed. Humana Press: Totowa, NJ, 2007; pp 119-138.
68. Jacobs, P. P.; Geysens, S.; Vervecken, W.; Contreras, R.; Callewaert, N., Engineering complex-type N-glycosylation in Pichia pastoris using GlycoSwitch technology. *Nat. Protoc.* **2009,** *4* (1), 58-70.
69. Strong, L. E.; Kink, J. A.; Mei, B.; Shahan, M. N.; Raines, R. T., First-in-human phase I clinical trial of QBI-139, a human ribonuclease variant, in solid tumors. *J. Clin. Oncol.* **2012,** *30* (15_suppl), TPS3113-TPS3113.
70. Strong, L. E.; Kink, J. A.; Pensinger, D.; Mei, B.; Shahan, M.; Raines, R. T., Efficacy of ribonuclease QBI-139 in combination with standard of care therapies. *Cancer Res.* **2012,** *72 (Suppl. 1)*, 1838.
71. Lomax, J. E.; Eller, C. H.; Raines, R. T., Rational design and evaluation of mammalian ribonuclease cytotoxins. *Methods Enzymol.* **2012,** *502*, 273-290.
72. Chao, T. Y.; Lavis, L. D.; Raines, R. T., Cellular uptake of ribonuclease A relies on anionic glycans. *Biochemistry* **2010,** *49* (50), 10666-10673.
73. Haigis, M. C.; Raines, R. T., Secretory ribonucleases are internalized by a dynamin-independent endocytic pathway. *J. Cell Sci.* **2003,** *116* (Pt 2), 313-324.
74. Leich, F.; Stohr, N.; Rietz, A.; Ulbrich-Hofmann, R.; Arnold, U., Endocytotic internalization as a crucial factor for the cytotoxicity of ribonucleases. *J. Biol. Chem.* **2007,** *282* (38), 27640-27646.
75. Mayor, S.; Pagano, R. E., Pathways of clathrin-independent endocytosis. *Nat. Rev. Mol. Cell Biol.* **2007,** *8*, 603.
76. Johnson, R. J.; Chao, T.-Y.; Lavis, L. D.; Raines, R. T., Cytotoxic ribonucleases: The dichotomy of Coulombic forces. *Biochemistry* **2007,** *46* (36), 10308-10316.

77. Chao, T.-Y.; Raines, R. T., Mechanism of ribonuclease A endocytosis: Analogies to cell-penetrating peptides. *Biochemistry* **2011,** *50* (39), 8374-8382.
78. Dube, D. H.; Bertozzi, C. R., Glycans in cancer and inflammation--potential for therapeutics and diagnostics. *Nat. Rev. Drug Discov.* **2005,** *4* (6), 477-488.
79. Eller, C. H.; Chao, T.-Y.; Singarapu, K. K.; Ouerfelli, O.; Yang, G.; Markley, J. L.; Danishefsky, S. J.; Raines, R. T., Human cancer antigen Globo H is a cell-surface ligand for human ribonuclease 1. *ACS Cent. Sci.* **2015,** *1* (4), 181-190.
80. Mariani-Costantini, R.; Barbanti, P.; Colnaghi, M. I.; Menard, S.; Clemente, C.; Rilke, F., Reactivity of a monoclonal antibody with tissues and tumors from the human breast. Immunohistochemical localization of a new antigen and clinicopathologic correlations. *Am. J. Pathol.* **1984,** *115* (1), 47-56.
81. Mariani-Costantini, R.; Colnaghi, M. I.; Leoni, F.; Menard, S.; Cerasoli, S.; Rilke, F., Immunohistochemical reactivity of a monoclonal antibody prepared against human breast carcinoma. *Virchows Arch. A Pathol. Anat. Histopathol.* **1984,** *402* (4), 389-404.
82. Bremer, E. G.; Levery, S. B.; Sonnino, S.; Ghidoni, R.; Canevari, S.; Kannagi, R.; Hakomori, S., Characterization of a glycosphingolipid antigen defined by the monoclonal antibody MBr1 expressed in normal and neoplastic epithelial cells of human mammary gland. *J. Biol. Chem.* **1984,** *259* (23), 14773-14777.
83. Danishefsky, S. J.; Shue, Y.-K.; Chang, M. N.; Wong, C.-H., Development of Globo-H cancer vaccine. *Acc. Chem. Res.* **2015,** *48* (3), 643-652.
84. Rutkoski, T. J.; Raines, R. T., Evasion of ribonuclease inhibitor as a determinant of ribonuclease cytotoxicity. *Curr. Pharm. Biotechnol.* **2008,** *9* (3), 185-189.
85. Lee, J. E.; Raines, R. T., Ribonucleases as novel chemotherapeutics: The ranpirnase example. *BioDrugs* **2008,** *22* (1), 53-58.
86. Wu, Y.; Mikulski, S. M.; Ardelt, W.; Rybak, S. M.; Youle, R. J., A cytotoxic ribonuclease. Study of the mechanism of onconase cytotoxicity. *J. Biol. Chem.* **1993,** *268* (14), 10686-10693.
87. Costanzi, J.; Sidransky, D.; Navon, A.; Goldsweig, H., Ribonucleases as a novel pro-apoptotic anticancer strategy: review of the preclinical and clinical data for ranpirnase. *Cancer Invest.* **2005,** *23* (7), 643-650.
88. Vasandani, V. M.; Burris, J. A.; Sung, C., Reversible nephrotoxicity of onconase and effect of lysine pH on renal onconase uptake. *Cancer Chemother. Pharmacol.* **1999,** *44* (2), 164-169.
89. Lomax, J. E.; Bianchetti, C. M.; Chang, A.; Phillips, G. N., Jr.; Fox, B. G.; Raines, R. T., Functional evolution of ribonuclease inhibitor: Insights from birds and reptiles. *J. Mol. Biol.* **2014,** *426* (17), 3041-3056.
90. Rutkoski, T. J.; Kink, J. A.; Strong, L. E.; Raines, R. T., Site-specific PEGylation endows a mammalian ribonuclease with antitumor activity. *Cancer Biol. Ther.* **2011,** *12* (3), 208-214.
91. Rutkoski, T. J.; Kink, J. A.; Strong, L. E.; Raines, R. T., Human ribonuclease with a pendant poly(ethylene glycol) inhibits tumor growth in mice. *Transl. Oncol.* **2013,** *6*, 392-397.
92. Leland, P. A.; Staniszewski, K. E.; Kim, B.-M.; Raines, R. T., Endowing human pancreatic ribonuclease with toxicity for cancer cells. *J. Biol. Chem.* **2001,** *276*, 43095-43102.
93. Conner, S. D.; Schmid, S. L., Regulated portals of entry into the cell. *Nature* **2003,** *422*, 37.
94. Polo, S.; Di Fiore, P. P., Endocytosis conducts the cell signaling orchestra. *Cell* **2006,** *124* (5), 897-900.
95. Vink, H.; Duling, B. R., Identification of distinct luminal domains for macromolecules, erythrocytes, and leukocytes within mammalian capillaries. *Circ. Res.* **1996,** *79* (3), 581-589.

96. In *Essentials of Glycobiology*, nd; Varki, A.; Cummings, R. D.; Esko, J. D.; Freeze, H. H.; Stanley, P.; Bertozzi, C. R.; Hart, G. W.; Etzler, M. E., Eds. Cold Spring Harbor Laboratory Press: Cold Spring Harbor (NY), 2009.
97. Reitsma, S.; Slaaf, D. W.; Vink, H.; van Zandvoort, M. A. M. J.; oude Egbrink, M. G. A., The endothelial glycocalyx: Composition, functions, and visualization. *Pflugers Archiv.* **2007,** *454* (3), 345-359.
98. Sun, D.; Chen, J.; Song, Y.; Zhu, C.; Pan, G.; Wan, L., Topography and functional information of plasma membrane. *Sci. China, C, Life Sci.* **2008,** *51* (2), 95-103.
99. Yang, N. J.; Hinner, M. J., Getting across the cell membrane: An overview for small molecules, peptides, and proteins. *Methods Mol. Biol.* **2015,** *1266*, 29-53.
100. Fu, A.; Tang, R.; Hardie, J.; Farkas, M. E.; Rotello, V. M., Promises and pitfalls of intracellular delivery of proteins. *Bioconjugate Chem.* **2014,** *25* (9), 1602-1608.
101. Varkouhi, A. K.; Scholte, M.; Storm, G.; Haisma, H. J., Endosomal escape pathways for delivery of biologicals. *J. Control. Release* **2011,** *151* (3), 220-228.
102. Bruce, V. J.; McNaughton, B. R., Inside job: Methods for delivering proteins to the interior of mammalian cells. *Cell Chem. Biol.* **2017,** *24* (8), 924-934.
103. Mukherjee, S.; Ghosh, R. N.; Maxfield, F. R., Endocytosis. *Physiol. Rev.* **1997,** *77* (3), 759-803.
104. Marsh, M.; McMahon, H. T., The structural era of endocytosis. *Science* **1999,** *285* (5425), 215-220.
105. Lee, Y.; Ishii, T.; Kim, H. J.; Nishiyama, N.; Hayakawa, Y.; Itaka, K.; Kataoka, K., Efficient delivery of bioactive antibodies into the cytoplasm of living cells by charge-conversional polyion complex micelles. *Angew. Chem. Int. Ed. Engl.* **2010,** *49* (14), 2552-2555.
106. Wang, M.; Alberti, K.; Sun, S.; Arellano, C. L.; Xu, Q., Combinatorially designed lipid-like nanoparticles for intracellular delivery of cytotoxic protein for cancer therapy. *Angew. Chem. Int. Ed. Engl.* **2014,** *53* (11), 2893-2898.
107. Peer, D.; Karp, J. M.; Hong, S.; Farokhzad, O. C.; Margalit, R.; Langer, R., Nanocarriers as an emerging platform for cancer therapy. *Nat. Nanotechnol.* **2007,** *2* (12), 751-760.
108. Duchardt, F.; Fotin-Mleczek, M.; Schwarz, H.; Fischer, R.; Brock, R., A comprehensive model for the cellular uptake of cationic cell-penetrating peptides. *Traffic* **2007,** *8* (7), 848-866.
109. Brock, R., The uptake of arginine-rich cell-penetrating peptides: Putting the puzzle together. *Bioconjugate Chem.* **2014,** *25* (5), 863-868.
110. Cronican, J. J.; Beier, K. T.; Davis, T. N.; Tseng, J. C.; Li, W.; Thompson, D. B.; Shih, A. F.; May, E. M.; Cepko, C. L.; Kung, A. L.; Zhou, Q.; Liu, D. R., A class of human proteins that deliver functional proteins into mammalian cells in vitro and in vivo. *Chem. Biol.* **2011,** *18* (7), 833-838.
111. Thompson, D. B.; Cronican, J. J.; Liu, D. R., Engineering and identifying supercharged proteins for macromolecule delivery into mammalian cells. *Methods Enzymol.* **2012,** *503*, 293-319.
112. Doane, T.; Burda, C., Nanoparticle mediated non-covalent drug delivery. *Adv. Drug Deliv. Rev.* **2013,** *65* (5), 607-621.
113. Baslé, E.; Joubert, N.; Pucheault, M., Protein chemical modification on endogenous amino acids. *Chem. Biol.* **2010,** *17* (3), 213-227.
114. Harris, J. M.; Chess, R. B., Effect of pegylation on pharmaceuticals. *Nat. Rev. Drug Discov.* **2003,** *2* (3), 214-221.
115. De Groot, A. S.; Scott, D. W., Immunogenicity of protein therapeutics. *Trends Immunol.* **2007,** *28* (11), 482-490.

116. Onoue, S.; Yamada, S.; Chan, H. K., Nanodrugs: Pharmacokinetics and safety. *Int. J. Nanomedicine* **2014,** *9*, 1025-1037.
117. Bruno, B. J.; Miller, G. D.; Lim, C. S., Basics and recent advances in peptide and protein drug delivery. *Ther. Del.* **2013,** *4* (11), 1443-1467.
118. Kirmse, W., 100 years of the Wolff rearrangement. *Eur. J. Org. Chem.* **2002,** *2002* (14), 2193-2256.
119. Saalfrank, R. W., Diazo compounds. Properties and synthesis. *Angew. Chem.* **1987,** *99* (12), 1335-1335.
120. Ford, A.; Miel, H.; Ring, A.; Slattery, C. N.; Maguire, A. R.; McKervey, M. A., Modern organic synthesis with α-diazocarbonyl compounds. *Chem. Rev.* **2015,** *115* (18), 9981-10080.
121. Josa-Culleré, L.; Wainman, Y. A.; Brindle, K. M.; Leeper, F. J., Diazo group as a new chemical reporter for bioorthogonal labelling of biomolecules. *RSC Adv.* **2014,** *4* (94), 52241-52244.
122. McGrath, N. A.; Andersen, K. A.; Davis, A. K. F.; Lomax, J. E.; Raines, R. T., Diazo compounds for the bioreversible esterification of proteins. *Chem. Sci.* **2015,** *6* (1), 752-755.
123. Le, W. E., Diazomethane poisoning; report of a fatal case with autopsy. *Am. J. Med. Sci.* **1949,** *218* (5), 556-562.
124. Schoental, R., Carcinogenic action of diazomethane and of nitroso-N-methyl urethane. *Nature* **1960,** *188*, 420.
125. Lewis, C. E., Diazomethane poisoning. Report of a case suggesting sensitization reaction. *J. Occup. Med.* **1964,** *6*, 91-92.
126. Mix, K. A.; Aronoff, M. R.; Raines, R. T., Diazo compounds: Versatile tools for chemical biology. *ACS Chem. Biol.* **2016,** *11* (12), 3233-3244.
127. Myers, E. L.; Raines, R. T., A phosphine-mediated conversion of azides into diazo compounds. *Angew. Chem.* **2009,** *48* (13), 2359-2363.
128. Chou, H.-H.; Raines, R. T., Conversion of azides into diazo compounds in water. *J. Am. Chem. Soc.* **2013,** *135* (40), 14936-14939.
129. Liederer, B. M.; Borchardt, R. T., Enzymes involved in the bioconversion of ester-based prodrugs. *J. Pharm. Sci.* **2006,** *95* (6), 1177-1195.
130. Testa, B.; Mayer, J. M., *Hydrolysis in Drug and Prodrug Metabolism: Chemistry, Biochemistry, and Enzymology*. John Wiley & Sons: 2003.
131. Lavis, L. D., Ester Bonds in Prodrugs. *ACS Chem. Biol.* **2008,** *3* (4), 203-206.
132. Grossberg, A. L.; Pressman, D., Nature of the combining site of antibody against a hapten bearing a positive charge. *J. Am. Chem. Soc.* **1960,** *82* (20), 5478-5482.
133. Doscher, M. S.; Wilcox, P. E., Chemical derivatives of alpha-chymotrypsinogen IV. A comparison of the reactions of alpha-chymotrypsinogen and of simple carboxylic acids with diazoacetamide. *J. Biol. Chem.* **1961,** *236*, 1328-1337.
134. Riehm, J. P.; Scheraga, H. A., Structural studies of ribonuclease. XVII. A reactive carboxyl group in ribonuclease. *Biochemistry* **1965,** *4*, 772-782.
135. Delpierre, G. R.; Fruton, J. S., Inactivation of pepsin by diphenyldiazomethane. *Proc. Natl. Acad. Sci. U.S.A.* **1965,** *54* (4), 1161-1167.
136. Mix, K. A.; Raines, R. T., Optimized diazo scaffold for protein esterification. *Org. Lett.* **2015,** *17* (10), 2358-2361.
137. Mix, K. A.; Lomax, J. E.; Raines, R. T., Cytosolic delivery of proteins by bioreversible esterification. *J. Am. Chem. Soc.* **2017,** *139* (41), 14396-14398.
138. Larsen, C., Dextran prodrugs — structure and stability in relation to therapeutic activity. *Adv. Drug Deliv. Rev.* **1989,** *3* (1), 103-154.

139. Kothari, D.; Das, D.; Patel, S.; Goyal, A., Dextran and Food Application. In *Polysaccharides: Bioactivity and Biotechnology*, Ramawat, K. G.; Mérillon, J.-M., Eds. Springer International Publishing: Cham, 2021; pp 1-16.
140. Sutherland, I. W., Novel and established applications of microbial polysaccharides. *Trends Biotechnol.* **1998,** *16* (1), 41-46.
141. Cheetham, N. W. H.; Fiala-Beer, E.; Walker, G. J., Dextran structural details from high-field proton NMR spectroscopy. *Carbohydr. Polym.* **1990,** *14* (2), 149-158.
142. Oben, J. A.; Foreman, J. C., A simple quantitative fluorimetric assay of in vitro phagocytosis in human neutrophils. *J. Immunol. Methods* **1988,** *112* (1), 99-103.
143. Barysch, S. V.; Jahn, R.; Rizzoli, S. O., A fluorescence-based in vitro assay for investigating early endosome dynamics. *Nat. Protoc.* **2010,** *5* (6), 1127-1137.
144. Chyan, W.; Kilgore, H. R.; Raines, R. T., Cytosolic uptake of large monofunctionalized dextrans. *Bioconjugate Chem.* **2018,** *29* (6), 1942-1949.
145. Li, L.; Wan, T.; Wan, M.; Liu, B.; Cheng, R.; Zhang, R., The effect of the size of fluorescent dextran on its endocytic pathway. *Cell Biol. Int.* **2015,** *39* (5), 531-539.
146. Solá, R. J.; Griebenow, K., Glycosylation of therapeutic proteins: An effective strategy to optimize efficacy. *BioDrugs* **2010,** *24* (1), 9-21.
147. Rutkoski, T. J.; Kurten, E. L.; Mitchell, J. C.; Raines, R. T., Disruption of shape-complementarity markers to create cytotoxic variants of ribonuclease A. *J. Mol. Biol.* **2005,** *354* (1), 41-54.
148. Stevens, J. M., Cytochrome c as an experimental model protein. *Metallomics* **2011,** *3* (4), 319-322.
149. Cai, J.; Yang, J.; Jones, D., Mitochondrial control of apoptosis: The role of cytochrome c. *Biochim. Biophys. Acta* **1998,** *1366* (1), 139-149.
150. Alvarez-Paggi, D.; Hannibal, L.; Castro, M. A.; Oviedo-Rouco, S.; Demicheli, V.; Tórtora, V.; Tomasina, F.; Radi, R.; Murgida, D. H., Multifunctional cytochrome c: Learning new tricks from an old dog. *Chem. Rev.* **2017,** *117* (21), 13382-13460.
151. Ow, Y. P.; Green, D. R.; Hao, Z.; Mak, T. W., Cytochrome c: Functions beyond respiration. *Nat. Rev. Mol. Cell Biol.* **2008,** *9* (7), 532-542.
152. Koppenol, W. H.; Rush, J. D.; Mills, J. D.; Margoliash, E., The dipole moment of cytochrome c. *Mol. Biol. Evol.* **1991,** *8* (4), 545-558.
153. Sorrentino, S., The eight human "canonical" ribonucleases: Molecular diversity, catalytic properties, and special biological actions of the enzyme proteins. *FEBS Lett.* **2010,** *584*, 2194-2200.
154. Lu, L.; Li, J.; Moussaoui, M.; Boix, E., Immune modulation by human secreted RNases at the extracellular space. *Front. Immuno.* **2018,** *9* (1012).
155. Kunitz, M., Isolation from beef pancreas of a crystalline protein possessing ribonuclease activity. *Science* **1939,** *90* (2327), 112-113.
156. Richards, F. M., The 1972 Nobel prize for chemistry. *Science* **1972,** *178* (4060), 492-493.
157. Richards, F. M., Linderström-Lang and the Carlsberg Laboratory: The view of a postdoctoral fellow in 1954. *Protein Sci.* **1992,** *1*, 1721-1730.
158. Kresge, N.; Simoni, R. D.; Hill, R. L., The thermodynamic hypothesis of protein folding: The work of Christian Anfinsen. *J. Biol. Chem.* **2006,** *281* (14), e11.
159. Cuchillo, C. M.; Nogués, M. V.; Raines, R. T., Bovine pancreatic ribonuclease: Fifty years of the first enzymatic reaction mechanism. *Biochemistry* **2011,** *50*, 7835-7841.

160. Plummer, T. H.; Hirs, C. H. W.; Tench, W. t. t. a. o. A. L., The isolation of Ribonuclease B, a glycoprotein, from bovine pancreatic juice. *J. Biol. Chem.* **1963,** *238* (4), 1396-1401.
161. Marshall, R. D., The nature and metabolism of the carbohydrate-peptide linkages of glycoproteins. *Biochem. Soc. Symp.* **1974,** (40), 17-26.
162. Imperiali, B.; Hendrickson, T. L., Asparagine-linked glycosylation: Specificity and function of oligosaccharyl transferase. *Bioorg. Med. Chem.* **1995,** *3* (12), 1565-1578.
163. Aebi, M.; Bernasconi, R.; Clerc, S.; Molinari, M., N-Glycan structures: Recognition and processing in the ER. *Trends Biochem. Sci.* **2010,** *35* (2), 74-82.
164. Levine, Z. G.; Walker, S., The biochemistry of O-GlcNAc transferase: Which functions make it essential in mammalian cells? *Annu. Rev. Biochem.* **2016,** *85*, 631-657.
165. Bause, E.; Hettkamp, H., Primary structural requirements for N-glycosylation of peptides in rat liver. *FEBS Lett.* **1979,** *108* (2), 341-344.
166. Peracaula, R.; Royle, L.; Tabares, G.; Mallorqui-Fernandez, G.; Barrabes, S.; Harvey, D. J.; Dwek, R. A.; Rudd, P. M.; de Llorens, R., Glycosylation of human pancreatic ribonuclease: Differences between normal and tumor states. *Glycobiology* **2003,** *13* (4), 227-244.
167. Bravo, J.; Fernández, E.; Ribó, M.; de Llorens, R.; Cuchillo, C. M., A versatile negative-staining ribonuclease zymogram. *Anal. Biochem.* **1994,** *219*, 82-86.
168. Beintema, J. J., Structure, properties and molecular evolution of pancreatic-type ribonucleases. *Life Chem. Rep.* **1987,** *4*, 333-389.
169. Beintema, J. J.; Lenstra, J. A., Evolution of mammalian pancreatic ribonucleases. In *Macromolecular Sequences in Systematic and Evolutionary Biology*, Goodman, M., Ed. Plenum: New York, 1982; pp 43-73.
170. Russo, N.; de Nigris, M.; Ciardiello, A.; Di Donato, A.; D'Alessio, G., Expression in mammalian cells, purification and characterization of recombinant human pancreatic ribonuclease. *FEBS Lett.* **1993,** *333*, 233-237.
171. Brooks, S. A., Strategies for analysis of the glycosylation of proteins: Current status and future perspectives. *Mol. Biotechnol.* **2009,** *43* (1), 76.
172. Gibson, D. G.; Young, L.; Chuang, R.-Y.; Venter, J. C.; Hutchinson, C. A., III; Smith, H. O., Enzymatic assembly of DNA molecules up to several hundred kilobases. *Nat. Methods* **2009,** *6*, 343-345.
173. Eller, C. H.; Lomax, J. E.; Raines, R. T., Bovine brain ribonuclease is the functional homolog of human ribonuclease 1. *J. Biol. Chem.* **2014,** *289* (38), 25996-26006.
174. Thomas, S. P.; Kim, E.; Kim, J.-S.; Raines, R. T., Knockout of the ribonuclease inhibitor gene leaves human cells vulnerable to secretory ribonucleases. *Biochemistry* **2016,** *55*, 6359-6362.
175. Kelemen, B. R.; Klink, T. A.; Behlke, M. A.; Eubanks, S. R.; Leland, P. A.; Raines, R. T., Hypersensitive substrate for ribonucleases. *Nucleic Acids Res.* **1999,** *27*, 3696-3701.
176. Bourgoin-Voillard, S.; Leymarie, N.; Costello, C. E., Top-down tandem mass spectrometry on RNase A and B using a Qh/FT-ICR hybrid mass spectrometer. *Proteomics* **2014,** *14* (10), 1174-1184.
177. Kyriakis, J. M., In the beginning, there was protein phosphorylation. *J. Biol. Chem.* **2014,** *289* (14), 9460-9462.
178. Tagliabracci, V. S.; Engel, J. L.; Wen, J.; Wiley, S. E.; Worby, C. A.; Kinch, L. N.; Xiao, J.; Grishin, N. V.; Dixon, J. E., Secreted kinase phosphorylates extracellular proteins that regulate biomineralization. *Science* **2012,** *336* (6085), 1150-1153.

179. Rudd, P. M.; Joao, H. C.; Coghill, E.; Fiten, P.; Saunders, M. R.; Opdenakker, G.; Dwek, R. A., Glycoforms modify the dynamic stability and functional activity of an enzyme. *Biochemistry* **1994,** *33*, 17-22.
180. Kim, B.-M.; Kim, H.; Raines, R. T.; Lee, Y., Glycosylation of onconase increases its conformational stability and toxicity for cancer cells. *Biochem. Biophys. Res. Commun.* **2004,** *315*, 976-983.
181. Goettig, P., Effects of glycosylation on the enzymatic activity and mechanisms of proteases. *Int. J. Mol. Sci.* **2016,** *17* (12).
182. Nogués, M. V.; Moussaoui, M.; Boix, E.; Vilanova, M.; Ribó, M.; Cuchillo, C. M., The contribution of noncatalytic phosphate-binding subsites to the mechanism of bovine pancreatic ribonuclease A. *Cell. Mol. Life Sci.* **1998,** *54*, 766-774.
183. Fisher, B. M.; Ha, J.-H.; Raines, R. T., Coulombic forces in protein-RNA interactions: Binding and cleavage by ribonuclease A and variants at Lys7, Arg10 and Lys66. *Biochemistry* **1998,** *37* (35), 12121-12132.
184. Fisher, B. M.; Grilley, J. E.; Raines, R. T., A new remote subsite in ribonuclease A. *J. Biol. Chem.* **1998,** *273* (51), 34134-34138.
185. Joao, H. C.; Scragg, I. G.; Dwek, R. A., Effects of glycosylation on protein conformation and amide proton exchange in RNase B. *FEBS Lett.* **1992,** *307*, 343-346.
186. Klink, T. A.; Woycechowsky, K. J.; Taylor, K. M.; Raines, R. T., Contribution of disulfide bonds to the conformational stability and catalytic activity of ribonuclease A. *Eur. J. Biochem.* **2000,** *267*, 566-572.
187. Arnold, U.; Ulbrich-Hofmann, R., Kinetic and thermodynamic thermal stabilities of ribonuclease A and ribonuclease B. *Biochemistry* **1997,** *36*, 2166-2172.
188. Arnold, U.; Schierhorn, A.; Ulbrich-Hofmann, R., Influence of the carbohydrate moiety on the proteolytic cleavage sites in ribonuclease B. *J Protein Chem.* **1998,** *17* (5), 397-405.
189. Arnold, U.; Schierhorn, A.; Ulbrich-Hofmann, R., Modification of the unfolding region in bovine pancreatic ribonuclease and its influence on the thermal stability and proteolyic fragmentation. *Eur. J. Biochem.* **1999,** *259*, 470-475.
190. Mitra, N.; Sinha, S.; Ramya, T. N.; Surolia, A., N-linked oligosaccharides as outfitters for glycoprotein folding, form and function. *Trends Biochem. Sci.* **2006,** *31* (3), 156-163.
191. Solá, R. J.; Griebenow, K., Effects of glycosylation on the stability of protein pharmaceuticals. *J. Pharm. Sci.* **2009,** *98* (4), 1223-1245.
192. Russell, D.; Oldham, N. J.; Davis, B. G., Site-selective chemical protein glycosylation protects from autolysis and proteolytic degradation. *Carbohydr. Res.* **2009,** *344* (12), 1508-1514.
193. Johnson, R. J.; McCoy, J. G.; Bingman, C. A.; Phillips, G. N., Jr.; Raines, R. T., Inhibition of human pancreatic ribonuclease by the human ribonuclease inhibitor protein. *J. Mol. Biol.* **2007,** *367*, 434-449.
194. Zhang, J.; Dyer, K. D.; Rosenberg, H. F., RNase 8, a novel RNase A superfamily ribonuclease expressed uniquely in placenta. *Nucleic Acids Res.* **2002,** *30* (5), 1169-1175.
195. Mullard, A., Top product sales forecasts for 2018. *Nat. Rev. Drug Discov.* **2018,** *17*, 86.
196. Mitragotri, S.; Burke, P. A.; Langer, R., Overcoming the challenges in administering biopharmaceuticals: Formulation and delivery strategies. *Nat. Rev. Drug Discov.* **2014,** *13*, 655.
197. Du, S.; Liew, S. S.; Li, L.; Yao, S. Q., Bypassing endocytosis: Direct cytosolic delivery of proteins. *J. Am. Chem. Soc.* **2018,** *140*, 15986-15996.
198. Rautio, J.; Kärkkäinen, J.; Sloan, K. B., Prodrugs—Recent approvals and a glimpse of the pipeline. *Eur. J. Pharm. Sci.* **2017,** *109*, 146-161.

199. Wang, D.; Zou, L.; Jin, Q.; Hou, J.; Ge, G.; Yang, L., Human carboxylesterases: A comprehensive review. *Acta Pharm. Sin. B* **2018,** *8* (5), 699-712.
200. Waldo, G. S.; Standish, B. M.; Berendzen, J.; Terwilliger, T. C., Rapid protein-folding assay using green fluorescent protein. *Nat. Biotechnol.* **1999,** *17*, 691-695.
201. Knowles, J. R., Tinkering with enzymes: What are we learning? *Science* **1987,** *236*, 1252-1258.
202. Kim, J.-S.; Souček, J.; Matoušek, J.; Raines, R. T., Mechanism of ribonuclease cytotoxicity. *J. Biol. Chem.* **1995,** *270*, 31097-31102.
203. Dickson, K. A.; Dahlberg, C. L.; Raines, R. T., Compensating effects on the cytotoxicity of ribonuclease A variants. *Arch. Biochem. Biophys.* **2003,** *415*, 172-177.
204. Hoang, T. T.; Tanrikulu, I. C.; Vatland, Q. A.; Hoang, T. M.; Raines, R. T., A human ribonuclease variant and ERK-pathway inhibitors exhibit highly synergistic toxicity for cancer cells. *Mol. Cancer Ther.* **2018,** *17*, 2622-2632.
205. Roberts, J. D.; Watanabe, W.; McMahon, R. E., The kinetics and mechanism of the reaction of diphenyldiazomethane and benzoic acid in ethanol. *J. Am. Chem. Soc.* **1951,** *73* (2), 760-765.
206. Roberts, J. D.; Watanabe, W.; McMahon, R. E., The kinetics and mechanism of the reaction of diphenyldiazomethane with 2,4-dinitrophenol in ethanol. *J. Am. Chem. Soc.* **1951,** *73* (6), 2521-2523.
207. Futami, J.; Maeda, T.; Kitazoe, M.; Nukui, E.; Tada, H.; Seno, M.; Kosaka, M.; Yamada, H., Preparation of potent cytotoxic ribonucleases by cationization: Enhanced cellular uptake and decreased interaction with ribonuclease inhibitor by chemical modification of carboxyl groups. *Biochemistry* **2001,** *40* (25), 7518-7524.
208. Haigis, M. C.; Kurten, E. L.; Raines, R. T., Ribonuclease inhibitor as an intracellular sentry. *Nucleic Acids Res.* **2003,** *31* (3), 1024-1032.
209. Note1, 2019.
210. Chao, T.-Y.; Raines, R. T., Fluorogenic label to quantify the cytosolic delivery of macromolecules. *Mol. BioSyst.* **2013,** *9*, 339-342.
211. Rosenberg, H. F., Recombinant human eosinophil cationic protein. Ribonuclease activity is not essential for cytotoxicity. *J. Biol. Chem.* **1995,** *270*, 7876-7881.
212. Leuschner, C.; Hansel, W., Membrane disrupting lytic peptides for cancer treatments. *Curr. Pharm. Des.* **2004,** *10*, 2299-2310.
213. Landry, J. J. M.; Pyl, P. T.; Rausch, T.; Zichner, T.; Tekkedil, M. M.; Stütz, A. M.; Jauch, A.; Aiyar, R. S.; Pau, G.; Delhomme, N.; Gagneur, J.; Korbel, J. O.; Huber, W.; Steinmetz, L. M., The genomic and transcriptomic landscape of a HeLa cell line. *G3* **2013,** *3*, 1213-1224.
214. Note2, 2019.
215. Fuchs, S. M.; Rutkoski, T. J.; Kung, V. M.; Groeschl, R. T.; Raines, R. T., Increasing the potency of a cytotoxin with an arginine graft. *Protein Eng. Des. Sel.* **2007,** *20* (10), 505-509.
216. Dimitrov, D. S., Therapeutic proteins. *Methods Mol. Biol.* **2012,** *899*, 1-26.
217. Pisal, D. S.; Kosloski, M. P.; Balu-iyer, S. V., Delivery of therapeutic proteins. *J. Pharm. Sci.* **2010,** *99* (6), 2557-2575.
218. Fuchs, S. M.; Raines, R. T., Arginine grafting to endow cell permeability. *ACS Chem. Biol.* **2007,** *2* (3), 167-170.
219. Pasteur, L., *Bull. Soc. Chim. Paris* **1861**, 30-31.
220. Organization, W. H., *WHO Model List of Essential Medicines*. World Health Organization: Geneva, Switzerland, 2017.
221. Ljungstrom, K. G., The antithrombotic efficacy of dextran. *Acta Chir. Scand. Suppl.* **1988,** *543*, 26-30.

222. Schmid, J.; Sieber, V.; Rehm, B., Bacterial exopolysaccharides: Biosynthesis pathways and engineering strategies. *Front. Microbiol.* **2015,** *6*, 1-24.
223. Turino, M. I.; de Valdez, G. F.; Mozzi, F., Biopolymers from lactic acid bacteria. Novel applications in foods and beverages. *Front. Microbiol.* **2015,** *6*, 1-16.
224. Khalikova, E.; Susi, P.; Korpela, T., Microbial dextran-hydrolyzing enzymes: Fundamentals and applications. *Microbiol. Mol. Biol. Rev.* **2005,** *69* (2), 306-325.
225. Yong-Ling, P. O.; Green, D. R.; Mak, T. W., Cytochrome c: Functions beyond respiration. *Nat. Rev. Mol. Cell. Biol.* **2008,** *9*, 532-542.
226. Rytomaa, M.; Mustonen, P.; Kinnunen, P. K., Reversible, nonionic, and pH-dependent association of cytochrome c with cardiolipin-phosphatidylcholine liposomes. *J. Biol. Chem.* **1992,** *267* (31), 22243-22248.
227. Rytomaa, M.; Kinnunen, P. K., Evidence for two distinct acidic phospholipid-binding sites in cytochrome c. *J. Biol. Chem.* **1994,** *269* (3), 1770-1774.
228. Rytomaa, M.; Kinnunen, P. K. J., Reversibility of the binding of cytochrome c to liposomes. *J. Biol. Chem.* **1995,** *270* (7), 3197-3202.
229. Tuominen, E. K.; Wallace, C. J.; Kinnunen, P. K., Phospholipid-cytochrome c interaction: Evidence for the extended lipid anchorage. *J. Biol. Chem.* **2002,** *277* (11), 8822-8826.
230. Kalanxhi, E.; Wallace, C. J., Cytochrome c impaled: Investigation of the extended lipid anchorage of a soluble protein to mitochondrial membrane models. *J. Biochem.* **2007,** *407* (2), 179-187.
231. van Donge, S. F. M.; Teeuwen, R. L. M.; Nallani, M.; van Berkel, S. S.; Cornelissen, J. L. M.; Noelt, R. J. M.; van Hest, J. C. M., Single-step azide introduction in proteins via an aqueous diazo transfer. *Bioconjugate Chem.* **2009,** *20*, 20-23.
232. Guo, M.; Bhaskar, B.; Li, H.; Barrows, T. P.; Poulos, T. L., Crystal structure and characterization of a cytochrome c peroxidase–cytochrome c site-specific cross-link. *Proc. Natl. Acad Sci. U.S.A.* **2004,** *101* (16), 5940-5945.
233. Morales-Cruz, M.; Figueroa, C. M.; Gonzalez-Robles, T.; Delgado, Y.; Molina, A.; Mendez, J.; Morales, M.; Griebenow, K., Activation of caspase-dependent apoptosis by intracellular delivery of Cytochrome c-based nanoparticles. *J. Nanobiotechnology* **2014,** *12*, 33.
234. Kim, S. K.; Foote, M. B.; Huang, L., The targeted intracellular delivery of cytochrome c protein to tumors using lipid-apolipoprotein nanoparticles. *Biomaterials* **2012,** *33* (15), 3959-3966.
235. Huang, W.-Y.; Davies, G.-L.; Davis, J. J., Engineering cytochrome-modified silica nanoparticles to induce programmed cell death. *Chem. Eur. J.* **2013,** *19* (52), 17891-17898.
236. Saxena, M.; Delgado, Y.; Sharma, R. K.; Sharma, S.; Guzmán, S. L. P. D. L.; Tinoco, A. D.; Griebenow, K., Inducing cell death in vitro in cancer cells by targeted delivery of cytochrome c via a transferrin conjugate. *PLoS ONE* **2018,** *13* (4), e0195542.
237. Barnes, M. P.; Shen, W. C., Disulfide and thioether linked cytochrome c-oligoarginine conjugates in HeLa cells. *Int. J. Pharm.* **2009,** *369* (1-2), 79-84.
238. Yeh, T. H.; Wu, F. L.; Shen, L. J., Intracellular delivery of cytochrome c by galactosylated albumin to hepatocarcinoma cells. *J. Drug Targ.* **2014,** *22* (6), 528-535.
239. Dhandayuthapani, S.; Marimuthu, P.; Hormann, V.; Kumi-Diaka, J.; Rathinavelu, A., Induction of apoptosis in HeLa cells via caspase activation by resveratrol and genistein. *J. Med. Food* **2013,** *16* (2), 139-146.
240. Li, L.; Qiu, R. L.; Lin, Y.; Cai, Y.; Bian, Y.; Fan, Y.; Gao, X. J., Resveratrol suppresses human cervical carcinoma cell proliferation and elevates apoptosis via the mitochondrial and p53 signaling pathways. *Oncol. Lett.* **2018,** *15* (6), 9845-9851.

241. Maia, J.; Carvalho, R. A.; Coelho, J. F. J.; Simoes, P. N.; Gil, M. H., Insight on the periodate oxidation of dextran and its structural vicissitudes. *Polymer* **2011,** *52* (2), 258-265.
242. Yaylayan, V. A.; Huyghues-Despointes, A.; Feather, M. S., Chemistry of the Amadori rearrangement products: Analysis, synthesis, kinetics, reactions and spectroscopic properties. *Crtic. Rev. Food Sci. and Nutri.* **1994,** *34* (4), 321-369.
243. Deriy, L. V.; Gomez, E. A.; Zhang, G. P.; Beacham, D. W.; Hopson, J. A.; Gallan, A. J.; Shevchenko, P. D.; Bindokas, V. P.; Nelson, D. J., Disease-causing mutations in the cystic fibrosis transmembrane conductance regulator determine the functional responses of alveolar macrophages. *J. Biol. Chem.* **2009,** *284* (51), 35926-35938.
244. Joao, H. C.; Dwek, R. A., Effects of glycosylation on protein structure and dynamics in ribonuclease B and some of its individual glycoforms. *Eur. J. Biochem.* **1993,** *218* (1), 239-244.
245. Makarov, A. A.; Ilinskaya, O. N., Cytotoxic ribonucleases: Molecular weapons and their targets. *FEBS Lett.* **2003,** *540* (1), 15-20.
246. Dicker, M.; Strasser, R., Using glyco-engineering to produce therapeutic proteins. *Expert Opin. Biol. Ther.* **2015,** *15* (10), 1501-1516.
247. Sinclair, A. M.; Elliott, S., Glycoengineering: The effect of glycosylation on the properties of therapeutic proteins. *J. Pharm. Sci.* **2005,** *94* (8), 1626-1635.
248. Méndez, J.; Morales Cruz, M.; Delgado, Y.; Figueroa, C. M.; Orellano, E. A.; Morales, M.; Monteagudo, A.; Griebenow, K., Delivery of chemically glycosylated cytochrome c immobilized in mesoporous silica nanoparticles induces apoptosis in HeLa cancer cells. *Mol. Pharm.* **2014,** *11* (1), 102-111.
249. Walsh, G., Biopharmaceutical benchmarks 2010. *Nat. Biotechnol.* **2010,** *28*, 917.
250. Imberty, A.; Pérez, S., Structure, conformation, and dynamics of bioactive oligosaccharides: Theoretical approaches and experimental validations. *Chem. Rev.* **2000,** *100* (12), 4567-4588.
251. Mertens, H. D. T.; Svergun, D. I., Structural characterization of proteins and complexes using small-angle X-ray solution scattering. *J. Struct. Biol.* **2010,** *172* (1), 128-141.
252. Guttman, M.; Weinkam, P.; Sali, A.; Lee, K. K., All-atom ensemble modeling to analyze small-angle x-ray scattering of glycosylated proteins. *Structure* **2013,** *21* (3), 321-331.
253. Yarema, K. J.; Bertozzi, C. R., Characterizing glycosylation pathways. *Genome Biol.* **2001,** *2* (5), reviews0004.0001.
254. Lederkremer, G. Z., Glycoprotein folding, quality control and ER-associated degradation. *Curr. Opin. Struct. Biol.* **2009,** *19* (5), 515-523.
255. Helenius, A.; Aebi, M., Roles of N-linked glycans in the endoplasmic reticulum. *Annu. Rev. Biochem.* **2004,** *73* (1), 1019-1049.
256. Itakura, E.; Chen, C.; de Bono, M., Purification of FLAG-tagged secreted proteins from mammalian cells. *Bio Protoc.* **2017,** *7* (15), e2430.
257. Anelli, T.; Sitia, R., Protein quality control in the early secretory pathway. *EMBO J.* **2008,** *27* (2), 315-327.
258. Reynaud, E. G.; Simpson, J. C., Navigating the secretory pathway. *EMBO Rep.* **2002,** *3* (9), 828-833.
259. Walter, P.; Ron, D., The unfolded protein response: From stress pathway to homeostatic regulation. *Science* **2011,** *334* (6059), 1081.
260. Rabouille, C.; Malhotra, V.; Nickel, W., Diversity in unconventional protein secretion. *J. Cell Sci.* **2012,** *125* (22), 5251.
261. Rabouille, C., Pathways of unconventional protein secretion. *Trends Cell Biol.* **2017,** *27* (3), 230-240.

262. Abel, R. L.; Haigis, M. C.; Park, C.; Raines, R. T., Fluorescence assay for the binding of ribonuclease A to the ribonuclease inhibitor protein. *Anal. Biochem.* **2002,** *306* (1), 100-107.
263. Dutta, D.; Donaldson, J. G., Search for inhibitors of endocytosis: Intended specificity and unintended consequences. *Cell Logist.* **2012,** *2* (4), 203-208.
264. Huttunen, K. M.; Raunio, H.; Rautio, J., Prodrugs—from serendipity to rational design. *Pharmacol. Rev.* **2011,** *63* (3), 750.
265. Fett, J. W.; Strydom, D. J.; Lobb, R. R.; Alderman, E. M.; Bethune, J. L.; Riordan, J. F.; Vallee, B. L., Isolation and characterization of angiogenin, an angiogenic protein from human carcinoma cells. *Biochemistry* **1985,** *24*, 5480-5486.
266. Kieran, D.; Sebastia, J.; Greenway, M. J.; King, M. A.; Connaughton, D.; Concannon, C. G.; Fenner, B.; Hardiman, O.; Prehn, J. H., Control of motoneuron survival by angiogenin. *J. Neurosci.* **2008,** *28* (52), 14056-14061.
267. Badet, J., Angiogenin, a potent mediator of angiogenesis. Biological, biochemical and structural properties. *Pathol. Biol.* **1999,** *47*, 345-351.
268. Sheng, J.; Xu, Z., Three decades of research on angiogenin: A review and perspective. *Acta Biochim. Biophys. Sin.* **2016,** *48* (5), 399-410.
269. Lyons, S. M.; Fay, M. M.; Akiyama, Y.; Anderson, P. J.; Ivanov, P., RNA biology of angiogenin: Current state and perspectives. *RNA Biol.* **2017,** *14* (2), 171-178.
270. Riordan, J. F., Angiogenin. *Methods Enzymol.* **2001,** *341*, 263-273.
271. Smith, B. D.; Raines, R. T., Genetic selection for critical residues in ribonucleases. *J. Mol. Biol.* **2006,** *362* (3), 459-478.
272. Hu, G. F.; Riordan, J. F.; Vallee, B. L., A putative angiogenin receptor in angiogenin-responsive human endothelial cells. *Proc. Natl. Acad. Sci. U.S.A.* **1997,** *94*, 2204-2209.
273. Skorupa, A.; King, M. A.; Aparicio, I. M.; Dussmann, H.; Coughlan, K.; Breen, B.; Kieran, D.; Concannon, C. G.; Marin, P.; Prehn, J. H., Motoneurons secrete angiogenin to induce RNA cleavage in astroglia. *J. Neurosci.* **2012,** *32* (15), 5024-5038.
274. Hu, G.-F.; Strydom, D. J.; Fett, J. W.; Riordan, J. F.; Vallee, B. L., Actin is a binding protein for angiogenin. *Proc. Natl. Acad. Sci. U.S.A.* **1993,** *90*, 1217-1221.
275. Moroianu, J.; Riordan, J. F., Nuclear translocation of angiogenin in proliferating endothelial cells is essential to its angiogenic activity. *Proc. Natl. Acad. Sci. U.S.A.* **1994,** *91*, 1677-1681.
276. Lixin, R.; Efthymiadis, A.; Henderson, B.; Jans, D. A., Novel properties of the nucleolar targeting signal of human angiogenin. *Biochem. Biophys. Res. Commun.* **2001,** *284* (1), 185-193.
277. Leland, P. A.; Staniszewski, K. E.; Park, C.; Kelemen, B. R.; Raines, R. T., The ribonucleolytic activity of angiogenin. *Biochemistry* **2002,** *41*, 1343-1350.
278. Emara, M. M.; Ivanov, P.; Hickman, T.; Dawra, N.; Tisdale, S.; Kedersha, N.; Hu, G. F.; Anderson, P., Angiogenin-induced tRNA-derived stress-induced RNAs promote stress-induced stress granule assembly. *J. Biol. Chem.* **2010,** *285* (14), 10959-10968.
279. Pizzo, E.; Sarcinelli, C.; Sheng, J.; Fusco, S.; Formiggini, F.; Netti, P.; Yu, W.; D'Alessio, G.; Hu, G. F., Ribonuclease/angiogenin inhibitor 1 regulates stress-induced subcellular localization of angiogenin to control growth and survival. *J. Cell Sci.* **2013,** *126* (Pt 18), 4308-4319.
280. Yamasaki, S.; Ivanov, P.; Hu, G. F.; Anderson, P., Angiogenin cleaves tRNA and promotes stress-induced translational repression. *J. Cell Biol.* **2009,** *185* (1), 35-42.
281. Ivanov, P.; Emara, M. M.; Villen, J.; Gygi, S. P.; Anderson, P., Angiogenin-induced tRNA fragments inhibit translation initiation. *Mol. Cell* **2011,** *43* (4), 613-623.

282. Saikia, M.; Hatzoglou, M., The many virtues of tRNA-derived stress-induced RNAs (tiRNAs): Discovering novel mechanisms of stress response and effect on human health. *J. Biol. Chem.* **2015,** *290* (50), 29761-29768.
283. Ivanov, P.; O'Day, E.; Emara, M. M.; Wagner, G.; Lieberman, J.; Anderson, P., G-quadruplex structures contribute to the neuroprotective effects of angiogenin-induced tRNA fragments. *Proc. Natl. Acad. Sci. U.S.A.* **2014,** *111* (51), 18201-18206.
284. Lyons, S. M.; Achorn, C.; Kedersha, N. L.; Anderson, P. J.; Ivanov, P., YB-1 regulates tiRNA-induced stress granule formation but not translational repression. *Nucleic Acids Res.* **2016,** *44* (14), 6949-6960.
285. Deng, J.; Ptashkin, R. N.; Chen, Y.; Cheng, Z.; Liu, G.; Phan, T.; Deng, X.; Zhou, J.; Lee, I.; Lee, Y. S.; Bao, X., Respiratory syncytial virus utilizes a tRNA fragment to suppress antiviral responses through a novel targeting mechanism. *Mol. Ther.* **2015,** *23* (10), 1622-1629.
286. Lee, F. S.; Shapiro, R.; Vallee, B. L., Tight-binding inhibition of angiogenin and ribonuclease A by placental ribonuclease inhibitor. *Biochemistry* **1989,** *28*, 225-230.
287. Blázquez, M.; Fominaya, J. M.; Hofsteenge, J., Oxidation of sulfhydryl groups of ribonuclease inhibitor in epithelial cells is sufficient for its intracellular degradation. *J. Biol. Chem.* **1996,** *271*, 18638-18642.
288. Fominaya, J. M.; Hofsteenge, J., Inactivation of ribonuclease inhibitor by thiol–disulfide exchange. *J. Biol. Chem.* **1992,** *267*, 24655-24660.
289. Kim, B.-M.; Schultz, L. W.; Raines, R. T., Variants of ribonuclease inhibitor that resist oxidation. *Protein Sci.* **1999,** *8*, 430-434.
290. Sundlass, N. K.; Eller, C. H.; Cui, Q.; Raines, R. T., Contribution of electrostatics to the binding of pancreatic-type ribonucleases to membranes. *Biochemistry* **2013,** *52* (37), 6304-6312.
291. Panero, R.; Rinaldi, A.; Memoli, D.; Nassa, G.; Ravo, M.; Rizzo, F.; Tarallo, R.; Milanesi, L.; Weisz, A.; Giurato, G., iSmaRT: a toolkit for a comprehensive analysis of small RNA-Seq data. *Bioinformatics* **2017,** *33* (6), 938-940.
292. Martin, M., Cutadapt removes adapter sequences from high-throughput sequencing reads. *EMBnet.journal* **2011,** *17* (1), 10-12.
293. Rueda, A.; Barturen, G.; Lebron, R.; Gomez-Martin, C.; Alganza, A.; Oliver, J. L.; Hackenberg, M., sRNAtoolbox: an integrated collection of small RNA research tools. *Nucleic Acids Res.* **2015,** *43* (W1), W467-W473.
294. Tarazona, S.; Furio-Tari, P.; Turra, D.; Pietro, A. D.; Nueda, M. J.; Ferrer, A.; Conesa, A., Data quality aware analysis of differential expression in RNA-seq with NOISeq R/Bioc package. *Nucleic Acids Res.* **2015,** *43* (21), e140.
295. de Hoon, M. J.; Imoto, S.; Nolan, J.; Miyano, S., Open source clustering software. *Bioinformatics* **2004,** *20* (9), 1453-1454.
296. Saldanha, A. J., Java Treeview--extensible visualization of microarray data. *Bioinformatics* **2004,** *20* (17), 3246-3248.
297. Backes, C.; Khaleeq, Q. T.; Meese, E.; Keller, A., miEAA: microRNA enrichment analysis and annotation. *Nucleic Acids Res.* **2016,** *44* (W1), W110-W116.
298. Supek, F.; Bosnjak, M.; Skunca, N.; Smuc, T., REVIGO summarizes and visualizes long lists of gene ontology terms. *PLoS One* **2011,** *6* (7), e21800.
299. Shannon, P.; Markiel, A.; Ozier, O.; Baliga, N. S.; Wang, J. T.; Ramage, D.; Amin, N.; Schwikowski, B.; Ideker, T., Cytoscape: a software environment for integrated models of biomolecular interaction networks. *Genome Res.* **2003,** *13* (11), 2498-2504.

300. Bailey, T. L., DREME: motif discovery in transcription factor ChIP-seq data. *Bioinformatics* **2011,** *27* (12), 1653-1659.
301. Zheng, L. L.; Xu, W. L.; Liu, S.; Sun, W. J.; Li, J. H.; Wu, J.; Yang, J. H.; Qu, L. H., tRF2Cancer: A web server to detect tRNA-derived small RNA fragments (tRFs) and their expression in multiple cancers. *Nucleic Acids Res.* **2016,** *44* (W1), W185-W193.
302. Kikin, O.; D'Antonio, L.; Bagga, P. S., QGRS Mapper: a web-based server for predicting G-quadruplexes in nucleotide sequences. *Nucleic Acids Res.* **2006,** *34* (Web Server issue), W676-W682.
303. Thomas, S. P.; Kim, E.; Kim, J. S.; Raines, R. T., Knockout of the ribonuclease inhibitor gene leaves human cells vulnerable to secretory ribonucleases. *Biochemistry* **2016,** *55* (46), 6359-6362.
304. Shapiro, R.; Vallee, B. L., Site-directed mutagenesis of histidine-13 and histidine-114 of human angiogenin. Alanine derivatives inhibit angiogenin-induced angiogenesis. *Biochemistry* **1989,** *28*, 7401-7408.
305. Hu, G. F., Neomycin inhibits angiogenin-induced angiogenesis. *Proc. Natl. Acad. Sci. U.S.A.* **1998,** *95* (17), 9791-9795.
306. Bárcena, C.; Stefanovic, M.; Tutusaus, A.; Martinez-Nieto, G. A.; Martinez, L.; García-Ruiz, C.; de Mingo, A.; Caballeria, J.; Fernandez-Checa, J. C.; Marí, M.; Morales, A., Angiogenin secretion from hepatoma cells activates hepatic stellate cells to amplify a self-sustained cycle promoting liver cancer. *Sci. Rep.* **2015,** *5*, 7916.
307. Saikia, M.; Krokowski, D.; Guan, B. J.; Ivanov, P.; Parisien, M.; Hu, G. F.; Anderson, P.; Pan, T.; Hatzoglou, M., Genome-wide identification and quantitative analysis of cleaved tRNA fragments induced by cellular stress. *J. Biol. Chem.* **2012,** *287* (51), 42708-42725.
308. Saxena, S. K.; Rybak, S. M.; Davey, R. T., Jr.; Youle, R. J.; Ackerman, E. J., Angiogenin is a cytotoxic, tRNA-specific ribonuclease in the RNase A superfamily. *J. Biol. Chem.* **1992,** *267*, 21982-21986.
309. Weng, C. H.; Dong, H. J.; Chen, G. D.; Zhai, Y. X.; Bai, R. P.; Hu, H.; Lu, L. R.; Xu, Z. P., miR-409-3p inhibits HT1080 cell proliferation, vascularization and metastasis by targeting angiogenin. *Cancer Lett.* **2012,** *323* (2), 171-179.
310. Li, S.; Hu, G. F., Emerging role of angiogenin in stress response and cell survival under adverse conditions. *J. Cell Physiol.* **2012,** *227* (7), 2822-2826.
311. Wang, Q.; Lee, I.; Ren, J.; Ajay, S. S.; Lee, Y. S.; Bao, X., Identification and functional characterization of tRNA-derived RNA fragments (tRFs) in respiratory syncytial virus infection. *Mol. Ther.* **2013,** *21* (2), 368-379.
312. Saikia, M.; Krokowski, D.; Guan, B. J.; Ivanov, P.; Parisien, M.; Hu, G.-f.; Anderson, P.; Pan, T.; Hatzoglou, M., Genome-wide identification and quantitative analysis of cleaved tRNA fragments induced by cellular stress. *J Biol Chem* **2012,** *287* (51), 42708-42725.
313. Sharma, U.; Conine, C. C.; Shea, J. M.; Boskovic, A.; Derr, A. G.; Bing, X. Y.; Belleannee, C.; Kucukural, A.; Serra, R. W.; Sun, F.; Song, L.; Carone, B. R.; Ricci, E. P.; Li, X. Z.; Fauquier, L.; Moore, M. J.; Sullivan, R.; Mello, C. C.; Garber, M.; Rando, O. J., Biogenesis and function of tRNA fragments during sperm maturation and fertilization in mammals. *Science* **2016,** *351* (6271), 391-396.
314. Li, Q.; Hu, B.; Hu, G. W.; Chen, C. Y.; Niu, X.; Liu, J.; Zhou, S. M.; Zhang, C. Q.; Wang, Y.; Deng, Z. F., tRNA-derived small non-coding RNAs in response to ischemia inhibit angiogenesis. *Sci. Rep.* **2016,** *6*, 20850.

315. Blanco, S.; Dietmann, S.; Flores, J. V.; Hussain, S.; Kutter, C.; Humphreys, P.; Lukk, M.; Lombard, P.; Treps, L.; Popis, M.; Kellner, S.; Holter, S. M.; Garrett, L.; Wurst, W.; Becker, L.; Klopstock, T.; Fuchs, H.; Gailus-Durner, V.; Hrabe de Angelis, M.; Karadottir, R. T.; Helm, M.; Ule, J.; Gleeson, J. G.; Odom, D. T.; Frye, M., Aberrant methylation of tRNAs links cellular stress to neuro-developmental disorders. *EMBO J* **2014,** *33* (18), 2020-2039.
316. Xu, Z. P.; Tsuji, T.; Riordan, J. F.; Hu, G. F., Identification and characterization of an angiogenin-binding DNA sequence that stimulates luciferase reporter gene expression. *Biochemistry* **2003,** *42* (1), 121-128.